INTERACTION BETWEEN SUPERCHARGED GUANIDINIUM-RICH PEPTIDES AND THE LIPID BIS(MONOACYLGLYCERO)PHOSPHATE ENABLES CYTOSOLIC PENETRATION INTO LIVE HUMAN CELLS: STRUCTURE-ACTIVITY RELATIONSHIPS AND MECHANISMS

A Dissertation

by

DAKOTA JAMES BROCK

Submitted to the Office of Graduate and Professional Studies of
Texas A&M University
in partial fulfillment of the requirements for the degree of

DOCTOR OF PHILOSOPHY

Chair of Committee,	Jean-Philippe Pellois
Committee Members,	Hays Rye
	Paul Straight
	Karen Wooley
Head of Department,	Dorothy Shippen

August 2019

Major Subject: Biochemistry

ABSTRACT

The effective delivery of hydrophilic, bioactive molecules, such as enzymes and nucleic acids, to the cytosol of cells has proven to be a multibillion-dollar problem for cell biologists and the pharmaceutical industry. In recent studies, unprecedented cytosolic delivery of such cargos was achieved by the utilization of cell-penetrating agents. These densely charged, polycationic molecules, whether of biological or synthetic origin, have shown the ability to penetrate human cells and, concomitantly, carry macromolecular cargos into the intracellular milieu, albeit with variable efficiencies.

Although this method of cell delivery seems promising, the molecular underpinnings involved in such transport remain unclear and, by proxy, limit advancements in this technology. In this study, I determine the effect of charge density (net charge / kDa) on cell penetration and gain insight into the proposed mechanism of transport by using the prototypical cell-penetrating peptide TAT. Cell penetrating peptide variants were synthesized containing one, two, or three copies of the TAT peptide on a synthetic scaffold to generate branched cell-permeable prototypes with increasing charge density. I establish that increasing TAT copies dramatically increases the cell penetration efficiency of the peptides while simultaneously enabling the efficient cytosolic delivery of macromolecular cargos. In previous studies, it has been shown that TAT-mediated cellular entry involves the leaky fusion of late endosomal membranes enriched with the anionic lipid BMP. We found that the derivatives with two and three

TAT branches, 2TAT and 3TAT, induce the leakage of lipid bilayers specifically containing BMP. Furthermore, these compounds lead to liposomal flocculation, fusion and an increase in lamellarity. In contrast, while the monomeric counterpart 1TAT binds to the same extent and causes liposomal flocculation, 1TAT does not induce fusion or a significant increase in lamellarity. Overall, these results indicate that an increase in the peptide density of these branched structures leads to the emergence of membrane-disruption and cell penetration activities.

Moreover, I sought to identify additional properties of BMP-containing membranes that play a role in endosomolysis. In this study, I found that late endosomal membranes are substantially more fluid or disordered than many other biological membranes. The source of this membrane fluidity stems from BMP itself. By utilizing phospholipid components with variable extents of unsaturation, I generated a series of late endosomal liposome mimics that increased in membrane fluidity as a function of unsaturation. As the liposomes increased in fluidity, 3TAT-induced membrane leakage increased as well. Conversely, liposomes containing saturated fatty acids leaked to a lesser extent than their unsaturated fatty acid counterparts. Taken together these results suggest that while the guanidinium-BMP interaction is necessary to cause endosomolysis, the intrinsic fluidity of BMP-enriched membranes directly impacts the extent of endosomolysis imparted by supercharged CPPs.

DEDICATION

I would like to dedicate this work to my God, wife, and family. My achievements are simply a product of God's wisdom and guidance and for that, I will be forever grateful. "'I can do all this through him who gives me strength' (New International Version, Phil. 4.13)." To my wife, Dr. Christina Brock, you have fervently loved me, supported me and stood by my side through this journey. You are my shining light, an inspiration to myself and everyone who gets to know you. To my mother, Dr. Kathryn Waggoner, I am so thankful to have had you as my spiritual and professional role model. You have always challenged me to excel in everything I do and to do everything for the glory of God. Finally, to my father and step mother, Bobby and Dorynda Brock, I am grateful for your support throughout my graduate career. I am particularly thankful for dragging me out of the lab so that I can spend time with family during my time in Texas.

ACKNOWLEDGEMENTS

First, I would like to thank my exceptional mentor, Dr. Jean-Philippe Pellois. You have molded my mind scientifically and challenged me to think critically, truly a testament to the outstanding professor that you are. Although I proved to be rather difficult to mentor at times (some would even say sassy), you provided guidance to me both in and out of the lab and truly serve as a scientific role model for what I hope to achieve. Additionally, I would like to acknowledge Dr. Hays Rye, Dr. Karen Wooley, and Dr. Straight for serving on my committee and providing me with helpful insight, guidance, and many contributions throughout my graduate career.

My graduate student colleagues of the Pellois lab truly embody the sense of community and support one needs to not only survive but excel through their graduate career. Of the previous members, Dr. Alfredo Erazo-Oliveras, Dr. Ting-Yi Wang, and Dr. Kristina Najjar stand out in particular. The three of you accepted me into the lab with open arms, mentored me along the way, and cultivated a truly remarkable lab atmosphere. While there is no doubt that the three of you helped me become the scientist I am today, Kristina has always been there for me as a mentor and dear friend. I cannot express how thankful I am for having you in my life. I would also like to express my appreciation for all of the current graduate members of the Pellois lab including Helena Kondow-McConaghy, Jason Allen, Joshua Diaz, Elizabeth Hager, Sean Xiao, and Aaron Jacobson. Helena and Jason, I am deeply thankful for Helena and Jason as they have both shown such support and patience with me through the scientific “debates” and

crazy ideas that I've had over the years. Liz, although I have not known you for quite as long, I value our friendship and your support. I would also like to thank all of my undergraduate mentees namely Kristin Graham and Chris Holt. Kristin truly taught me how to be a mentor as she is an excellent student and demonstrates and for that, I am truly grateful.

Finally, I would like to thank the entirety of the BioBio family including my close friends, the BGA, the staff, and my graduate advisor Rafael Almanzar for their support and for teaching me how to be a leader.

CONTRIBUTORS AND FUNDING SOURCES

This work was supervised by a dissertation committee consisting of Professor Jean-Philippe Pellois (advisor) and Professors Hays Rye and Paul Straight of the Department of Biochemistry & Biophysics and Professor Karen Wooley of the Department of Chemistry.

All work for the dissertation was completed independently by the student.

This work was made possible in part by National Institute of Health (NIH) Grant Award Number R01GM110137. Its contents are solely the responsibility of the authors and do not necessarily represent the official views of the NIH.

NOMENCLATURE

3-NBS	3-nitrobenzenesulfonate
AFM	atomic force microscopy
ATP	adenosine triphosphate
ATCC	American Type Culture Collection
β-gal	beta-galactosidase
BAS	burst analysis spectroscopy
BBB	blood-brain barrier
BHK	baby hamster kidney
BMP	bis(monoacylglycero)phosphate
BSA	bovine serum albumin
CCD	charge-coupled device
CFP	cyan fluorescent protein
CHO	Chinese hamster ovary
Chol	cholesterol
COI	cargo of interest
CPP	cell-penetrating peptide
DAPI	4′,6-diamidino-2-phenylindole
DCM	dichloromethane
DEAC	7-(diethylaminocoumarin)-3-carboxylic acid
DENV	Dengue virus
DENV C	Dengue virus capsid protein

DENV E	Dengue virus envelope protein
DiD	1,1'-dioctadecyl-3,3,3',3'-tetramethylindodicarbocyanine
DIEA	N,N-diisopropylethylamine
DLS	dynamic light scattering
DMEM	Dulbecco's modified eagle medium
DMF	dimethylformamide
DNA	deoxyribonucleic acid
DN	dominant negative
DO	dioleoyl
DOPC	dioleoylphosphatidylcholine
DOPE	dioleoylphosphatidylethanolamine
DPPC	dipalmitoylphosphatidylcholine
DRBD	double-stranded ribonucleic acid-binding domain
ds	double-stranded
DSPC	distearoylphosphatidylcholine
EDTA	ethylenediaminetetraacetic acid
EE	early endosome
EED	endosomal escape domain
EGFP	enhanced green fluorescent protein
EIPA	5-(N-ethyl-N-isopropyl) amiloride
EM	electron microscopy
ESI	electrospray ionization

FACS	fluorescence activated cell sorting
FBS	fetal bovine serum
FCS	fluorescence correlation spectroscopy
FDA	U.S. Food and Drug Administration
FITC	fluorescein isothiocyanate
Fl	carboxy-fluorescein
FRET	Förster resonance energy transfer
GP	generalized polarization
H2B	histone 2B
HA2	haemagglutinin protein II
HCTU	O-(1H-6-Chlorobenzotriazole-1-yl)-1,1,3,3-tetramethyluronium hexafluorophosphate
HEPES	4-(2-hydroxyethyl)-1-piperazineethanesulfonic acid
HIV	Human immunodeficiency virus
HM	heavy membranes
HNF	human newborn fibroblasts
HPLC	high-performance liquid chromatography
HRP	horseradish peroxidase
HSPG	heparin sulfate proteoglycan
IGF2/MPR	insulin-like growth factor type 2/mannose-6-phosphate receptor
IgG	immunoglobulin G
ILV	interlumenal vesicle

IP	intraperitoneal
iPSC	induced pluripotent stem cells
IPTG	isopropyl -D-1-thiogalactopyranoside
ITC	isothermal calorimetry
kDa	kilo Dalton
L-15	Leibovitz's 15
LB	Luria broth
LBPA	lysobisphosphatidic acid (aka bis(monoacylglycero)phosphate)\
LDL	low-density lipoproteins
LE	late endosome
LFA	LipofectAMINE2000
LNPs	lipid nanoparticles
LSL	lox-stop-lox
LUV	large unilamellar vesicle
mAb	monoclonal antibody
MALDI	matrix-assisted laser desorption/ionization
MAP	model amphipathic peptide
MBHA	methylbenzhydrylamine
MHC	major histocompatibility complex
MLV	multivesicular liposomes
MOF	metal-organic framework
MTT	3-(4,5-Dimethylthiazol-2-yl)-2,5-diphenyltetrazolium bromide

MVB	multivesicular bodies
NCL	native chemical ligation
NLS	nuclear localization signal
NMR	nuclear magnetic resonance
NP	nanoparticle
NPC	Niemann-Pick type C
ns	not significant
ON	oligonucleotide
PAS	proline/alanine-rich sequences
PBS	phosphate buffer saline
PCI	photochemical internalization
PCR	polymerase chain reaction
PEI	polyethylenimine
PG	phosphatidylglycerol
PM	plasma membrane
PNA	peptide nucleic acid
POI	protein of interest
Ptd	phosphatidyl
Ptd-Ser	phosphatidyl serine
RBC	red blood cell
RFP	red fluorescent protein
RNA	ribonucleic acid

RNase A	ribonuclease A
ROS	reactive oxygen species
rp	reversed-phase
RPM	rotations per minute
SAR	structure-activity relationship
SDS-PAGE	sodium dodecyl sulfate polyacrylamide gel electrophoresis
sfGFP	superfolder green fluorescent protein
siRNA	small-interfering ribonucleic acid
SNAP	soluble N-ethylmaleimide sensitive factor attachment protein
SPPS	solid-phase peptide synthesis
ssDNA	single-stranded deoxynucleic acid
TAT	trans-activator of transcription
TCEP	tris(2-carboxyethyl)phosphine
TFA	trifluoroacetic acid
TGN	trans-Golgi network
TMR	5(6)-carboxytetramethylrhodamine
TOF	time-of-flight
TP	transportan
VLP	virus-like particle
WNV	West Nile virus
WT	wild-type
YFC	yellow fever virus

TABLE OF CONTENTS

Page

LIST OF FIGURES

Page

LIST OF TABLES

Page

CHAPTER I

INTRODUCTION

1.1 Significance of the delivery of macromolecules into the cytosol of live cells

Delivery of macromolecular cargo, such as nucleic acids and proteins, into the cytosolic space of live cells is of great value to the field of cell biology. For example, cellular delivery of a domain of *Pseudomonas* exotoxin A has been used to learn more about *Pseudomonas* cytotoxicity (1). Similarly, advancements in the pharmaceutical/biomedical field has been demonstrated by the delivery of bioactive molecular cargoes such as the transcription factors Oct4, Sox2, and Klf4, which led to the reprograming of human dermal fibroblasts into pluripotent stem cells (2). Large macromolecular cargoes, however, are often unable to reach the cytosolic space of cells due to the inability to cross the plasma membrane. In this sense, the cell's plasma membrane acts as a natural barrier against the translocation of large, hydrophilic macromolecules to their place of action: the cytosol. As a result, direct plasma membrane translocation of macromolecular was the first approach taken toward successful delivery into the cytosolic space. Many methods have been developed to tackle this problem, such as scrape-loading, microinjection, and electroporation (3-6). However, these techniques have limited utility because they target only a very small population of cells. For applications requiring much larger populations of cells, such as drug delivery, a variety of different chemical and biological delivery tools have been developed. These delivery tools include bacterial toxins, virus-like particles (VLPs), cationic lipids, nanoparticles and lipid nanoparticles (LNPs), and liposomes; these tools

allow for the delivery of nucleic acids, proteins, and even well-known small molecule drugs (7-11). Many of these chemical and biological tools, however, suffer from drawbacks, including drastic cytotoxicity, host immunological response, inefficiency both in material used and administration time, and poor cargo delivery efficiency (1). Although these delivery tools are commonly used for several applications, the drawbacks listed above strongly suggest that there remains room for improvement in the cellular delivery field. Cell-penetrating peptides (CPPs) have emerged as an effective chemical means to cytosolic delivery and a possible solution to circumvent many of the issues highlighted above (12).

1.2 Supercharged cell-penetrating peptides as cytosolic delivery tools

1.2.1 History of cell-penetrating peptides

Two independent labs, led by Paul Loewenstein and Carl Pabo, discovered in 1988 that the transactivator of transcription protein of HIV-1 (TAT) was capable of traversing the plasma membrane and retaining activity to activate gene expression once within the cytosol of human cells (13,14). This shared observation of cell permeability of this small, cationic protein spurred curiosity into the mechanism by which this protein is able to cross the plasma membrane. In work that followed, it was found that TAT enters cells by utilizing endocytosis (15). This discovery led to the potential applications of TAT as a cell delivery tool. Lebleu and coworkers sought to determine the exact sequence or domain that was responsible for the transduction of the protein. This group found that TAT was able to penetrate cells due to a protein transduction domain (PTD) made up of a short sequence of predominantly basic residues between positions 48-60 of

the 86-mer (16). It was found that a truncated form of this PTD, NH_3^+-RKKRRQRRR-COO^-, was the minimum sequence required for cell penetration and, thus, the genesis of the first CPP: the TAT peptide.

CPPs are short peptide sequences typically consisting of less than 30 residues. CPPs have been used to deliver bioactive molecules into the cytosolic space of cells. Delivery is performed by either coincubation of the cargo of interest and CPP with cells or by covalent conjugation of the cargo of interest to the peptide by using chemical means or molecular biology (e.g., as a fusion construct with a protein of interest) (16). CPPs are classified into categories based on origin or molecular properties.

Classification based on origin divides CPPs into the following three categories. The first category, to which TAT belongs, consists of peptides originating from proteins, such as penetratin, VP22 and pVEC (17,18). Penetratin, for example, is a 16 amino acid peptide derivative of *Drosophila antennapedia* homeodomain (Antp) (19). Members of the second category are chimeric peptides composed of two units. Chimeric CPPs include transportan (TP), MPG, and pep-1 (20). TP was generated by the fusion of the neuropeptide galanin to the peptide mastoparan from wasp venom (21). The final category includes CPPs derived from synthetic origins. CPPs in this category were identified by structural activity relationship (SAR) studies of well-studied CPPs, such as TAT and penetratin. Members of the synthetic CPP group include the model amphipathic peptide (MAP) MAP-17, GALA, R6W3, and polyarginine peptides. Notable CPPs that do not fall into one of these categories include CADY, Xentry, and PPTG1 (20,22-26).

CPP classification based on molecular properties is divided into the following four categories. The first category consists of cationic peptides. These peptides are cationic at physiological pH owing to an abundance of basic residues (e.g., arginine and lysine). This category is primarily composed of guanidinium-rich peptides, such as TAT and polyarginines. The second category includes amphipathic peptides. Amphipathic molecules have both hydrophobic and hydrophilic spatial arrangements. In addition to the canonical amphipathic CPP penetratin, well-known members of the amphipathic category of CPPs include MAP-17, GALA, and P28 (27-29). Hydrophobic CPPs make up the third category: an emerging class of CPPs exhibiting hydrophobicity are stapled peptides, although these peptides have been the last of categories to gain traction in the literature. Stapled peptides are peptides forced to maintain a given conformation by the incorporation of an often hydrophobic, synthetic chemical moiety (e.g., hydrocarbon) that acts as the "staple". This "staple" maintains a peptides conformation by restricting the rotational degrees of freedom of the peptide itself (30). Interestingly, these stapled peptides seem to penetrate cells independent of residue specificity but, rather, do so as a result of the activity of the hydrophobic staple itself (16). The final CPP category is composed of cyclic peptides. Although originating as products commonly sourced from plants, the advent of recent chemical technologies has granted the ability to generate synthetic cyclic peptides as well. SFTI-1 is an example of a naturally occurring cell permeable cyclic peptide; groups such as Pei and coworkers have sought to advance this class of CPPs by creating synthetic variants that exhibit highly efficient cell penetration (31,32).

Peptide:	Origin:	Sequence:
Protein-derived peptides		
TAT peptide	Tat(48-57)	GRKKRRQRRR
Penetratin	Antennapedia(43-58)	RQIKIWFQNRRMKWKK
pVEC	Cadherin(615-632)	LLIILRRRRIRKQAHAHSK
Chimeric peptides		
Transportan	Galanine/Mastropran	GWTLNSAGYLLGKINLKALAALAKKIL
MPG	HIV-gp41/SV40 T-antigen	GALFLGFLGAAGSTMGAWSQPKKKRKV
Pep-1	HIV-reverse transcriptase/ SV40 T-antigen	KETWWETWWTEWSQPKKKRKV
Synthetic peptides		
MAP	*de novo*	KLALKLALKALKAALKLA
GALA	pH dependent	WEAALAEALAEALAE-HLAEALAEALEALAA
Polyarginine	derived from TAT peptide	R_n n≥6
R6W3	derived from Penetratin	RRWWRRWRR
Cyclic peptides		
STFI-1	*Helianthus annuus*	Cyclic-GR(CTKSIPPIC)FPD
CPP12	derived from TAT peptide	Cyclic(FfΦRrRrQ)
MCoTI-II (MCo)	*Momordica cochinchinensis*	Cyclic-(GGVCPKILKKCRRDSDC-PGACICRGNGYCGSGSD)

Table 1-1 Categorization of CPPs by their origin and corresponding sequences. Lower case letters indicate the use of D-amino acids; Φ indicates the use of the non-natural amino acid L-2-naphthylalanine.

1.2.2 Importance of charge density and guanidinium density in cytosolic penetration of polycationic peptides

While polycationic CPPs universally possess a net positive charge, the total charge and size (in terms of mass) of each CPP varies. David Liu linked these parameters by coining the term "charge density", which is defined as the quotient of the total charge of a molecule divided by the mass in kDa (33). Liu and coworkers went on to find that supercharged molecules, or molecules that possess a charge density of ≥ 0.75, have a propensity to penetrate cells and can even be used as delivery tools for nucleic acids and other functional proteins (33-36). While able to deliver cargo, the cytosolic penetration efficiency of the supercharged variants of superfolder GFP (sfGFP) was very poor. It was then revealed by fluorescence microscopy that the majority of the supercharged fluorescent protein remained trapped in endocytic vesicles. One reason for this lack of activity could be that in supercharging the sfGFP template molecule, the majority of residue substitutions replaced lysine residues as opposed to arginine residues. While the charge density of supercharged GFP(+36) was certainly much higher than that of sfGFP (from -0.2 to 1.3), the change in terms of arginine or guanidinium density was less impressive (from 0.3 to 0.7). Undoubtedly, the enhancement in charge density led to a significant increase in endocytic uptake of the supercharged molecule. However, the ability to penetrate the cytosolic space of cells seems reliant on more than charge density alone.

The importance of arginine residues in the cell penetration activity of CPPs has been corroborated by Mitchell, Wender, and Futaki (37-39). Wender and coworkers performed an alanine scan over the TAT peptide and determined that the mutation of arginine residues, specifically, led to a lower cell penetration activity. At physiological pH, TAT has nine positive charges: six charges come from arginine residues, two charges from lysine residues, and the final charge comes from the N-terminal amine. Wender et al. found that the same activity could be reproduced by hexa-arginine even though it only possessed a net charge of +7 (38). Additionally, increasing arginine content led to even higher penetration activity than TAT itself. Complementary to this work, Rothbard and coworkers found that polyarginine peptides exhibited greater cell penetration activity than polylysine or polyornithine peptides with a similar or the same number of residues (37). Taken together, these results show that cytosolic penetration is not simply dependent on the charge density of a molecule; rather, it is more dependent on guanidinium content. However, cytosolic penetration is more complex than can be explained by this single parameter.

Rothbard et al. went on to show that molecular properties such as side chain length and chirality did not affect cell penetration (37). However, the importance of guanidinium was further underscored whenever Rothbard and coworkers synthesized peptides where arginine was replaced with the isostere citrulline. The newly synthesized peptides thus substituted the guanidino group for a urea group. It was found that heptacitrulline did not lead to cellular internalization, in contrast to heptaarginine, even when cells were incubated with peptide in great excess (at concentrations up to 100 μM).

A notable difference between these two functional groups is their charge. While guanidino groups have a pKa ~ 12, urea groups have a pKa of ~ 0.1 and, as such, do not yield a charged compound. The positive charge of the guanidinium groups on heptaarginine allows for stable hydrogen bond generation between the peptide and phosphate or sulfate moieties on the cell surface. This interaction is uniquely important for cellular internalization and will be discussed further below.

It is important to highlight a significant technical shortcoming in the two studies that are relevant to the work presented here. These findings were based on the use of flow cytometry. Flow cytometry measures the total fluorescence intensity of each event as it passes through the flow cell. However, this measurement does not distinguish where on the cell (inside or outside) the signal originates (e.g., attached to the surface, trapped in vesicles, localized to an organelle or distributed cytosolically) (40). Futaki and coworkers sought to combat this lack of cellular localization by utilizing fluorescence microscopy. Using this technique, they found that several fluorescently labeled arginine-rich peptides were capable of cytosolic penetration (i.e., cytosolic distribution) in RAW264.2 cells (a macrophage cell line). From these studies, the authors expanded on the enhanced activity observed by Wender and Rothbard groups and determined that a minimum of eight arginine residues was required for efficient cytosolic penetration (39). Although suggestive, it is important to note that these experiments were performed after cellular fixation. One artifact of interest results in a false positive for cell penetration when extracellular peptide stains cellular components following membrane permeabilization (40,41). To circumvent this potential artifact, cell penetration of

fluorescent polyarginine peptides was evaluated in live cells via fluorescence microscopy (42,43). In these studies, it was found that cellular penetration of arginine-rich peptides was much higher than that of other polycationic peptides (such as polylysine).

1.2.3 Cytosolic delivery of molecular cargo: in cellulo applications

CPPs have been used to delivery a variety of molecular cargo such as small molecule drugs, peptide-based probes, proteins, liposomes, nanoparticles, and nucleic acids (44). Examples of CPP-mediated delivery of bioactive proteins and nucleic acids will be highlighted below.

Delivery of proteins

Use of CPPs to deliver protein cargos has been accomplished via a conjugation method, through which the cargo of interest (COI) is covalently attached to the CPP, or via simple coincubation of the cargo and CPP with cells (45). Generally, protein cargoes are divided into two groups: reporters, which are probes for delivery itself (further investigated in section 1.5), and functional, bioactive proteins or peptides, which result in a cellular response in some fashion. Shortly after its discovery, Fawell and coworkers showed that TAT could be used to deliver β-galactosidase (β-gal), horseradish peroxidase (HRP), a domain of *Pseudomonas* exotoxin A, and ribonuclease A (RNase A) via direct conjugation (1). They showed that cell delivery appears to be independent of cell type and can be employed in a variety of cell lines, including HeLa cells and primary human keratinocytes. Fawell et al. went on to compare β-gal activity between TAT-mediated delivery and transfection. They observed a drastic difference in the

timescale of activity for each method; TAT-mediated delivery of β-gal resulted in activity on timescales ranging from minutes-to-hours, whereas β-gal activity produced via transfection required a longer timescale (overnight). These results suggested that cytosolic β-gal levels were much higher with the TAT delivery method. However, variability in the expression levels of the plasmids used as well as transfection efficiency could, in part, explain this difference. Furthermore, cell fixation was used to quantify the extent of protein delivery. Taken together, it is not clear from this study that TAT-mediated delivery of β-gal was successful.

In the studies that followed, stronger evidence for TAT-mediated delivery of protein cargos was presented. In 1997, Kim and coworkers described the use of a TAT conjugate as a therapeutic and prophylactic vaccine (46). Upon macrophage infection, proteins or peptides of pathogenic origin can be degraded into peptide fragments that are then presented on the major histocompatibility complex (MHC) classes I and II for T-cell recognition. One caveat of this defense mechanism for MHC class II-deficient cells, however, is that the pathogenic proteins or peptides must reach the cytosolic space of cells, rendering traditional protein-based vaccines useless for invoking an immune response because they cannot cross the plasma membrane. Kim et al. produced a TAT-ovalbumin conjugate as a proof of concept and showed that this conjugate evoked MHC class I responses in T-cells (46).

Transcription factors have also been delivered by CPPs to complement traditional transfection-based means of transient expression. Kim and coworkers produced polyarginine fusion constructs with Oct4, Sox2, Klf4, and c-Myc, all of which

have exhibited induction of pluripotency in stem cells (47,48). Each construct was expressed in HEK293 cells, and cell extracts were used to treat newborn human fibroblasts (HNF). They found that multiple subsequent 16-hr treatments of HNF cells led to a change in HNF morphology consistent with that of induced pluripotent stem cells (iPSC) (47). Additionally, they found expression markers indicative of iPSCs. Taken together, these results paved the way for the use of CPPs in therapeutic applications in which stem cell programming is required (e.g., organ transplants).

One commonality between the successful deliveries presented above is that very little protein must reach the cytosolic space of live cells in order to exhibit a phenotype or activity. While these assays have proven useful in these signal amplification scenarios, the total amount of material delivered remains relatively low. This highlights the need for improvement of these delivery tools to broaden their applications and effectiveness. Factors that contribute to the high sensitivity of these systems and the relative delivery efficiency of these tools in terms of total molecules delivered are discussed in greater detail in section 1.5.

Delivery of nucleic acids

Nucleic acids can also be delivered either as reporters or therapeutic tools. For example, cellular gene delivery can be used to induce dysregulation of disease-associated genes (49). Because of their large size and high level of negative charges, nucleic acids cannot easily traverse the plasma membrane. Many approaches have been employed to deliver nucleic acids as therapeutic tools. In particular, viral vectors have been particularly successful ultimately resulting in integration of DNA cargo into host

genomes. However, viral delivery faces many obstacles such as immunogenicity, cytotoxicity, and the nonscalable production of viral vectors (50). Consequently, an alternative approach for nucleic acid delivery is needed.

RNAi is an effective way to manipulate cells and can be used to screen for druggable targets in an array of different diseases. This technique relies on the cellular internalization of exogenous siRNA which exhibits poor efficiency and high cytotoxicity (51). Initial efforts to employ CPPs for RNAi delivery were unsuccessful. Direct conjugation of siRNA to cationic CPPs led to charge neutralization that inactivated the cell penetration activity of the CPP and drastically limited siRNA delivery (49). In 2009, however, Dowdy and coworkers demonstrated that a TAT fusion construct with a double-stranded (ds) RNA-binding domain (DRBD) could bind siRNA with a high affinity and deliver the siRNA in multiple cell lines (51). Notably, many of these cell lines had previously been deemed difficult to transfect. Additionally, little to no cytotoxicity was observed, and a variety of different siRNAs were successfully delivered.

In addition to RNA, CPPs have been used to deliver oligonucleotides into live cells. Oligonucleotides (ONs) are a class of nucleic acids that have recently garnered interest for therapeutic applications. ONs can be used to form RNA-DNA duplexes which can block RNA recognition, inhibiting gene expression or inducing RNA cleavage through RNase H (52,53). Examples of ON-based (antisense) therapeutic applications include the modification of nuclear splicing genes as well as silencing of endogenous microRNAs (54,55). One highly impactful application of ONs is their

specific ability to block protein translation. Since ONs need not be recognized by endogenous cellular machinery, they can be produced by synthetic means. Synthesis of ONs not only allows for mass production but also chemical modification, which can greatly expand their therapeutic potential.

Peptide nucleic acids (PNAs) are synthetic analogs of ONs that have gained attention due their enhanced ability to inhibit gene expression. PNAs share the same purine and pyrimidine bases as DNA and RNA. However, the backbone of a PNA is different from those of DNA and RNA. Rather than a sugar phosphate backbone linked together by phosphodiester bonds, PNAs consists of a N-(2-aminoethyl)-glycine backbone linked by amide (peptide) bonds. As a result, the backbone of PNAs possesses a net neutral charge as opposed to the net negative charge of DNA and RNA. This characteristic allows PNAs to draw from the best of both worlds: PNAs exhibit strong, sequence-specific base recognition and binding of RNAs while decreasing the charge repulsion associated with a phosphoester backbone. Unfortunately, despite the lack of net charge, PNAs are generally cell impermeable. CPPs have however been employed as a means of cytosolic PNA delivery. The first report of PNA-CPP conjugates was published by Langel et al. in 2004 (56). Langel and coworkers used a 21-base PNA coupled to either Penetratin or transportan and showed that the PNA-CPP conjugates would form a duplex with galanin receptor mRNA, thereby inhibiting expression in Bowes cells. Many subsequent studies followed, in which PNA therapeutics were linked to CPPs such as TAT, polyarginine, and penetratin. Each construct proved, however, incapable of inducing the intended biologic effect at low concentrations. The reason for

this lack of biological activity stemmed from poor cytosolic penetration efficiency of these covalent constructs. In an attempt to improve the cytosolic penetrative activity of these compounds, chloroquine and ionic calcium were also employed to try and drive endosomal escape (57,58). As shown by these examples, endosomal entrapment (explored at greater lengths in section 1.3) remains a major bottleneck for most cell penetrating agents, and much effort has been focused on enhancing cytosolic penetration activity of these delivery tools (see section 1.4).

1.2.4 Cytosolic delivery of molecular cargo: in vivo applications

The use of proteins as biologics *in vivo* has, on the whole, been limited to extracellular targets such as cell surface receptors. As discussed previously, this is substantial because most proteins cannot cross the plasma membrane or gain access to the cytoplasm even if taken into an endocytic compartment. Overcoming these obstacles has been achieved in part by conjugating protein biologics to CPPs. An early example of the *in vivo* application of CPPs towards delivery of protein biologics was demonstrated by the Dowdy group. In 1999, Dowdy and coworkers were able to successfully deliver β-gal to a multitude of different tissues in mice *in vivo* by intraperitoneal (IP) injection of a TAT-β-gal fusion construct (59). Expanding upon this work, many others have adopted this protein biologic conjugation approach with CPPs in order to study and treat diseases such as cancer, diabetes, and ischemia (to be discussed below). These studies highlight the therapeutic potential of CPPs, demonstrating successful passage of a protein therapeutic across both epithelia and the blood-brain barrier (BBB).

The therapeutic potential of TAT has been demonstrated by delivering tumor suppressing proteins. In cancerous cells, the expression of tumor suppressing proteins is dysregulated. The protein p53 is a well-studied tumor suppressor protein arrests growth and induces apoptosis in response to cellular stress-based stimuli (60). In over half of all cancers, the p53 gene is mutated. One potential therapeutic application of CPPs would thus be to restore p53 activity by delivering a nonmutated gene or functional form of the tumor suppressor. In practice, this approach is challenging. Previous attempts to deliver a wildtype copy of the p53 gene have not been successful most likely because of low deliver efficiencies in combination with the host immune response (61). In an alternative approach, a C-terminal truncated form of p53 was derived (p53C'). Upon successful delivery into cancerous cells, the host-cell p53 mutant DNA-binding activity was restored, resulting in normal function of the mutated tumor suppressor (62). It is important to note, however, that the mechanism by which this occurs remains unknown. As with many biologics, cellular internalization of p53C' was still poor. Consequently, in 2004, Dowdy and coworkers introduced a proteolytically stable TAT-p53C' conjugate into a cancerous mouse model and showed that the conjugate induced apoptosis in cancerous cells (63). They further corroborated the previous *in cellulo* findings of Lane et al. by demonstrating that the TAT-p53C' conjugate displayed apoptotic activation that required p53 expression in the target cell. Cancerous or non-cancerous cells lacking p53 (mutant or otherwise) failed to show apoptotic activation upon administration of the conjugate (63). The use of TAT as a therapeutic delivery tool *in vivo* was further validated by similar studies in which the CPP was conjugated to other peptide

therapeutics, such as the MDM2-binding domain of p53 as well as peptides derived from the p16 tumor suppressor (64-66).

An alternative anti-cancer approach involves targeting the serine-threonine kinase casein kinase 2 (CK2). Elevation of cellular CK2 levels leads to increased cell growth and proliferation, and CK2 acts as a potent suppressor of apoptosis. These characteristics highlight the role CK2 plays in cancer (67). The cyclic peptide p15 is a potential peptide therapeutic thought at the time to combat CK2 elevation by inhibiting CK2 phosphorylation (shown *in vitro*) (68). Conjugation of the cyclic peptide to TAT and intratumoral administration of the fusion construct to a TC-1 lung epithelial tumor on a mouse led to a decrease in tumor volume that extended beyond completion of the treatment. These resulted suggested that the conjugate was cell penetrative and exhibited anti-tumor properties.

In addition to anti-cancer therapeutics, other protein therapeutics have been delivered *in vivo* by CPPs. These protein therapeutics include a suppressor of cytokine signaling as well as Bcl-2 family members. These protein therapeutics were used to treat systemic/local inflammation and cerebral ischemia secondary to cerebral infarction, respectively (69,70). This study of *in vivo* delivery of the Bcl-2 family members also demonstrated successful BBB crossing, which was attributed to CPP conjugation. While these results are highly promising, TAT-containing therapeutics have notoriously failed in clinical trials. In fact, there are presently no FDA-approved TAT-containing therapeutics (71,72). Although TAT-containing drugs have frequently entered Phase I and II clinical trials, they have failed, so far, for a variety of reasons.

1.2.5 The limitations and failures of the application of CPPs

To date, the most effective use of CPPs as delivery vectors and therapeutic tools has been with *in cellulo* and *in vivo* applications. While a number of CPPs, such as TAT, have demonstrated their superior ability to be endocytosed into cells, CPPs have failed to escape endocytic vesicles. Endosomal entrapment has been extensively documented by fluorescence microscopy of cells treated with fluorescently labeled CPPs (40,73,74). Thus, endosomal escape is the primary limiting factor for the effective use of CPPs for many applications. However, the underlying mechanisms that govern escape remain opaque. Another limitation of CPPs, both *in cellulo* and *in vivo*, is their susceptibility to proteolytic degradation. Incorporation of unnatural amino acids or *D*-amino acids can improve proteolytic stability of CPPs. This approach has proven successful in some *in vivo* applications (as is the case with p53C' *in vivo* studies).

Another notable limitation of CPPs stems from conjugation to fluorophores. In early studies, CPPs were (and still are) often labeled with fluorophores to monitor cell penetration. Two major drawbacks come with the addition of a fluorescent label to CPPs. First, the fluorescent moiety affects (even improves) the cell penetrative activity of CPPs (75). For some applications, this enhancement may prove beneficial, but the removal of the fluorophore for downstream "traceless" applications may yield decreased penetrative activities. Second, the prolonged excitation of fluorophores generates radical oxygen species (ROS). ROS oxidize membranes which leads to membrane permeabilization (76). This oxidation leads to the overestimation of cytosolic penetration (as discussed previously), as well as cell death. Improvement of CPPs by implementing

"tracelessness" is a necessity to advance a number of CPP *in cellulo* and *in vivo* applications and is crucial for the implementation of CPP-based therapeutics.

1.3 Proposed mechanisms of cytosolic penetration of TAT and TAT derivatives

While CPPs facilitate delivery into the cytosolic space of cells, the mechanisms of cellular internalization remain unclear. Two major routes of cellular internalization have emerged for CPPs. The first route, direct plasma membrane translocation, is an energy-independent route where the CPPs will translocate across the plasma membrane of the cell. The second route is energy-dependent and employs the endocytic pathway. The major route of cellular internalization is influenced by a number of factors. These factors include the peptide sequence, concentration, target cell type, target cell differentiation state, and the nature and size of the cargo/detection fluorophore (77-84). Notably, most CPPs undergo both routes of cellular internalization (85). These topics will be discussed in greater detail below.

1.3.1 Direct plasma membrane translocation

CPPs can traverse the plasma membrane of a cell through an energy independent mechanism known as direct plasma membrane translocation. This mode of cellular internalization was first observed by fluorescence microscopy over live cells incubated at 4°C (39,86). At this temperature the cells reach an energy depletion state and endocytosis is greatly decreased. Under these conditions, cellular uptake and internalization were not inhibited for TAT. This suggests that TAT can adopt an endocytosis-independent cellular internalization route. Three models have been proposed

to explain the mechanism behind direct plasma membrane translocation. These include the inverted micelle, carpet, and barrel stave or toroidal pore models (87).

Antp is a 16 amino acid amphipathic CPP that interacts with the plasma membrane of cells to form inverted micelles and translocate into the cytosol (88). Following this observation, Daniele Derossi and coworkers proposed the inverted micelle model. First, a CPP interacts with the plasma membrane of the cell. Upon interaction, membrane disruption occurs, and the peptide is encapsulated within an inverted micelle within the lipid bilayer. Further CPP-induced disruption results in micelle dissociation and deposition of the CPP within the cytosolic space of a cell. However, these studies do not fully clarify this route of cellular internalization for much larger cell permeable agents (e.g., CPP-protein conjugates). Size limitations dictate the improbability of micelle encapsulation and, by proxy, cellular internalization through this route.

The carpet model, also known as the membrane-thinning model, was proposed to explain the major membrane destabilization that occurs in the presence of high concentrations of CPP. First, the CPP will bind and “carpet”, or saturate, the membrane. This saturated state induces a change in the secondary structure of the CPP, which allows for non-polar residues to interact with the hydrophobic fatty acid tails of the membrane. This results in a transient disruption allowing for translocation into the cytosol. This multibodied event can be envisioned as membrane thinning, as the transient disruptions that occur *en masse* allow for the insertion and intercalation of the CPPs within the membrane itself. This model relies on CPPs being enriched in

hydrophobic residues and has been demonstrated with peptides such as melittin and alamethicin (89). However, this route of cellular internalization is less likely for CPPs such as TAT that are not rich in hydrophobic residues.

Finally, CPP-induced pore formed inside the plasma membrane leads to direct membrane translocation. The barrel stave and toroidal pore models have been proposed to explain this phenomenon. In these models, the peptide first interacts with and inserts into the membrane followed by oligomerization to form a pore (87,90). The barrel stave and toroidal pore models differ in how the peptide interacts with the lipid bilayer. The barrel stave model involves interaction of hydrophobic residues of CPPs with the fatty acids of the plasma membrane. This interaction leads to a ring-shape, or "barrel", structured by the hydrophilic residues. In the toroidal pore model, however, the peptide interacts exclusively with the phospholipid head, typically through electrostatic interactions. These interactions disrupt the plasma membrane leading to the characteristic toroidal pore. The pores formed in each mechanism act as a gateway for extracellular cargo and other CPP molecules to enter the cytosolic space of the cell.

Each of the models presented can be used to explain the cellular internalization mechanisms of CPPs such as short, amphipathic peptides. Notably, plasma membrane perturbation exhibits intrinsic cytotoxicity which is unfavorable for live cell applications. Additionally, this form of cellular internalization is unfavorable for the translocation of much larger molecules. This suggests that a different route of cellular internalization is likely adopted by hydrophilic CPPs.

1.3.2 Endocytosis-mediated translocation

Uncertainties stem from many sources; in earlier studies, uncertainties stemmed from the techniques used to visualize cellular internalization of CPPs. These early studies utilized cellular fixation which was problematic since a) crucial initial steps in the mechanism were overlooked (e.g., interaction with receptors at the cell surface) (38,40,41,91).

Early studies (utilizing cell fixation) suggested that cellular of internalization of TAT was through endocytosis. However, progress towards understanding this process was initially limited as crucial steps in the mechanism were overlooked (e.g., interaction with receptors at the cell surface) (38,40,41,91). Endocytosis is a naturally occurring process by which cells uptake biomolecules and required nutrients but also undesirable molecules, such as toxins (85,92-94). Endocytosis falls under two categories: phagocytosis (cell eating) and pinocytosis (cell drinking). Typically undergone by macrophages, phagocytosis is the engulfment of cell debris, bacteria, and other large particles (95). Pinocytosis involves the regulated uptake of smaller particles and is split into two categories: receptor-mediated endocytosis (e.g., clathrin- or caveolae-mediated endocytosis) and micropinocytosis (92,96). Endocytosis-mediated cell penetration begins with CPP interaction with the cell surface. CPPs are then internalized through endocytic uptake but remain trapped within endosomes. Finally, endosomal escape must occur for CPPs to translocate into the cytosolic space. Each of these processes will be investigated in more detail below.

1.3.3 Interaction with components on the cell surface

Basic residues of hydrophilic CPPs form H-bonds with anionic groups present on the cell surface, such as phosphates, sulfates, and carboxylates (97-99). These anionic moieties are presented on the surface of the cell by proteoglycans. Examples include the transmembrane syndecans as well as the lipid-linked glypicans (100). Sulfates and occasionally carboxylates can also be found as substituents to linear glycosaminoglycans (GAGs) (101). Heparin sulfate proteoglycan (HSPG) in particular has proven crucial to the uptake of arginine-rich CPPs (102-105). Isothermal calorimetry (ITC) experiments demonstrated the high affinity of TAT towards heparin sulfate, revealed the multiple TAT-binding sites of HSPG, as well as the nature of these binding events (106). Seelig and coworkers also showed that these binding events are predominantly driven by electrostatic interactions and, to a lesser extent, hydrogen bonding. Dynamic light scattering (DLS) was used to show that HSPG clusters form upon interaction with guanidinium groups. Additionally, when TAT was unable to interact with HSPG on the cell surface (i.e., pretreatment with heparin, HSPG degradation, or downregulation) endocytic uptake and cell penetration efficiency decreased (103,107). Taken together, these experiments suggest that TAT interacts with HSPG on the cell surface. In subsequent studies, it was shown that HSPG and proteoglycans induce F-actin organization and macropinocytosis (102,108). HSPG and bound ligand (e.g. TAT) become endocytosed into the lumen of the newly formed vesicle. The process of cytosolic penetration of TAT through endocytosis will be described below.

1.3.4 Cytosolic penetration of TAT is a two-step endocytosis-mediated process

Several studies have suggested TAT and other CPPs hijack a number of pinocytic pathways that involve membrane ruffling (102). Membrane ruffling is defined as, "the formation of motile cell surface protrusions containing a meshwork of newly polymerized actin filaments" (109). To investigate cellular internalization of TAT through endocytosis, cells were forced into an energy-depleted state (through low temperature incubation or ATP depletion). (110). In each case, this led to a decrease in TAT internalization (103,111). Futaki and coworkers showed that endocytosis-mediated cellular internalization is also adopted by other cationic, arginine-rich CPPs as well (112,113). These results suggest the involvement of endocytosis in TAT cell penetration. To investigate the specific route of endocytosis adopted by TAT, molecular inhibitors were used to inhibit individual endocytic pathways. Incubation of cells with inhibitors of micropinocytosis (e.g., cytochalasin D, amiloride, and EIPA) led to a decrease in the cytosolic penetration of TAT and TAT-cargo conjugates (111,114). However, inhibition of endocytosis creates artifacts that alter the normal behavior of a cell (81). To complement these findings, colocalization of TAT with markers of different endocytic routes was performed. TAT colocalized with dextran and FM4-64 (markers of macropinocytosis and general endocytosis) but did not colocalize with transferrin (a marker of clathrin-mediated endocytosis), (85,112-114). Coincubation with TAT and TAT-conjugated to dextran markers exhibited a dose-dependent response, which suggested an increase in endocytic uptake via macropinocytosis (111,114). Based on these results, macropinocytosis is recognized as the major route of cellular

internalization adopted by TAT. Notably, other reports also suggest that clathrin- and caveolae-mediated endocytosis may also be involved to a lesser extent (85,103,115,116).

Macropinocytosis is a membrane ruffling event often stimulated by growth that involves the maturation of endocytic organelles through the endocytic pathway (92). This process occurs when the distal edges of the membrane ruffle begin to encapsulate the local extracellular fluid (as well as nutrients, cargos, etc.). The fully formed macropinosome results from the constriction and pinching inward of the membrane ruffles into a fully formed vesicle whose lumenal environment matches that of the extracellular material. As membrane ruffling is an essential process for macropinosome formation, actin restructuring can be monitored to determine the involvement of macropinocytosis in CPP internalization. Treatment of cells with R8 induced rearrangement of F-actin in a way that is comparable to treatment by epidermal growth factor (a known inducer of F-actin rearrangement) (113). Furthermore, incubation of cells with cytochalasin D, a drug that induces F-actin depolymerization, results in decrease of CPP uptake. Finally, the size of the molecular cargo influences the route of internalization. Macropinosomes range from 0.2-10 μm in diameter, allowing them to encapsulate much larger cargo (117). However, clathrin- and caveolae-dependent endocytosis bud into smaller vesicles averaging 50 and 100 nm in diameter, respectively (118,119). Based on these dimensional constraints, larger cargos such as high-mass dextrans are restricted to internalization through macropinocytosis.

The second step of endocytosis-mediated cell penetration is endosomal escape of CPPs and accompanying cargo. The endocytic pathway is a dynamic and complex

endocytic organelle maturation process. Notably, the process involves lumenal acidification, sorting and fusion events, membrane compositional changes, and the acquisition of lumenal degradative enzymes (120). First, budded vesicles containing the arginine-rich CPP merge with early endosomes via homotypic fusion (121). This endocytic organelle is characterized by cisternal regions of thin tubular-like structures that extend up to 60 nm as well as a central vesicle (ranging from 300-400 nm) that encapsulates interlumenal vesicles (ILVs) (122). Early endosomes (EEs) possess mosaic membranes with definitive segregation of phospholipids and proteins maintained by molecular machines which allow for the formation of functionalized domains. These domains not only act as docking and fusion points for other vesicles but are also involved in other cellular processes such as the intracellular trafficking of the EE. Trafficking of endocytic organelles along actin cytoskeletal structures is regulated by small Rab GTPases (123). Over 60 unique members of the Rab family are associated with different cellular membranes. Rab proteins interact with membranes through a geranylgeranyl functionalization conjugated to the C-terminus of the small proteins an exhibit specificity towards different target membranes. Rab5 is an early endosomal marker and plays a regulatory role in the maturation of the endocytic organelle. The maturation of EEs into multi-vesicular bodies (MVBs) is a process whereby the vesicular component of the EE detaches from the rest of the organelle. The newly formed MVBs, ranging from 400-500 nm in diameter, act as the intermediary organelle between EEs and late endosomes (LEs) (121). These endocytic organelles have proven

difficult to isolate and study, thus, knowledge about the membrane composition (i.e., lipid profile and protein content) remains unclear.

Late endosomes (LEs) are acidic organelles (lumenal pH = 5.5) that vary in diameter and morphology but possess both a tubular and a multivesicular region. Proteins that associate with late endosomes include Rab7 and lysosomal-associated membrane protein-1 (LAMP1) (124). The lipid profile of late endosomes is highly enriched with the negatively charged phospholipid bis(monoacylglycero)phosphate (BMP) (125,126). In particular, the ILVs and inner leaflet of LEs exhibit very high BMP content. TAT binds to this anionic phospholipid with very high affinity (127). Furthermore, TAT exhibits membrane lytic activity *in vitro* towards BMP-containing liposomes. BMP and cell penetration involving the anionic phospholipid will be discussed in more detail in section 1.6. The final step in the endocytic pathway is fusion of LEs with lysosomes. Lysosomes are highly acidic organelles that play a large role in the hydrolytic degradation of proteins, nucleic acids, carbohydrates, and other biological molecules (128,129). Endosomal escape of TAT and accompanying cargo must occur upstream of the lysosome. Upon reaching the lysosome, TAT would lose cell-penetrative activity upon degradation. Furthermore, release of the lumenal contents of the lysosome, such as ionic calcium, would lead to cell death (130). The process of endosomal escape will be discussed below.

1.3.5 Endosomal escape: the final frontier

Endosomal escape is a crucial step for the COI to reach the cytosolic space of cells. However, it is estimated that TAT escapes endosomes in <1% of cells (131). While

this level of endosomal escape is sufficient for some applications, this poor efficiency limits the utility of TAT as a delivery tool. Fluorescence and mass spectrometry-based experiments have been conducted to demonstrate the presence and extent of endosomal entrapment of CPPs (132-136). One example includes a TAT-ubiquitin fusion construct (136). Upon reaching the cytosol, deubiquitanase would cleave the ubiquitin cargo liberating TAT. However, even though the fusion construct was endocytosed, the presence of liberated TAT was undetected. This suggests that the majority of the construct never reached the cytosolic space.

In addition to limiting application, poor endosomal escape activity of TAT has limited progress towards elucidation of the mechanism of endosomal escape. Despite difficulties, efforts have been made to isolate which endocytic organelle(s) are involved in endosomal escape. Appelbaum and coworkers found that TAT colocalizes with Rab5 and Rab7, markers of EEs and LEs, respectively (133). The dominant-negative variant of Rab5 ($Rab5^{Q79L}$; DN-Rab5) arrests procession of the endocytic pathway downstream of EEs. Cells expressing DN-Rab decreased the endosomal escape of TAT into the cytosolic space. In our lab, we corroborated these results with a dimeric, fluorescent variant of TAT, dfTAT, using another DN-Rab5, $Rab5^{S34N}$ (137,138). We expanded upon this finding by using a dominant-negative form of Rab7 (Rab7T22N; DN-Rab7), which disrupts trafficking to late endosomes. Again, we saw that dfTAT penetration of cells was dramatically reduced. Taken together, these results suggest the involvement of late endosomes or lysosomes in endosomal escape. This is corroborated by the high affinity of TAT towards BMP (found only in LEs and lysosomes). While the mechanism

of endosomal escape remains largely unanswered, a number of approaches have been taken to enhance cytosolic penetration activity. These approaches will be investigated in the following section.

1.4 Approaches towards the enhancement of cytosolic penetration activity

Many approaches have been taken to enhance the endosomal escape property of CPPs. Examples of these approaches include lysomotropic agents, pH-dependent membrane-active peptides (PMAPs), endosomal escape domains (EEDs), photochemical internalization (PCI), and multivalency (139-141). Lysomotropic agents are small molecules that ultimately localize inside of lysosomes. The prototypical lysomotropic agent is chloroquine, a base that accumulates in acidic organelles (e.g., late endosomes and lysosomes) upon protonation. At high concentrations, chloroquine causes endosomal swelling by an accumulation of anions (142,143). Chloroquine-enhanced cytosolic penetration has been observed for both TAT-Cre and TAT-PNA (114,144,145). However, pursuits of enhancing cytosolic penetration activity via chloroquine and other lysomotropic agents has been stifled by intrinsic cytotoxicity associated with the small molecules. Additionally, HA2-TAT conjugated cargo can remain tethered to endosomes even after membrane perturbation.

PMAP-CPP fusion constructs have been implemented as a means to enhance cytosolic penetration. Upon protonation in the endocytic pathway, PMAPs undergo a conformational change that causes the PMAP to insert into the limiting endosomal membrane (146). As this process is driven by the acidification of the endosomal lumen, the plasma membrane is left unperturbed (147). One example of a PMAP exhibiting this

behavior is the hemagglutinin-derived peptide HA2. The first instance of the use of HA2 to enhance cytosolic penetration was used in conjunction with TAT-Cre (114). Although TAT-Cre delivery will be discussed in more detail in the following section, cytosolic deliver of the conjugate is determined by the induced expression of EGFP. Another example of enhanced cytosolic penetration by HA2 conjugation was demonstrated by conjugation to p53-R11 (148). Notably, simple coincubation of cargo with a TAT-HA2 construct (no conjugation required) allowed for successful delivery (140). This is of interest because conjugation to the COI may affect its activity. Unfortunately, PMAPs are inherently cytotoxic, so they prove to be an unfavorable solution for enhancing endosomal escape.

EEDs are short, hydrophobic peptides that, when fused to arginine-rich CPPs, enhance endosomal escape efficiency. Implementing the split GFP system (a delivery detection system to be discussed in the following section), Dowdy and coworkers demonstrated how EEDs can enhance cargo delivery (141). They showed that creating a fusion construct of TAT-β11-EED (EED sequence: GFWFG) led to increased cargo delivery as opposed to TAT-β11 alone. Although this seems to be a promising approach, the mechanism of action of the EED remains unclear. Additionally, β11 provides technical difficulty as the peptide is relatively hydrophobic and, thus, limits applications.

Another approach towards enhancing endocytic escape is through the use of membrane-disrupting photosensitizers. Ferrer and coworkers demonstrated how endosomally entrapped fluorescein and Alexa-Fluor 633 labeled-CPPs were able to be released into the cytosolic space by irradiation with λ=488 nm or 633 nm, respectively

(149). This process was defined as CPP-mediated photochemical internalization (PCI). Use of a FITC-R11-p53 variant also demonstrated the use of PCI as a means to enhance the delivery of bioactive cargo as well (150). In our lab, we not only investigated the use of PCI as a means of enhancing endosomal escape but have also corroborated and identified key negative effects associated with the technique. We found that irradiation of TAT labeled with the fluorophore tetramethylrhodamine yielded singlet oxygen, a reactive oxygen species (ROS) that is highly membrane lytic (151). Intriguingly, TMR-labeled K9, which accumulates in endosomes as well, was unable to escape endosomes upon irradiation (152). These results suggest that synergy exists, in which PCI only acts as an enhancer to cell penetration as opposed to independently causing cell penetration. The downside to utilizing PCI is, as with many of the previously discussed approaches, inherent cytotoxicity results from the permeabilization of not only endosomal membranes but also the plasma membrane (153).

1.4.1 Enhancing endosomal escape efficiency through multivalency

For this work, multivalency is defined as the conjugation of multiple copies of a functional moiety (TAT, or a CPP) together to create a single molecule. Inspiration for multivalency comes from biological examples such as viral and bacterial adherence to the surface components of a host cell as well as the human immune response (154,155). Multivalent CPPs can interact with a multivalent receptor or even multiple monovalent, or single-copy, receptors (156). Multivalency imparts an enhanced avidity associated with multivalent compounds. The avidity effect is the increase in local concentration of a molecule or particular moiety as a result of the restriction in spatial freedom of said

moieties (157). Employing multivalent systems is an appealing approach toward enhancing the endosomal escape efficiency of arginine rich CPPs.

1.4.2 Established multivalent CPP systems

Several approaches have been utilized towards generating multivalent CPPs (mCPPs) have been generated through several methods. These methods include complexation, oligomerization/aggregation, as well as other coupling mechanisms. Torchillin and colleagues generated a multivalent system through complexation where over 100 TAT copies were applied to a liposome whose phosphatidylethanolamine component was functionalized by p-nitrophenylcarbonyl-PEG (158). The resulting TAT complexation was used as a delivery vector for DNA transfection in multiple cell lines (159,160). Alternatively, superparamagnetic nanoparticles (NPs) have also served as a complexation scaffold to develop multivalent CPP systems (161,162). As with their liposomal progenitors, these mCPP-NP systems displayed a dose-dependent enhancement in cytosolic penetration respective to the number of TAT copies conjugated and have shown application potential in multiple cell lines (163,164).

Some COIs serve as scaffolds in the mCPP systems (157). These cargos are able to oligomerize or aggregate. One example of this mCPP can be exploits the tetramerization domain of p53 (165,166). First, SPPS was used to generate a fusion construct between TAT, decaarginine, or decalysine with the tetramerization domain of p53 (p53tet, residues 325-355) (167,168). Following tetramerization, the mCPP exhibited a 10-to-100-fold enhancement in cell penetration activity over their monomeric, non-multimerizing subunit counterparts. The mCPPs also demonstrated an

enhanced ability to delivery DNA cargo; in particular, 10R-p53tet showed promise as the most efficient of the mCPPs. Additional mCPP systems in this category include the fusion of Antp or TAT with the SH2 domain of Grb10 or the BH4 domain of Bcl-XL (169,170). In practice, and as a result of β-strand driven aggregation, these domains are predicted to form aggregates in solution.

Another approach towards multimerization is through branching. One example of a branching system includes the use of a functionalized dendritic scaffold, onto which multiple copies of CPPs can be conjugated (171-175). A loligomer is a "squid-like" dendritic construct that has been used to form mCPPs (176-179). One example of a loligomer is a branched polylysine scaffold that allows for conjugation of CPPs to form an octomeric mCPP. These constructs have been successfully employed as cytosolic delivery vectors for DNA (178). Another example of loligomer-based delivery is of an antigenic epitope into T-cells which triggered a cytotoxic response (179). An alternative branching system, and a form of the approach taken in my studies, is the use of a peptide-based linear scaffold to conjugate CPPs. In previous studies from our lab, we demonstrated the use of this branching system. A TAT peptide with a C-terminal thioester functionalization was conjugated to the thiol of a (Lys(ε-NH-Cys)Gly)n (where n = the number of copies of CPP subunit) scaffold by means of native chemical ligation (NCL) (180,181). Additionally, dimeric CPPs have been generated by exploiting the ability of cysteine-containing CPPs to form disulfide bonds (137,182,183). A model dimeric CPP generated in our lab, dfTAT, has shown promise. The mCPP dfTAT demonstrates an unprecedented enhancement of endosomal escape with little-to-no

repercussions commonly associated with this enhancement (e.g., cytotoxicity, transcript up- and downregulation, etc.) (137).

1.4.3 Limitations and challenges of the multivalent approach

Multivalent systems are inherently more complex to synthesize than their monomeric subunits. This difficulty is often realized in the form of low yields, structural and chemical restrictions on the mCPP formed, and a lack of purity/homogeneity of the fully synthesized probe (180). With respect to transitioning to *in vivo* systems, mCPPs face the challenge of immunogenicity, as they can often display structural similarities to multiple antigenic peptides (MAPs) (184). MAPs, such as PAMAM, are synthetic dendrimeric peptides that present multiple copies of antigenic peptides for enhanced T-cell recognition and are often used as diagnostic reagents. As such, one could expect that the mCPPs would face a shorter lifetime extracellularly than their monomeric counterparts. Finally, cellular internalization mechanisms of mCPPs could be altered from that of their progenitor monomeric substituents. New mCPPs must be evaluated to determine if they retain the same major route of internalization or if this has changed by proxy of the multivalency (e.g., an endocytosis-mediated monomeric CPP switching to direct membrane translocation upon multivalent display).

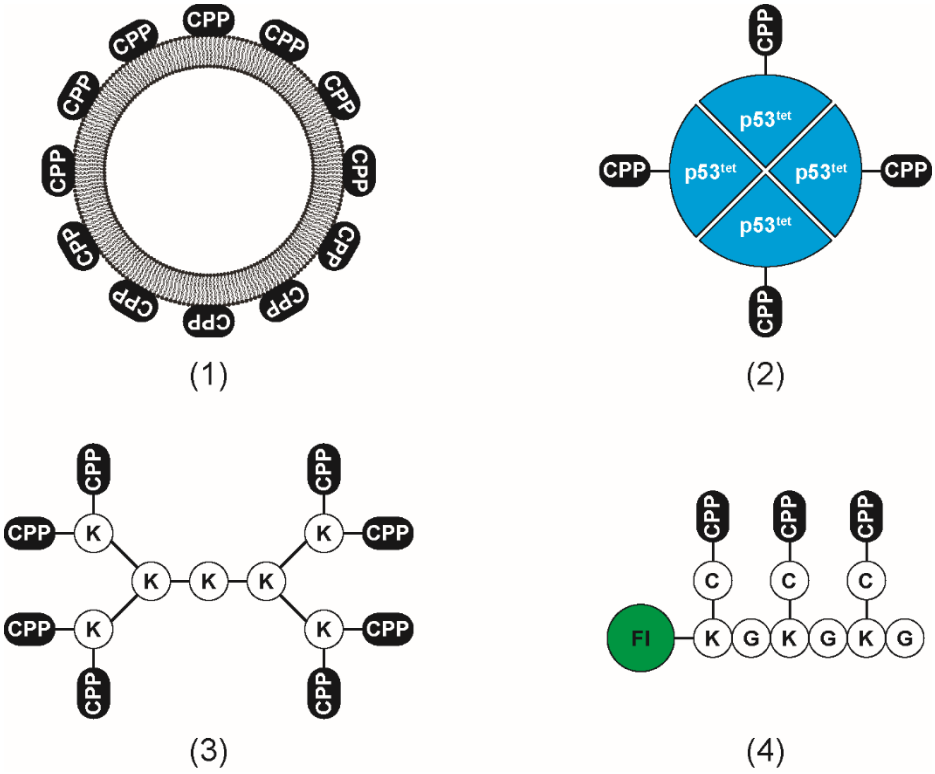

Figure 1-1 Strategies used to generate mCPPs.
(1) A liposomal-mCPP assembly was generated by first synthesizing CPP-conjugated phospholipids. Phosphatidylethanolamine was modified via a p-nitrophenylcarbonyl-PEGylation to form PE-pNP. Following this modification, the CPP was conjugated to individual PE-pNP subunits and liposomes, modified with >100 CPP copies were generated. (2) The $p53^{tet}$-mCPP assembly involves conjugation of the tetramerization domain of the human tumor repressor protein p53 ($p53^{tet}$) to a CPP. The monomeric peptide fusion constructs were synthesized via SPPS. Spontaneous self-assembly of the monomeric units yielded the $p53^{tet}$-mCPP tetramer. (3) Loligomers are a dendrimeric mCPP assembly. Multiple copies of a CPP are attached to the ε-NH branches of a polylysine scaffold. The scaffold and the peptide are synthesized through SPPS. CPP valency is dictated by the number of conjugation steps of lysine branches (CPP valency = 2^n where *n* is the number of lysine conjugations). (4) One example of a branched CPP assembly involves the synthesis of a peptide scaffold composed of Lys(ε-NH-Cys)Gly repeats to which a thioesterified CPP is conjugated via native chemical ligation (NCL). Each component was synthesized through SPPS. A fluorophore was conjugated to the N-terminal amine of the scaffold peptide to serve as a fluorescent reporter as well as a small molecular cargo.

1.4.4 What is dfTAT and how does dfTAT-mediated delivery work?

*Structure and activity of dfTAT**

dfTAT is composed of two copies of the prototypical TAT peptide derived from the protein HIV-1 transactivator of transcription (13,14,137,185). Both copies are conjugated to the fluorophore tetramethylrhodamine and are connected by a disulfide bond. When incubated with cells at concentrations of 5 μM or higher, dfTAT displays a cytosolic distribution, while its monomeric counterpart remains entrapped in endosomes. As shown in Figure 1-2, dfTAT can be coincubated with a variety of cargos to promote their endocytic uptake. As dfTAT and cargo traffic into the endocytic pathway, the endosomolytic peptide mediates the permeabilization of endosomal membranes, thereby releasing the cargo into the cell.

Conditions where dfTAT successfully penetrates live cells

Using the simple coincubation method, dfTAT has been successful at delivering cargos that are diverse in size, chemical properties, and function. These cargos include transcription factors, antibodies, and metal–organic framework (MOF) nanoparticles, as shown in Figure 1-2 (137,186). Given their well-defined sizes (50–100 nm in diameter), successful MOF nanoparticle delivery indicates that dfTAT-mediated endosomal leakage involves membrane disruptions that are wide enough to accommodate large cargos. Moreover, the ability to introduce dfTAT and the cargo as separate entities

---

*This section was reprinted with permission from Allen, J. K., Brock, D. J., Kondow-McConaghy, H. M., and Pellois, J.-P. (2018) Efficient Delivery of Macromolecules into Human Cells by Improving the Endosomal Escape Activity of Cell-Penetrating Peptides: Lessons Learned from dfTAT and its Analogs. *Biomolecules* **8**, E50.

enables the controlled titration of material into cells through the modulation of cargo concentration independent of dfTAT. This can be exceedingly difficult to achieve using other methods where the cargo must be covalently fused to the penetrating agent. One example of dfTAT's versatility was the delivery of the transcription factor HOXB4 (homeobox B4) into cells. To evaluate the dfTAT-mediated delivery of HOXB4, a HOXB4-inducible promoter was used to regulate the expression of luciferase in cells. In the absence of dfTAT, luciferase expression remained completely suppressed. However, with dfTAT, varying levels of luciferase expression could be controlled based on the amount of HOXB4 titrated into the incubation mixture (137).

Conditions where dfTAT fails to penetrate live cells

The polycationic nature of dfTAT is critical for its function (Figure 1-2). As described below, electrostatic interactions are important for cell penetration. However, these interactions can be abrogated if the charge of the peptide is screened in any way. For example, electrostatic interactions of dfTAT with negatively charged cargos (such as DNA) can cause aggregation, inhibiting the ability for dfTAT to induce endocytosis and endosomal leakage. This is also a consideration when delivery is performed in the presence of fetal bovine serum (FBS), which is a common supplement that is added to cell culture media. This is because FBS is rich in negatively charged albumin. Due to the binding of dfTAT to albumin, the introduction of FBS to the incubation medium reduces the activity of dfTAT in a manner that is proportional to the levels of FBS added (137).

Characteristics of the delivery process

The penetration of dfTAT, as observed by fluorescence microscopy, appears to be a binary event (Figure 1-2). In particular, after peptide incubation, two distinct cell populations can be observed: one with a diffuse fluorescence signal (with cytosolic and nucleolar staining, establishing that the signal is intracellular), and one with a punctate distribution, which is indicative of endosomal entrapment. The cells with a diffuse signal typically show very few puncta, and the cells with puncta show no diffuse fluorescence. At low concentrations of dfTAT, almost all of the cells show puncta only. As peptide concentration is increased, this population shifts towards cells of diffuse fluorescence, until cell penetration is achieved in close to 100% of the cells. Overall, this indicates that for any given cell, dfTAT penetration is either achieved efficiently, or not at all. This is in contrast to a situation where a uniform level of translocation would be achieved over the entire population. In this case, the concentration of peptide that is added controls how much gets in. Overall, these results instead indicate that the peptide activity is dependent on a concentration threshold (137,138). This threshold may itself be dependent on multiple parameters (some of which are described below). Nonetheless, in practice, this means that small variations can have a big impact on delivery outcome, as they may shift the threshold of penetration. Conversely, using excess peptide concentrations well above the threshold required for successful penetration can alleviate this issue.

The process of dfTAT-mediated delivery necessitates a minimum incubation period. dfTAT must be first taken up into the endocytic pathway. The peptide must then

traffic to the organelles that constitute the specific site of membrane leakage (i.e., late endosomes, see Section 2). Using pulse-chase experiments, it was established that this process requires 10 to 45 min (137). Based on these results, our typical protocol involves a 60-min incubation. Remarkably, this protocol does not lead to toxicity, it does not affect cell proliferation rates, and it does not impact the transcriptome (137). This means that efficient delivery can be performed without inducing dramatic disturbances in the cell.

For successful delivery to occur, dfTAT does not need to interact with its cargo. Instead, dfTAT and cargo simply need to traffic together within the endocytic pathway of a cell. In turn, this means that the delivery process must also be carried out by pre-incubation of the cargo first, and by adding dfTAT second. If the two incubation steps are performed immediately one after the other, dfTAT will "catch up" to the cargo within the endocytic pathway, and cell penetration of both peptide and cargo will be achieved. This can be particularly beneficial when attempting to deliver cargos prone to aggregation, as the peptide does not come into contact with the cargo until it reaches the same endocytic organelles as the pre-incubated cargo. In some cases, this two-step incubation process may therefore result in higher delivery efficiencies than a coincubation protocol. However, it should be noted that if time is allowed to pass between the two incubation steps, dfTAT will penetrate cells, but delivery of cargo will fail. This is because the cargo may reach lysosomes before dfTAT may have a chance to cause endosomal leakage.

In most of our experiments, dfTAT and cargo coincubation leads to a pulse delivery of cargo into cells. This means that a high concentration of cargo may enter cells during a typical 60-min coincubation. However, the cargo, which is now subjected to intracellular degradation, may soon vanish, depending on its intrinsic half-life. However, for many applications, a sustained cargo activity may be desirable (this is what is typically expected in DNA transfection experiment where gene products are continually produced by the cell). Notably, due to the low toxicity of dfTAT, it is also possible to repeat several dfTAT deliveries on the same cell population within a short time frame (137). We have not established whether there is a limit to the number of delivery steps that can be performed on cells before toxicity arises. It is also unclear whether cells can sustain endosomal leakage for a prolonged period of time: cells may be able to sustain a burst of endosomal membrane leakage but also may die if membranes are kept permanently permeable.

A limitation of using the endosomal pathway as a route of cell entry is related to degradation. Endosomes contain various hydrolases, and both dfTAT and cargo can be subjected to degradation while transiting within the lumen of these organelles. The degradation of dfTAT by endosomal proteases can significantly impact the membrane-leakage activity of the peptide, thereby diminishing delivery efficiencies (187). Degradation of the cargo may vary as it is presumably cargo-dependent. In principle, unfolded peptides or proteins are more prone to degradation than their folded counterparts, and this should be a consideration when delivering such cargos into cells (188-190).

Figure 1-2 Macromolecular delivery by the endosomolytic cell-penetrating peptide (CPP) dfTAT in cell cultures.
dfTAT mediates cell penetration of various macromolecules by permeabilizing endosomal membranes efficiently. The stepwise process of cell entry—endocytic uptake followed by endosomal escape—is highlighted. Examples of cargos that have been successfully delivered are provided. Red boxes point to the limitations that are associated with this approach. Experimental evidence of the high efficiency of the delivery process is also shown in the form of microscopy images for two fluorescent cargos: the cell-impermeable small molecule SNAP-Surface 488 (which is delivered into cells expressing the nuclear tag SNAP-H2B), and the coumarin-labeled, nucleoli-staining peptide DEAC-k5. pI: isoelectric point; FBS: fetal bovine serum. The figure is used with permission (191).

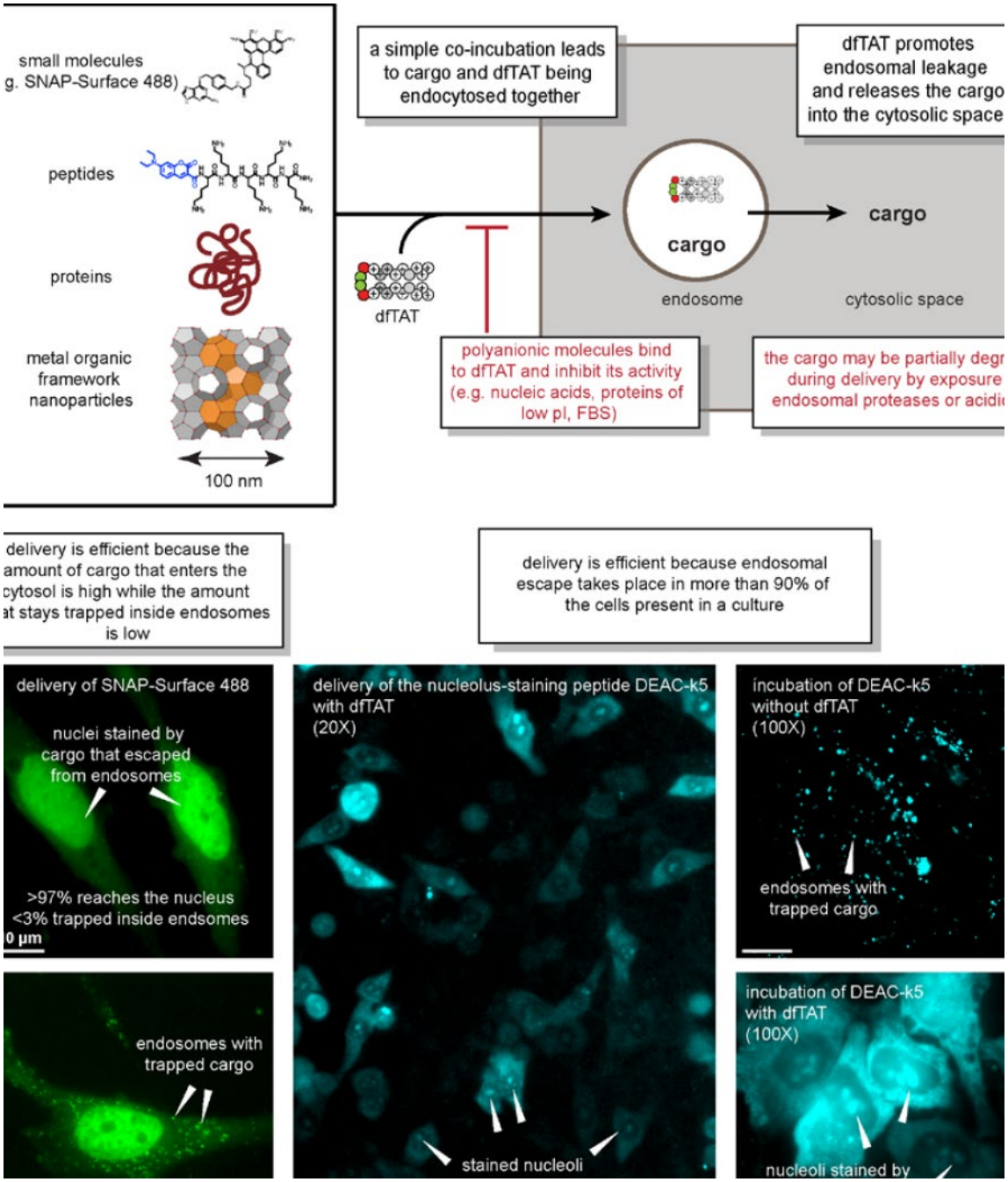
small molecules
g. SNAP-Surface 488)
peptides
proteins
metal organic
framework
nanoparticles
100 nm
a simple co-incubation leads to cargo and dfTAT being endocytosed together
dfTAT promotes endosomal leakage and releases the cargo into the cytosolic space
cargo
cargo
endosome
cytosolic space
dfTAT
polyanionic molecules bind to dfTAT and inhibit its activity (e.g. nucleic acids, proteins of low pI, FBS)
the cargo may be partially degr
during delivery by exposure
endosomal proteases or acidi
delivery is efficient because the
amount of cargo that enters the
cytosol is high while the amount
at stays trapped inside endosomes
is low
delivery is efficient because endosomal escape takes place in more than 90% of the cells present in a culture
delivery of SNAP-Surface 488
nuclei stained by
cargo that escaped
from endosomes
>97% reaches the nucleus
<3% trapped inside endsomes
0 µm
endosomes with
trapped cargo
delivery of the nucleolus-staining peptide DEAC-k5
with dfTAT
(20X)
stained nucleoli
incubation of DEAC-k5
without dfTAT
(100X)
endosomes with
trapped cargo
incubation of DEAC-k5
with dfTAT
(100X)
nucleoli stained by

1.5 Methods to quantify the cytosolic delivery of molecular cargo*

With the emergence of highly efficient delivery tools like dfTAT, the need for standardized, quantification techniques for cytosolic delivery has become more apparent. However, the issue of endosomal escape efficiency is complicated. In particular, it includes several intertwined questions. To what extent do delivery agents and macromolecules escape from endosomes? To what extent does the endocytosed material remain trapped within the endosomal lumen? How many endosomes undergo leakage in a given cell? How does this process vary from cell-to-cell within the same experiment? These questions remain unanswered in many instances. Herein, several reports using a variety of delivery agents have been highlighted that address these questions quantitatively.

---

*This section was reprinted with permission from Brock, D. J., Kondow-McConaghy, H. M., Hager, E. C., and Pellois, J.-P. (2019) Endosomal Escape and Cytosolic Penetration of Macromolecules Mediated by Synthetic Delivery Agents. *Bioconjugate Chemistry* **30**, 293-304. Copyright 2018 American Chemical Society.

Figure 1-3 Examples of approaches used to detect the efficiency of cellular delivery and of endosomal escape.
(a) Measuring the efficiency of DNA nuclear delivery by using a DsRed2-H2A reporter. Once endocytosed, a plasmid encoding the histone H2A labeled with the fluorescent protein DsRed2 escapes endosomes, penetrates the cytosol, and translocates into the nucleus. Expression of the delivered plasmid leads to a fluorescent DsRed2 signal sequestered in the nuclei of cells by incorporation of H2A into chromatin. Nuclei are extracted and analyzed by flow cytometry to establish protein expression level. Nuclei of various intensities are then sorted, and their plasmid content is quantified by real-time PCR. This analysis can therefore reveal how many plasmids enter the nucleus of cells for a given transfection reagent and relate delivery efficiency to gene expression outcomes. (b) Measuring the efficiency of enzyme delivery by using Cre recombinase as a model. Cells transfected with a GFP gene under a loxP split promoter are treated with Cre recombinase and a delivery agent. Upon successful delivery of Cre recombinase, the split promoter is recombined allowing downstream expression of GFP. Cells are then scored for delivery based on the presence or absence of cytosolic GFP fluorescence. (c) Quantitative measurement of the concentration of a peptide or protein delivered into the cytosol of cells. Cells are treated with a fluorescently labeled cell-penetrating species. Cells are then washed to remove all traces of fluorescent signal outside cells and imaged by confocal microscopy. A focal volume within the cytoplasmic area of a cell is chosen and fluorescence correlation spectroscopy (FCS) is performed. Autocorrelation analysis is performed, and the y-intercept of the autocorrelative curve generated is used to determine the cytosolic concentration of fluorescent molecules (192). (d) Quantitative determination of how leaky endosomes are upon treatment with a delivery agent. Cells are transfected with a gene encoding a fusion construct of the histone H2B labeled with a SNAP-tag. Cells are then treated with the delivery agent and the cell- impermeable fluorophore SNAP-Surface 488 (SS488). Depending on the efficiency of the delivery agent and of its membrane disruption activity, endocytosed SS488 is either entrapped in the endosome or released in the cytosol of cells. Once in the cytosol, SS488 is sequestered to the nucleus via an irreversible reaction with the SNAP-tag. As a result, the fluorescence of SS488 is either punctate (trapped inside endosomes), or nuclear (bound to SNAP-H2B). More specifically, the nuclear capture depletes the cytosolic signal, thereby revealing more clearly the signal left inside endosomes. In turn, this approach can be used to estimate the efficiency of endosomal leakage, that is, how much signal is in the nucleus versus how much is left trapped inside endosomes. The figure is used with permission (193).

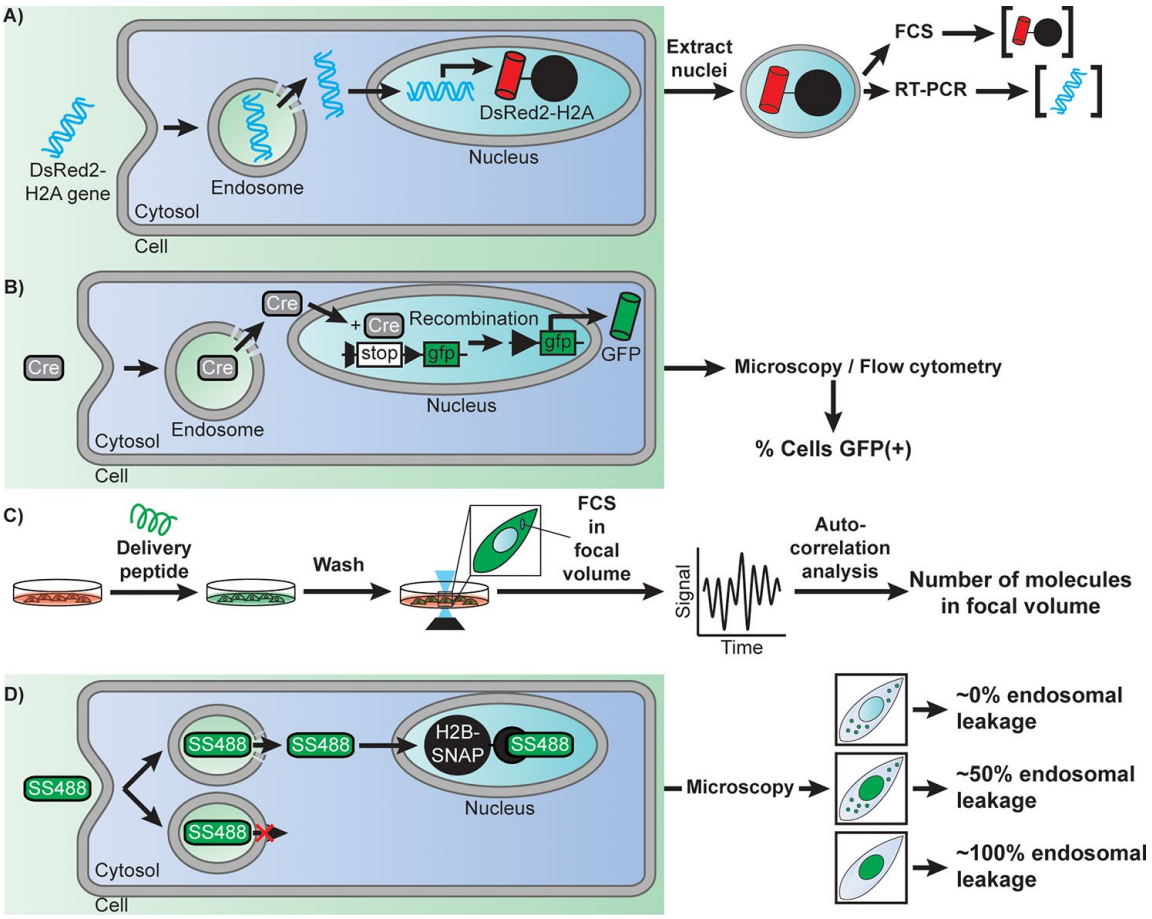
A)
DsRed2-
H2A gene
Endosome
Cytosol
Cell
DsRed2-H2A
Nucleus
Extract
nuclei
FCS
RT-PCR
B)
Cre
Cre
Cre
+
Cre
stop
gfp
Recombination
gfp
GFP
Nucleus
Endosome
Cytosol
Cell
Microscopy / Flow cytometry
% Cells GFP(+)
C)
Delivery
peptide
Wash
FCS
in
focal
volume
Signal
Time
Auto-
correlation
analysis
Number of molecules
in focal volume
D)
SS488
SS488
SS488
SS488
H2B-
SNAP
Nucleus
Cytosol
Cell
Microscopy
~0% endosomal
leakage
~50% endosomal
leakage
~100% endosomal
leakage

1.5.1 Reagents with low apparent endosomal escape activity

The efficiency of plasmid DNA transfection by LipofectAMINE2000 (LFA), a cationic lipid formulation, and PEI have been assessed by Glover et al. (194). The goal of their study was not to measure endosomal escape per se, but instead to assess how many plasmids reach the nucleus of cells. Furthermore, the authors were interested in establishing how nuclear access correlates with expression of a gene encoded in the delivered plasmid. To address these questions, cells were transfected with a plasmid encoding DsRed2-H2A, a fluorescently tagged histone that is incorporated into chromatin upon expression (Figure 1-3a). The nuclei of cells containing both the delivered plasmid and its protein product were subsequently isolated (the viability of cells was not directly discussed in this report; yet, one can infer that cells capable of expressing DsRed2-H2A are likely alive prior to nuclear isolation). Real-time PCR was then used to quantitatively measure the amount of plasmid DNA present, while flow cytometry was used to determine the amount of protein expressed based on its fluorescence signal. This analysis reveals that cells exposed to 4 μg of plasmid (2.2×10^6 plasmids per cell) for 24 hr accumulate 350 plasmids/h in the first 8 hr of exposure: this rate subsequently accelerates. At the end of the 24 hr incubation, PEI could deliver 1.8×10^4 plasmids per nucleus while LFA delivered 8.3×10^3, representing overall yields (nuclear plasmid per cell/total DNA administered per cell) of 0.8% and 0.4%, respectively. Notably, while LFA delivers less plasmid into the nucleus of cells than PEI, it leads to equivalent levels of DsRed-H2A expression per cell, while also transfecting a higher percentage of cells overall. These results are in agreement with the

notion that cationic lipids dissociate from their DNA cargo upon endosomal escape and cytosolic egress, leaving a naked strand of DNA that may enter the nucleus only inefficiently. In contrast, PEI remains associated with DNA after endosomal escape and subsequently promotes the nuclear delivery of the cargo (195,196). While this may be an advantage for delivery, it is possible that the PEI that remains bound to DNA upon reaching the nuclear destination may then interfere with transcription. Overall, these results indicate that the multistep process of DNA transfection is of relatively poor efficiency. However, they do not reveal directly whether endosomal escape is itself a bottleneck. However, cells incubated with fluorescently labeled polyplexes or lipoplexes typically show a punctate distribution of fluorescence signal, as observed by high-magnification microscopy. This punctate signal corresponds to the accumulation of fluorescent material within endosomes. By contrast, no signal is typically detectable in the cytosol or nucleus of cells. Overall, this indicates that the vast majority of endocytosed complexes stay trapped within the endocytic pathway and that endosomal escape is a limiting step.

The TAT peptide is a ubiquitous delivery agent that has been used with a variety of cargo in many applications. Despite its popularity, how well TAT works often remains unclear. To assess the extent to which TAT is capable of delivering enzymes into cells, Dowdy and coworkers have used Cre recombinase (Figure 1-3b) as a model (114). In this assay, cells are transfected with a LoxP-STOP-LoxP-eGFP plasmid. Upon introduction of Cre recombinase into the cytosol and nucleus of cells, the enzyme excises the STOP signal present in the reporter DNA, leading to expression of eGFP.

The expression of eGFP was quantitated via flow cytometry, excluding dead cells stained with propidium iodide (PI) from analysis. The authors showed that incubation of cells with the fusion TAT-Cre for 1 hr led to a majority (~80%) of cells expressing eGFP 18 hr later. On one hand, these results clearly highlight that TAT can successfully bring cargo into cells. However, as described with lipoplexes, microscopy observation of a fluorescently labeled TAT-Cre shows exclusive retention of the protein inside endosomes. It is therefore likely that, while the endosomal escape activity of TAT is limited, TAT may be capable of delivering a few copies of TAT-Cre per cell. Given the catalytic properties of Cre, these few copies may be sufficient to activate the reporter plasmids present in the cell (as few as 4 Cre molecules, 4 Cre-bound sites being required for excision). Moreover, this assay is binary: there is either enough Cre recombinase that enters cells to activate eGFP expression or there is not. Therefore, above a given Cre recombinase threshold, eGFP is expressed regardless of how many enzymes are delivered. This, in turn, does not allow the testing of cell-to-cell variability. To assess how many peptides may enter the cytosol of cells, two groups have recently reported the use of fluorescence correlation spectroscopy (Figure 1-3c) (192,197). In these assays, fluorescently labeled peptides are incubated with cells. In one instance, live cells are isolated by FACS (based on size and granularity) and lysed. Cell lysates are then subjected to ultracentrifugation to isolate a cytosolic fraction. Samples are subsequently analyzed by bulk fluorescence correlation spectroscopy (FCS) and the concentration of fluorophore present is extracted from autocorrelation curves, using standards of known concentration as calibration. In another instance, FCS is directly performed in the focal

volume contained in the cytoplasmic space of cells (cells observed are determined to be viable based on their ability to remain adherent after a brief treatment with trypsin). Autocorrelation analysis yields an estimate of the number of molecules present in this volume. Using these alternative approaches, TAT was found to enter the cytosol of cells with an efficiency of 2% ([TAT]cytosol vs [TAT]outside cells). More specifically, a 30-min incubation with 500 nM of peptide yields a cytosolic concentration of 10 nM (192). Similarly, Antp, a cationic CPP (RQIKIWFQNRRMKWKK) also used for delivery applications, was found to enter at very low level (197). In particular, incubation of 1×10^6 cells with 1 μM peptide for 2 hr ($\sim 1.2 \times 10^8$ molecules/cell), yields approximately 9.0×10^5 molecules/cell of Antp internalized. Moreover, only 1.8×10^4 molecules/cell are present in the cytosol, the remainder being trapped inside endosomes. Overall, this represents efficiencies of 2% (cytosol/endosome) and 0.015% (cytosol/ total outside cells). Notably, the authors observed that addition of PAS (GKPILFF), a hydrophobic peptide previously shown to enhance endosomal escape by Futaki and coworkers, showed an increase in both total internalization (i.e., endocytosis, up to 1.5×10^7 molecules/cell) and cytosolic release (up to 4.2×10^6 molecules/cell), corresponding in yields of 28% (cytosol/endosome) and 3.5% (cytosol/total) (198). Notably, despite this higher endosomal escape activity, the distribution of fluorescence signal remains punctate in microscopy images. Because endosomal escape remains relatively low, it is unknown whether the cytosolic delivery achieved involves just a few molecules escaping many endosomes in a cell, or conversely, many molecules escaping a single endosome among hundreds of organelles.

1.5.2 Reagents with high apparent endosomal escape

Several reports have highlighted how some reagents are efficient enough that the molecules they deliver can readily be observed in the cytosol of cells by fluorescence microscopy (111,194,199). For instance, when PCI is used as a delivery method, molecules trapped inside endosomes can be seen bursting out into the cytoplasm upon irradiation of photosensitizers (200). Similarly, dfTAT, a disulfide-bonded dimer of TAT labeled with two tetramethylrhodamine fluorophores, can release high levels of molecules in the cytosol of cells, albeit in the absence of light-activation (138). Herein, we use dfTAT as an example to illustrate how efficient endosomal escape can be. Like monomeric TAT, at low incubation concentrations (<2 μM, 1 hr), dfTAT accumulates within endosomes without any apparent access to the cytosol. However, as incubation concentration is increased, a majority of cells display a diffuse fluorescence signal throughout the cell, with noticeable staining of nucleolar compartments. This staining is, in turn, confirmation that some of the signal detected is indeed intracellular, and not simply caused by out- of-focus fluorescence from peptide bound to the exterior of the cell. This staining is detectable in close to 100% of cells when 5 μM of peptide or more is used (dead cells, identified by SYTOX nuclear staining, represent less than 5% of the total population and are excluded from quantitation). In contrast, monomeric TAT remains trapped inside endosomes, even when the amount of TAT internalized in endosomes exceeds that of dfTAT by more than 2-fold (50 μM TAT vs 5 μM dfTAT incubation). The cytosolic entry of dfTAT is such that microscopy images typically show little to no fluorescence left inside endosomes. Inhibitors of endocytosis and of

endosomal trafficking, nonetheless, all confirm that the peptide enters the cytosol by escaping from endosomes (137). Endosomal escape therefore appears highly efficient. However, one may envision how, above a certain level of cytosolic entry, the cytosolic fluorescence may mask the signal left trapped inside endosomes. To address this question, an assay based on the cell- impermeable fluorophore SNAP-Surface was developed (Figure 1-3d). In this assay, cells are transfected with SNAP-H2B, a histone protein fused to the SNAP-tag. Upon cell entry, as mediated by endocytosis and dfTAT-induced endosomal escape, SNAP-Surface diffuses freely into the cytosol of cells. However, upon nuclear entry, SNAP-H2B covalently captures the fluorophore. This leads to the retention of the fluorophore in the nuclear compartments and to a depletion of the signal in the cytosol. Importantly, this means that the signal that remains trapped inside endosomes, that is, signal from failed endosomal escape, is better revealed. Based on this assay, up to 90% of the fluorescent molecules reach the nucleus of cells in the presence of dfTAT (0% in its absence). The number of observable endosomes loaded with fluorophore is as low as a dozen, while hundreds are present when dfTAT is absent. Overall, this suggests that dfTAT can release a majority of internalized molecules into the cytosol and that this activity involves the leakage of many organelles in a cell. Notably, because dfTAT can stimulate an increase in cellular fluid-phase uptake (as reported for TAT and other arginine-rich peptides), the concentration of macromolecules that reach the interior of cells can exceed the extracellular concentration. Nonetheless, when comparing these results to the previous studies described, it is important to note that the number of molecules that enter cells remain an overall small percentage of the

number of molecules extracellularly administered. Specifically, with cells exposed to 1.5 × 10^{10} molecules/cell of GFP, dfTAT-mediated delivery yields to 4.2 × 10^{8} molecules/cell of protein internalized overall (leading to a 2.8% yield). As with SNAP-surface, the fluorescence of the protein is almost exclusively in the cytosol of cells, indicating that the cytosol/ endosome yield of release is close to 100%. This notion is further supported by the delivery of the transcription factor HOXB4: while TAT can deliver HOXB4 and induce the expression of a luciferase gene-reporter, dfTAT can improve this activity by more than 60-fold (201).

1.5.3 Summary of cell delivery quantification techniques

The efficiency of endosomal escape of various delivery agents appears to vary widely. It is important to note that, in many instances, high efficiency is not required. As pointed out earlier with the example of DNA plasmid or Cre recombinase, low levels of cell entry are adequate if few macromolecules delivered are sufficient to execute a biological function. For other applications, this may, however, not be satisfactory and more robust delivery tools are then required. Additionally, more efficient endosomal escape may, in principle, provide other advantages. This may include lower variability or a higher percentage of cells with successfully delivered cargo. Moreover, by improving endosomal escape, lower levels of externally administered cargo may be required. While this may only provide added convenience in cell cultures by reducing the loss of reagents, which are often challenging and costly to prepare, this may prove absolutely necessary for *in vivo* applications where delivery agents and their cargo cannot be introduced in high concentrations.

1.6 Significance of the late endosomal and lysosomal-enriched lipid, Bis(monoacylglycero)phosphate

1.6.1 What is Bis(monoacylglycero)phosphate?

In 1998, Gruenberg and coworkers sought to understand the lipid composition of endocytic vesicles (122,125,126,202). Individual endocytic membranes from BHK cells were isolated including heavy membranes (HM), early endosomal membranes (early endosome; EE), and late endosomal membranes (late endosome; LE). While phospholipids such as DOPC and DOPE were found in all membranes, a unique lipid was highly enriched in late endosomal membranes (77% of the total membrane content) (125,126). This unique phospholipid was lysobisphosphatidic acid (LBPA) also known as bis(monoacylglycerol)phosphate (BMP). BMP is a negatively charged phospholipid and a structural isomer of phosphatidylglycerol (PG). Where the fatty acids of PG are conjugated to a single glycerol substituent, the fatty acids of BMP are conjugated symmetrically to each glycerol substituent of the phospholipid. Owing to its structure, BMP has a unique behavior that will be discussed in detail in the following subsection.

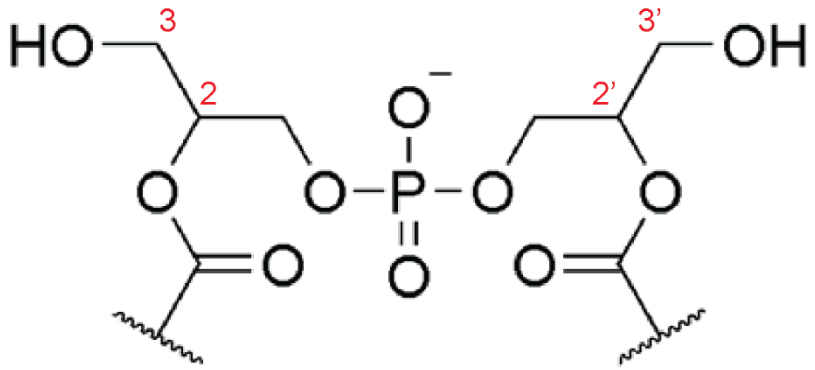

Figure 1-4 The minimal structure of 2,2'-bis(monoacylglycerol)phosphate (BMP). Fatty acid conjugation positions are specified as 2 or 3 for the first glycerol substituent and 2' or 3' for the second glycerol substituent.

1.6.2 BMP is highly fusogenic

In a later study, Gruenberg and coworkers showed that liposomes enriched in BMP exhibited fusogenicity which led to the formation of multivesicular liposomes (MVLs) (203,204). These results suggested that the fusogenic behavior was dependent on an acidic interlumenal pH (pH 5.5). This lumenal pH-dependent fusogenic behavior is corroborated *in cellulo* by the acidic lumen of late endosomal membranes which are highly enriched with BMP. Additionally, Gruenberg et al. found that five proteins were found to associate selectively for BMP; among these proteins was Alix (203). Alix is also associated with exosomes, phagosomes, and the yeast homolog Vps31p is involved in multivesicular endosome biogenesis (205-207). Alix inhibits MVL formation of liposomes in a pH-independent manner. In the cell, the fusogenicity of BMP is exploited in interlumenal vesicle (ILV) formation and inward budding of ILVs into late endosomes is regulated, in part, by Alix (208). The ability of this organelle to form and compartmentalize these interlumenal membrane structures is critical for the biologic function of sorting and distributing endosomal cargos. The involvement of BMP in the sorting of cholesterol will be investigated in greater detail below.

1.6.3 The biological function of BMP as regulator to endosomal cholesterol content

Cellular cholesterol acquisition is a well-characterized process. Low-density lipoproteins (LDL) are carriers of cholesterol which undergo receptor-mediated endocytosis (209). Following endocytic uptake, cholesterol carrying LDLs travel through the endocytic pathway until they reach the lysosome where they are degraded, releasing their sterol cargo. However, how the freed cholesterol gets distributed among

different cellular membranes had remained unclear. In 1999, Gruenberg and coworkers showed that late endosomes are involved in the regulation of cholesterol transport using cells affected by the lysosomal storage disease Niemann-Pick type C (NPC) (202). Symptoms of this disease include unesterified cholesterol accumulation as well as an abundance of multivesicular membrane structures in late endosomal and lysosomal organelles (210). Vesicles that had accumulated cholesterol associated with the late endosomal markers GTPase Rab7 and CD63 as well as BMP (211,212). These findings suggest that cholesterol accumulation was not restricted to lysosomes but to late endosomes as well. One role of the late endosome is the sorting of IGF2/MPR (insulin-like growth factor type 2 aka mannose-6-phosphate receptor). IGF2/MPR distributes newly-synthesized lysosomal enzymes from the *trans*-Golgi network (TGN) to LEs and then gets recycled for the next distribution (213). Gruenberg et al. observed prolonged redistribution of IGF2/MPR from the TGN to LEs (24-48 hr time scale). This sorting deficiency of the late endosome can be imparted upon the lysosome via late endosomal fusion.

1.6.4 Involvement of BMP in cellular internalization of cell penetrating agents

In the past decade, BMP has been implicated in the endosomal escape of CPPs. In addition to a high binding affinity of TAT toward BMP, TAT mediates the lysis of BMP-containing membranes (127). In our lab, we sought to similarly characterize dfTAT to provide insight into the unprecedented endosomal escape efficiency of the mCPP. The peptide displayed a high affinity towards BMP-containing liposomes and selectively induced membrane lysis over BMP-containing LUVs. Additionally, induced

inverted micelle formation that encapsulated the hydrophilic peptide and allowed it to partition into a hexane phase (138). Taken together, these results suggest that BMP plays a role in the endosomal escape of dfTAT.

In addition to TAT compounds, viruses and viral particles interact with BMP in infection mechanisms. Examples include Dengue, Bluetongue, and Yellow fever viruses (214-218). Dengue virus (DENV), a member of the *Flaviviridae* family, is an enveloped virus with a positive sense, single-stranded genomic RNA (219). In 2010, Chernomordik demonstrated that DENV interacts with BMP in the mechanism of cytosolic deposition of the viral RNA genome (214). The virus is internalized via endocytosis where, upon acidification of the lumen, the envelope protein (DENV E) dissociates into monomeric subunits that subsequently interact with the limiting membrane of the EE. This interaction leads to restricted hemifusion of the viral envelope with the limiting membrane where the virus is trapped until introduction of the anionic lipid. Maturation of the EE into a LE introduces BMP into the inner leaflet of the endocytic organelle allowing for the fusion loop of DENV E to insert into the membrane. The monomeric subunits undergo conformational change which allows for homotrimerization. The homotrimers drive the completion of the fusion event and result in the deposition of the nucleic acid cargo. Freire et al. demonstrated how the capsid protein of Dengue virus (DENV C) alone is capable of delivering nucleic acids via interaction with BMP (216). Multiple units of DENV C form a nucleocapsid which store the genomic RNA of the virus. DENV C is a supercharged dimeric protein with a net charge of +42 and a charge density of +1.97/kDa (220). The capsid protein contains a lipid binding motif (pepM,

residues 45-72) as well as a putative RNA binding domain (pepR, residues 67-100). Friere and coworkers demonstrated how DENV C delivered single-stranded DNA (ssDNA) as well as siRNA into BHK-21 cells, astrocytes, and HepG2 cells. Additionally, pepM and pepR were independently able to penetrate cells yet remain relatively innocuous. Finally, DENV C, pepM and pepR have anionic lipid-specific interactions with BMP that are crucial to the leaky fusion event that leads to cytosolic penetration. Taken together, these results underscore the utility of supercharged viral capsid proteins as transfection reagents. Datamining revealed that several other capsid proteins from the Flaviviridae family are supercharged proteins (> +0.75/kDa) and possess putative nucleic acid binding domains (216-218). Viruses such as Human adenovirus C type 1, HIV 1 and 2, and Chikungunya virus outside of the Flaviviridae family also have supercharged capsid proteins. By extrapolating the results of DENV and its interaction with BMP, opportunities arise as these other capsid proteins could be similarly harnessed as transfection reagents and a potentially widespread antiviral therapeutic can even be developed by targeting this interaction.

1.7 Goal of this research

In this study, I used a multivalent approach to determine the role that multivalency and, by proxy, charge or guanidinium density play in the endosomal escape of CPPs. While many multivalent synthetic approaches have exhibited poor yields due to inefficient means of multimerization, my approach has overcome this limitation, allowing for the preparation a sufficient amount of material to execute the studies discussed herein. As such, I was able to synthesize constructs via solid-phase peptide

synthesis (SPPS) that contain one, two, or three copies of the peptide TAT. These constructs share a universal scaffold to maintain high structural similarity and allow for the evaluation of the difference in penetrative activity contributed by only the varied charge/guanidinium density. To determine the contribution of the charge/guanidinium density to endosomal escape activity, each construct was compared *in cellulo* to discern differences or similarities in their inherent activities, including the ability to penetrate cells, deliver bioactive cargo, and induce cytotoxicity. In a more controlled environment, *in vitro* studies were also conducted in model membrane systems to gain insight into the endosomolytic nature of polycationic cell-penetrative compounds. In particular, the use of model membranes allowed for the determination of membrane restructuring events, as induced by the endosomolytic cell penetrative compounds, as well as provided a deeper understanding of the role of BMP in the mechanism of cell penetration by supercharged compounds. The results from this work will not only lead to the development of more efficient cell penetrating delivery agents and cell-permeable probes/therapeutics but can be extrapolated beyond CPPs to broadly apply to the mechanism of cellular internalization for all classes of supercharged polycationic molecules, including supercharged viral particles.

CHAPTER II

EFFICIENT CELL DELIVERY MEDIATED BY LIPID-SPECIFIC ENDOSOMAL ESCAPE OF SUPERCHARGED BRANCHED PEPTIDES*

2.1 Introduction

Reagents that can deliver exogenously administered macromolecules into live cells are useful in applications ranging from basic cell biology, *ex vivo* cell manipulations for biotechnological purposes or *in vivo* therapeutic strategies. Crossing cellular membranes to gain access to the cell interior is, however, a significant challenge and, whether it is because of low efficiencies or toxicity, the search for ideal delivery agents remains a research focus. A general class of delivery agents consists of polycationic molecules. It includes lipid particles, polymers, artificial or viral proteins and cell-penetrating peptides (CPPs) (221-224). For many decades, polycationic molecules have been recognized for their propensity for cellular internalization by endocytosis. It is thought that electrostatic interactions between polycationic species and anionic cell-surface glycosaminoglycans are important for this process (225,226). However, while advantageous as a first step of cellular entry, endocytic uptake itself does not lead to successful delivery. In fact, endosomal entrapment is typically useless in most applications, as macromolecular cargos shuttled in endocytic organelles cannot reach intended targets that may be localized in other parts of the cell. Notably, polycationic species, in some cases, appear to also be able to escape from endosomes, thereby releasing their cargo into to the

*This chapter is reprinted with permission from Brock, D. J., Kustigian, L., Jiang, M., Graham, K., Wang, T. Y., Erazo-Oliveras, A., Najjar, K., Zhang, J., Rye, H., and Pellois, J. P. (2018) Efficient cell delivery mediated by lipid-specific endosomal escape of supercharged branched peptides. *Traffic* **19**, 421-435.

to also be able to escape from endosomes, thereby releasing their cargo into to the cytosolic space of cells. For instance, this is the case for cationic, lipid-based DNA transfection reagents or for CPP-mediated delivery of enzymes (45,137,227,228). While the percentage of molecules that escape is relatively low (often estimated to be less than 1% of what remains trapped inside endosomes), intracellular activities can nonetheless be detected. Recently, a number of studies have highlighted how increasing the charge density of polycationic delivery agents to a relatively high degree may help increase their endosomal escape activities. An example is supercharged green fluorescent protein (GFP), a GFP mutant obtained by replacing anionic residues of wild-type superfolder GFP with cationic amino acids. While GFP has a charge of −7 at pH 7, supercharged GFP has an overall charge of +48 (33,34). When fused to other proteins, supercharged GFP is capable of escaping endosomes and delivering a variety of cargos (35). Remarkably, cell-permeable supercharged proteins also appear to occur in nature. Viral capsid proteins seem especially prone to "supercharging." This is the case of proteins of flaviviruses, including DENV C (+42 charge, +1.97/kDa, dengue virus) or YFC (+52 charge, +2.30/kDa, yellow fever virus) and WNV (+46 charge, +1.74/kDa, West Nile virus) (216-218). These proteins, which are involved in the entry of viruses into host cells at endosomal sites, can also be used as delivery agents for exogenous cargos. The notion of supercharging molecules for increased membrane permeation may be expanded to CPPs. For instance, CPPs incorporated into multimeric proteins have shown better delivery outcomes than their monomeric counterparts (157). Similarly, increasing the number of protein transduction fusion tags incorporated recombinantly at the N-

terminus of a protein can improve the cell penetration of the macromolecule (141). In our laboratory, we have recently observed that dimerization of the prototypical CPP TAT (GRKKRRQRRR, residues 48-57 form HIV-1 Trans-Activator of Transcription) could lead to a reagent, dfTAT (dimeric fluorescent TAT), with dramatically increased endosomal escape activity (137). In particular, dfTAT is capable of causing the endosomal release and cytosolic egress of more than 90% of material initially trapped inside endosomes. Because of this improved activity, dfTAT can deliver relatively high concentrations of small molecules, peptides and proteins in a simple coincubation assay. More specifically, dfTAT and its cargo do not need to interact: they simply need to be endocytosed together and, by making endosomes leaky, dfTAT mediates the cytosolic release of the cargo. Mechanistically, dfTAT escapes specifically from late endosomes, which are organelles where the cationic CPP encounters the anionic lipid BMP (138). dfTAT is in turn capable of causing the leaky fusion of late endosomal BMP-rich membranes. One promising approach towards the generation of supercharged cell-penetrating agents is by the branching of polycationic moieties of a molecular scaffold. When exploited in solid phase peptide synthesis (SPPS), this technique allows one to greatly increase the cationic content of potential cell-penetrating agents with relative ease when compared with linear peptide synthesis. One early example utilized branched-chain arginine-rich peptides to study plasma membrane translocation (229). In more recent work, branched polycationic peptides have even been successfully employed as gene transfection tools as well (230,231). Herein, we were interested in elucidating how multimerization of the TAT peptide leads to an enhanced endosomal escape activity. To

address this question, we generated branched structures that present a variable number of copies of the peptide on a common scaffold. The cell penetration activities of the constructs were evaluated in cell cultures and their propensities to disrupt membranes were characterized *in vitro*. We establish that multivalent display of the TAT peptide leads to dramatic increases in endosomal leakage, cytosolic escape and overall delivery efficiencies. These improved performances result from BMP-specific activities that are present in the branched species but not in the monomeric parent compound. They include a glue-like behavior that promotes lipid bilayer contact and the ability to induce the leaky fusion of BMP-containing bilayers.

2.2 Results

Several new CPP constructs were synthesized. These compounds are named 1TAT, 2TAT and 3TAT in relation of the number of TAT copies attached to a common scaffold (Figure 2-1a). This scaffold consists of the peptide KGKGKG, where the amino side-chains of the lysine residues are connected to either the C-terminus of a TAT peptide or to an acetyl capping group. The N-terminus of the scaffold is labeled with carboxytetramethylrhodamine (TMR), a red fluorophore used herein for peptide quantification and fluorescence microscopy tracking of the peptide behavior in cells. The peptides were synthesized by solid-phase peptide synthesis, purified by high-performance liquid chromatography (HPLC) and analyzed by mass spectrometry (Figures A-1 and A-2 in Appendix A, Supporting Information).

To first test the peptide reagents, cells were treated with 1TAT, 2TAT and 3TAT for 30 min, a time that is, in our experience, convenient for delivery protocols in cell

cultures. Under this condition, 1TAT, 2TAT and 3TAT displayed 2 distinct cellular localizations. In the case of 1TAT, a punctate distribution was observed at all concentrations tested (1, 3, 9 μM; Figure 2-1b). Colocalization of the red puncta with LysoTracker Green, a marker of acidic-organelles such as late endosomes and lysosomes, indicated that 1TAT is trapped in the lumen of endocytic organelles (Figure A-3 in Appendix A), as previously reported for similar peptides (232). In the case of 2TAT and 3TAT, a similar punctate distribution was observed at low concentration (1 μM). However, as the incubation concentration is increased, a population of cells displaying a diffuse cytoplasmic staining can be observed (Figure 2-1b). The red fluorescence of these cells also includes a distinct nucleolar staining, a feature previously observed for other cationic peptides (137,233,234). In this particular instance, nucleolar staining serves to demonstrate that the fluorescence signal detected is, at least in part, intracellular (as opposed to originating from surface binding). Notably, the percentage of cells showing cytoplasmic/nucleolar staining was low in the case of 2TAT (less than 10% at an incubation concentration of 4.5 μM). In contrast, approximately 50% of the cells showed cytosolic penetration by 3TAT. The cells counted in this assay exclude SYTOX Green positive cells, indicating that the cells do not have a compromised plasma membrane. However, it should be noted that less than 10% of cells become positive to SYTOX Green when exposed to 3 μM 3TAT, indicating that the peptide is modestly toxic at this concentration. Importantly, 3TAT was significantly more toxic at 5 μM (Figure 2-1d). This increased toxicity, which gives rise to peptide-stained cellular debris during imaging, made quantifying cell penetration difficult. Achieving delivery

while killing cells is also counterproductive. For these reasons, in the context of our mechanistic studies, 3TAT was not tested at a concentration higher than 3 μM (longer incubation times were, however, tested to characterize the cytotoxicity of the peptides more fully, Figure A-4 in Appendix A). Overall, this concentration alone was sufficient to exemplify that 3TAT is significantly more active than 1TAT and 2TAT. This is apparent when the peptides are compared at equal incubation concentrations, or at concentrations that lead to similar overall TAT content (i.e., 9 μM 1TAT vs 4.5 μM 2TAT vs 3 μM 3TAT). In particular, 3 μM 3TAT is internalized by cells at a higher level than 1TAT or 2TAT, at all concentrations tested. This indicates that 3TAT enters cells, being either trapped inside endosomes or diffused in the cytoplasm, in a larger amount than the analogs with fewer peptide copies. This in turn may suggest that this higher propensity for uptake is correlated to its ability to enter the cytosolic space of cells. However, it should be noted that, under conditions where 3TAT is internalized to a lower extent than 2TAT (i.e., 4.5 μM 2TAT vs 1 μM 3TAT), 3TAT displays more cytosolic penetration than 2TAT.

Figure 2-1 Cell penetrative and cytotoxic activities of supercharged peptides. (a) Representative scheme of the peptide constructs 1TAT, 2TAT and 3TAT. The constructs consist of a KGKGKG scaffold labeled with the TAT peptide or an acetyl capping group on the side chain of the lysine residues. Additionally, the scaffold is labeled with the fluorophore carboxytetramethylrhodamine (TMR) at its N-terminus. The molecular weight and expected charge of each construct at pH 7 and below are represented. (b) 2TAT and 3TAT reach the cytosol and nucleoli of cells but 1TAT does not. Fluorescence microscopy images of cells treated with each peptide for 30 min at indicated concentrations, washed, and stained with SYTOX Green and the nuclear stain Hoechst 33342. Cells were imaged 1 hr after incubation with peptides. Images are overlay of images pseudocolored red for TMR, blue for Hoechst 33342, and green for SYTOX Green (only present if cells have a disrupted plasma membrane; scale bars: 20×: 50 µm, 100×: 10 µm). (c) The cell penetration activity of 3TAT is superior to that of 2TAT and 1TAT. Quantitative evaluation of the percentage of cells positive for penetration (i.e., showing nucleolar staining while excluding SYTOX Green) after incubation for 30 min (1 hr wait) at the concentrations indicated. The data represented correspond to the mean of biological triplicates (>500 cells counted per experiment). (d) Evaluation of the toxicity of the peptides by a SYTOX Green exclusion assay. Cells were treated as in b and c. The number of cells displaying a nucleus stained by SYTOX Green were counted. The data represented correspond to the mean of biological triplicates (>500 cells counted per experiment). The red dashed line indicates a threshold toxicity at which, in our hands, cell penetration cannot be reliably quantified because of high levels of fluorescently stained cellular debris. (e) Evaluation of the levels of peptide uptake in cells by quantification of the TMR fluorescence intensity of cell lysates. Cells were treated as in b and c. Cells were washed, trypsinized, and homogenized. The fluorescence of the cell lysate was measured and normalized to the number of cells in each sample, assessed by flow cytometry. The data reported corresponds to the mean of technical triplicates. The figure is used with permission (235).

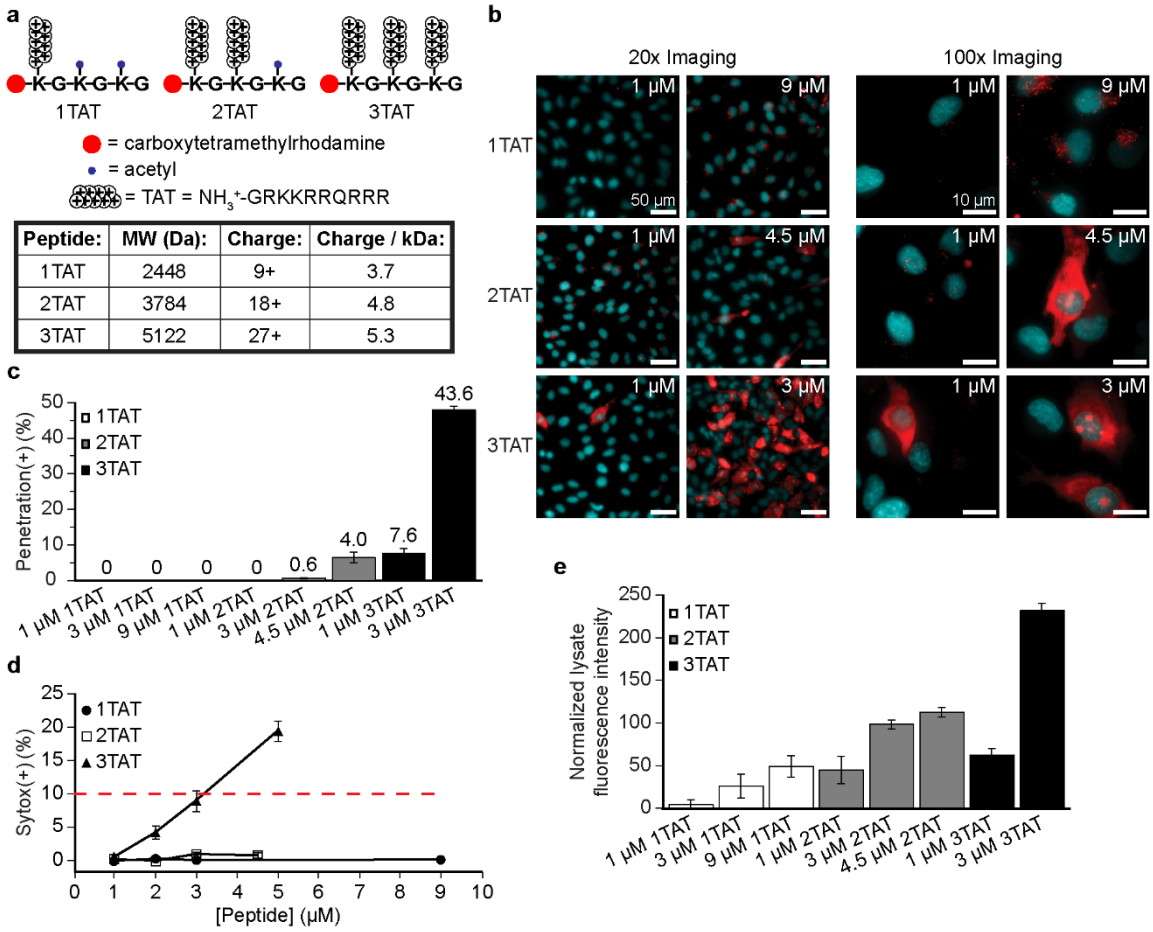

Peptide:	MW (Da):	Charge:	Charge / kDa:
1TAT	2448	9+	3.7
2TAT	3784	18+	4.8
3TAT	5122	27+	5.3

The usefulness of these peptides is not found in whether they penetrate cells per se, but instead in whether they can mediate the cytosolic delivery of other molecules. To address how 1TAT, 2TAT and 3TAT compare in this respect, we chose 2 cargoes, the enzyme Cre recombinase and the cell-impermeable small molecule SNAP-Surface 488. The cytosolic delivery of Cre recombinase, and the subsequent accumulation of the enzyme in the cell nucleus, can be quantified by the expression of an enhanced GFP (EGFP) reporter incorporated in a Cre-Lox recombination system (Figure 2-2a) (236). Similarly, the cytosolic delivery of SNAP-Surface 488 in cells expressing SNAP-H2B, a histone fusion, results in cells displaying fluorescent nuclei (Figure 2-2b) (137,237). In principle, the successful delivery of only a few Cre recombinase molecules is sufficient to induce GFP expression. In contrast, micromolar intracellular concentrations of molecules are required for microscopy detection of SNAP-Surface (based on calibration experiments performed in-house). We, therefore, envisioned that these 2 assays span a range of detection sensitivities that may reveal differences between the CPPs tested. As shown in Figure 2-2a, the percentage of cells positive for GFP expression was small when Cre recombinase was incubated with 1TAT (~10%, 3 μM 1TAT, 4 μM Cre recombinase; Cre recombinase used is expressed as a TAT fusion to promote endocytic uptake and the protein itself displays some cell-permeation activity, ~5%). In comparison, incubating Cre recombinase with 2TAT and 3TAT led to more than 50% of GFP positive cells.

Interestingly, the delivery activities of 2TAT and 3TAT were relatively equivalent, indicating that both compounds are capable of delivering enough enzyme to initiate expression of the EGFP reporter (however, the amount of enzyme actually delivered could, in principle, vary). In contrast, 3TAT was dramatically more effective at inducing the delivery of SNAP-Surface 488 to the nucleus of cells than 1TAT or 2TAT. These results closely match the results obtained with the peptides in Figure 2-1 and indicate that 3TAT is able to induce the cytosolic of delivery of a significantly higher amount of SNAP-Surface 488 than 1TAT and 2TAT.

Overall, these data indicate that 1TAT is ineffective, that 2TAT is active enough to mediate the delivery of few molecules, and that 3TAT, in contrast, can deliver larger quantities. Additionally, these data suggest that 2TAT and 3TAT are capable of delivering a variety of bioactive cargo as the two cargoes tested drastically differ in their respective chemical makeups.

Figure 2-2 Molecular cargo delivery efficiency of supercharged peptides.
(a) 2TAT and 3TAT deliver the enzyme TAT-Cre into cells. Cells transfected with a plasmid containing EGFP downstream of an LSL cassette were coincubated with TAT-Cre (4 μM) and peptide at indicated concentrations for 30 min. Because successful cellular entry of TAT-Cre results in EGFP expression, the number of cells positive for EGFP fluorescence were counted 24 hr after each peptide/TAT-Cre incubations. Fluorescence microscopy images, pseudocolored green for EGFP, are representative examples of the cells 24 hr after enzyme delivery (scale bars: 20×: 50 μm, 100×: 10 μm). The data reported corresponds to the normalized mean of biological triplicates (>500 cells per experiment). NS, $p>0.05$; * $p<0.05$. (b) 3TAT delivers the cell-impermeable green fluorophore SNAP-Surface 488 into the cytosolic space of cells. Cells transfected with a plasmid coding for histone H2B-$SNAP_f$ were coincubated with SNAP-Surface 488 (50 μM) and peptide at indicated concentrations for 30 min. Cells were then washed and stained with Hoechst 33342. Upon entry into cells, SNAP-Surface 488 is retained in the nucleus of cells by reaction with H2B-SNAP. Successful delivery was therefore assessed by counting the number of cells displaying a green nucleus. Fluorescence microscopy Images, pseudocolored green for SNAP-Surface 488 and colored white for Hoechst 33342, are representative examples of the cells 1 hr after incubation (scale bars: 20×: 50 μm, 100×: 10 μm). The data reported corresponds to the normalized mean of biological triplicates (>500 cells per experiment). The figure is used with permission (235).

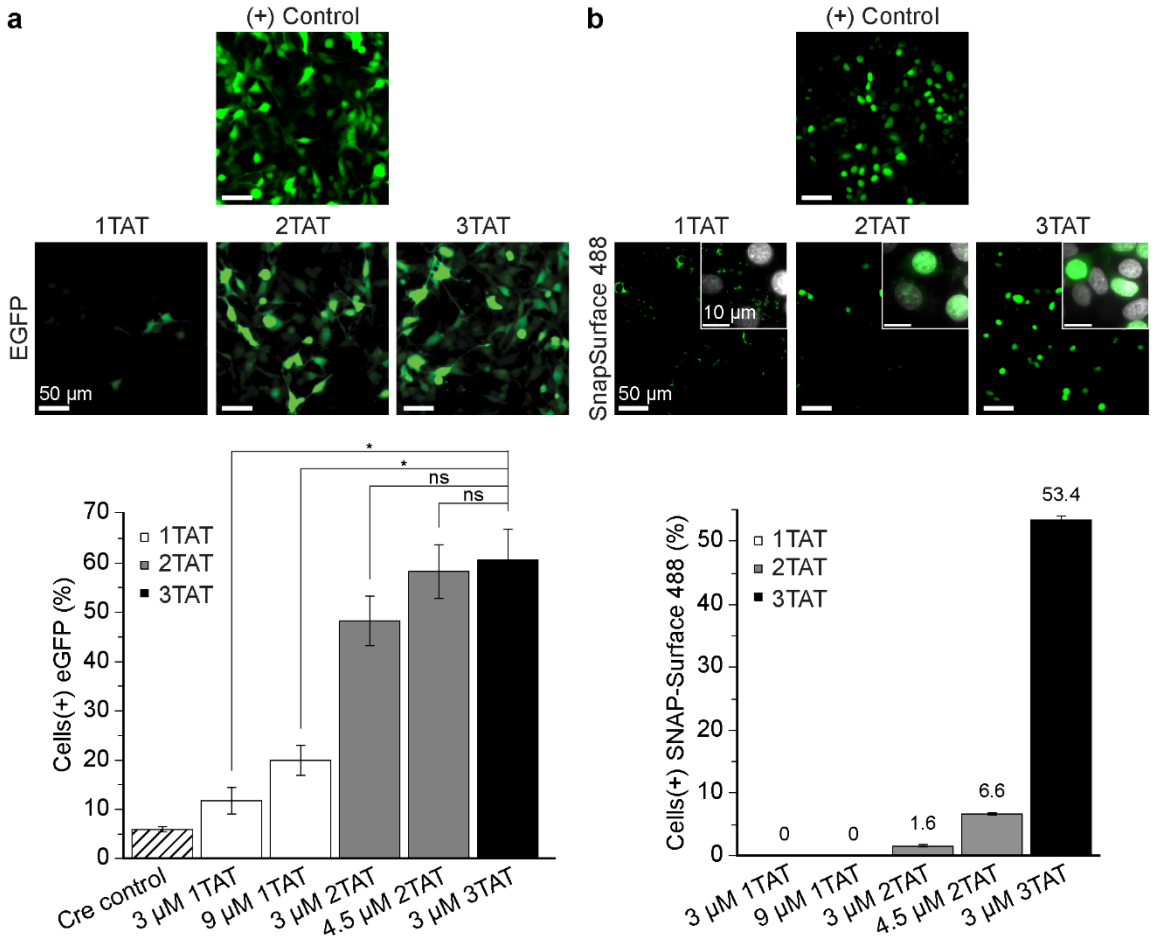
a
(+) Control
1TAT
2TAT
3TAT
EGFP
50 µm
b
(+) Control
1TAT
2TAT
3TAT
SnapSurface 488
10 µm
50 µm
*
*
ns
ns
Cells(+) eGFP (%)
1TAT
2TAT
3TAT
Cre control
3 µM 1TAT
9 µM 1TAT
3 µM 2TAT
4.5 µM 2TAT
3 µM 3TAT
Cells(+) SNAP-Surface 488 (%)
0
0
1.6
6.6
53.4

2.2.1 Cell penetration involves endosomal escape

We have previously demonstrated that dfTAT delivers macromolecular cargos by causing endosomal leakage. To test whether 3TAT has a similar activity, the intracellular localization of the peptide was first monitored in a pulse-chase experiment (Figure 2-3a). Cells were incubated with 3 μM 3TAT for 5 min, washed and examined by fluorescence microscopy. At early time points, cells displayed a punctate distribution consistent with endosomal entrapment. At later time points, this distribution change to a cytosolic and nucleolar staining. Because the peptide is not present extracellularly during the post-treatment period, these data, therefore, suggest that the peptide, initially trapped inside endosomes, is subsequently able to escape from endosomes and reach a cytosolic destination. To ensure cells under each condition assayed were exposed to the same amount of internalized peptide, uptake measurements were performed, as before, at the indicated time points. These measurements indicate that the relative amount of peptide taken up by the cells was relatively equivalent across the 2 conditions.

To further assess how 3TAT enters cells and mediates the delivery of cargos, we next tested whether the peptide could cause the release of material preloaded inside endosomes. Cells were preincubated with DEAC-k5, a peptide labeled with a blue fluorescent coumarin and containing cationic D-lysine residues that confer protease-resistance and that facilitate endocytic uptake (140,234). Cells were washed, treated with or without 3TAT and imaged by fluorescence microscopy (Figure 2-3b; Figure A-8 in Appendix A). Cells incubated with DEAC-k5 for 1 hr displayed punctate fluorescence signal (Figure 2-3b). The blue fluorescent puncta colocalized with LysoTracker Green,

consistent with endosomal accumulation of DEAC-k5 (Figure 2-3b; Figure A-5 in Appendix A). Upon addition of 3TAT, the blue fluorescence was redistributed throughout the cell cytosol. In addition, like 3TAT, DEAC-k5 showed a distinct nucleolar staining, confirming that the signal detected is intracellular. The cytosolic penetration of both 3TAT and DEAC-k5 was inhibited by addition of bafilomycin (cells are treated after DEAC-k5 loading), suggesting that blocking endosomal acidification prevents endosomal escape. Cytosolic delivery of DEAC-k5 was also abolished when addition of 3TAT was delayed by 2 hr, a time frame that allows accumulation of DEAC-k5 in lysosomes (138). Together, these data indicate that 3TAT is capable of reaching endosomes preloaded with DEAC-k5 and of causing a membrane leakage that results in the release of both peptides. When the time window between DEAC-k5 and 3TAT is short, endocytic organelles containing 3TAT presumably fuse with endocytic organelles containing DEAC-k5, leading to content mixing. When the time window is longer, DEAC-k5 reaches organelles further downstream in the endocytic pathway (i.e., lysosomes), away from sites of 3TAT-mediated escape.

Previous reports on dfTAT have established that endosomal escape involves the disruption of the membrane of late endosomes (138). In particular, dfTAT mediates its membrane-disrupting activity by interacting with the anionic lipid BMP in late endosomes. Because lipid bilayers of both late endosomes and lysosomes contain BMP, 3TAT may have the capacity to disrupt either of these organelles. To determine the major route of endosomal escape, a delivery assay of preloaded lysosomal cargo was performed (Figure 2-3b, exp 4). Cells first incubated with DEAC-k5 were then treated

with 3TAT following 2 hr wait to ensure that a majority of the endocytosed cargo was sequestered to the lysosome (a time frame in which one would expect this to happen). This experiment displayed very poor delivery of DEAC-k5 (<3%). Furthermore, whenever cells were treated shortly after the DEAC-k5 delivery, cells displayed a substantial amount of DEAC-k5 delivery (54%). Taken together, these data suggest that cargo must not be sequestered to the lysosome for successful delivery.

Notably, anti-BMP, a monoclonal antibody raised against BMP, can prevent the fusion of late endosomal membranes (late endosomes are organelles that contain vesicles in their lumen) and thereby block the endosomal escape of dfTAT (138). To establish whether 3TAT would respond to a similar treatment, cells were preincubated with anti-BMP or with the control antibody anti-IgG, a monoclonal antibody that does not recognize BMP as an epitope. Cells were then incubated with 3TAT and imaged. As shown in Figure 2-3c, anti-IgG did not prevent 3TAT from reaching the cytosol and nucleoli of cells. In contrast, anti-BMP inhibited cytosolic penetration, most of the cells displaying instead a punctate distribution of the peptide. Importantly, neither antibodies led to a significant reduction in peptide uptake, as measured by the total fluorescence of cell lysates. This indicates that the peptide is capable of accumulating inside endosomes but becomes unable to escape endosomes when anti-BMP is present.

Figure 2-3 3TAT utilizes endocytosis to penetrate the cytosolic space of cells. (a) 3TAT enters the cytosol of cells after endocytic uptake. Cells were incubated with 3TAT (3 μM) for 5 min, washed, and then imaged by fluorescence microscopy at different time points to determine the extent of cell penetration. The number of cells displaying nucleolar staining (i.e., penetration positive) were counted as previously described. The fluorescence microscopy images represented, pseudocolored red for TMR, highlight that cells first display a punctate distribution consistent endosomal entrapment at first and that nucleolar staining appear subsequently. The data reported corresponds to the mean of biological triplicates (>500 cells per experiment). Total peptide uptake at the 6- and 35-min time points was determined by lysing cells and measuring the bulk lysate for TMR fluorescence. The fluorescence of the cell lysate was measured and normalized to the number of cells in each sample, assessed by flow cytometry. The data reported corresponds to the mean of technical triplicates. NS, $p>0.05$. (b) 3TAT releases a cargo entrapped inside endocytic vesicles into the cytosol of cells. First, experiments were performed to determine the lysosomal accumulation of DEAC-k5 as a function of time after incubation. In experiments 1-3, cells were incubated with the blue fluorescent peptide DEAC-k5 (25 μM) for 1 hr. Cells were then washed and incubated in L15 medium for the indicated time periods (exp 1 = 0 hr, exp 2 = 0.75 hr, and exp 3 = 2.75 hr). Following L15 incubation, cells were treated with LysoTracker Green (500 nM) for 15 min prior to imaging by fluorescence microscopy. Colocalization analysis was performed over representative images taken of DEAC-k5 and LysoTracker Green taken under 100× magnification. From this analysis, Pearson's R value is reported to represent the extent of colocalization. For experiments 4-7, cells were treated with DEAC-k5 for 1 hr, as before. For experiments 2 and 3, cells were washed, incubated with L-15 ± bafilomycin (200 nM) for 20 min, and then treated with 3TAT (3 μM) ± bafilomycin for 30 min. For experiment 4, following DEAC-k5 incubation, cells were washed and incubated with L15 for 2 hr. Cells were then treated with 3TAT (3 μM) for 30 min. Following a 30 min wait for experiments 2-4, fluorescence microscopy images were taken at 20× and 100× magnification to quantify DEAC-k5 delivery. Cells were scored, as before, for successful DEAC-k5 penetration if nucleoli staining was observed (biological triplicates, >500 cells per experiment). Prior to 3TAT treatment, DEAC-k5 displays a punctate distribution consistent with endosomal entrapment. After treatment with 3TAT, DEAC-k5 redistributes throughout the cell (nucleolar staining, presumably attributable to the polycationic nature of the peptide, can be observed). This effect is blocked by bafilomycin, an inhibitor of endosomal acidification and trafficking. However, whenever DEAC-k5 is accumulated predominantly in the lysosome, cell delivery of the molecular cargo is abolished. (c) Preincubation with an anti-BMP mAb inhibits 3TAT cytosolic penetration but not endocytic uptake. Cells were preincubated with anti-BMP or the control antibody, anti-IgG (50 μg/mL), for 1 hr, washed, and then treated with 3TAT (3 μM) for 30 min. Cell penetration was then visualized and quantified by fluorescence microscopy as previously described. The percentage of penetration positive cells

reported is the mean of biological triplicates (>500 cells per experiment). Fluorescence images are pseudocolored red for 3TAT (scale bars: 20×: 50 μm, 100×: 10 μm). Total peptide uptake was determined by lysing cells and measuring the bulk lysate for TMR fluorescence. The fluorescence of the cell lysate was measured and normalized to the number of cells in each sample and to the level of uptake observed for 3TAT alone, assessed by flow cytometry. Each condition was normalized to cells treated with 3TAT (3 μM) for 30 min. The data reported corresponds to the mean of technical triplicates. NS, p>0.05. The figure is used with permission (235).

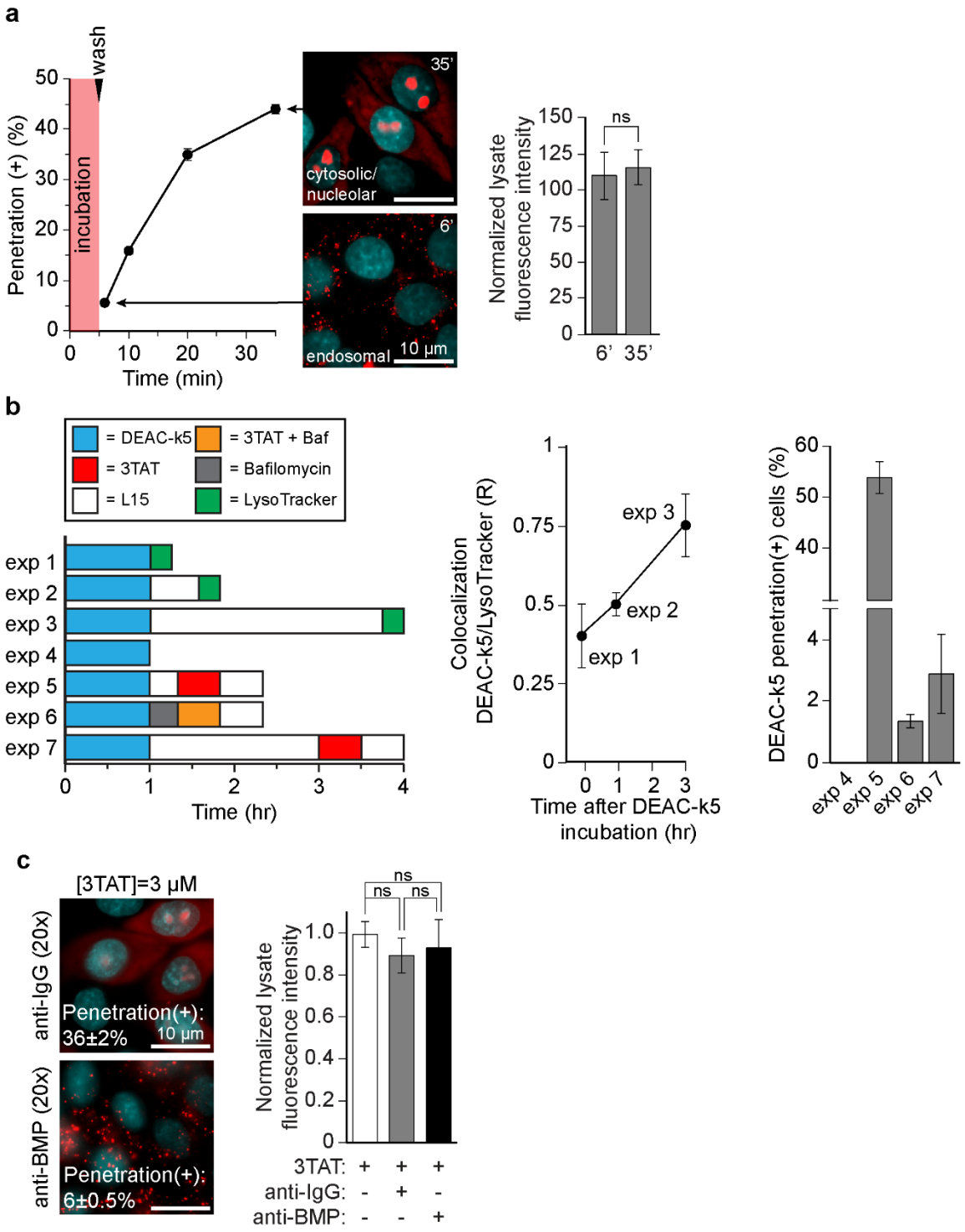
a
wash
incubation
Penetration (+) (%)
Time (min)
35'
cytosolic/
nucleolar
6'
endosomal
10 μm
Normalized lysate
fluorescence intensity
ns
6' 35'
b
= DEAC-k5
= 3TAT
= L15
= 3TAT + Baf
= Bafilomycin
= LysoTracker
exp 1
exp 2
exp 3
exp 4
exp 5
exp 6
exp 7
Time (hr)
Colocalization
DEAC-k5/LysoTracker (R)
Time after DEAC-k5
incubation (hr)
DEAC-k5 penetration(+) cells (%)
c
[3TAT]=3 μM
anti-IgG (20x)
Penetration(+):
36±2%
10 μm
anti-BMP (20x)
Penetration(+):
6±0.5%
Normalized lysate
fluorescence intensity
ns
3TAT:
anti-IgG:
anti-BMP:

2.2.2 In vitro characterization of 1TAT, 2TAT and 3TAT

To test whether the involvement of late endosomes and BMP could be corroborated *in vitro*, lipid bilayer leakage assays were performed. Large unilamellar vesicles (LUVs) were prepared with membrane com- position mimicking that of the plasma membrane or early endosomes (PM/EE LUV: 65:15:20 PC:PE:Chol) or that of late endosomes (LE LUV: 77:19:4 BMP:PC:PE). The lipid composition for early and late endosomes is adapted from studies performed by Gruenberg et al. (126). It should be noted that in this and more recent studies, it was not possible to differentiate the lipid compositions between late endosomes and lysosomes. These LUVs were loaded with the green fluorophore calcein and membrane leakage upon treatment with peptides was evaluated by measuring calcein release (126). When mixed at a peptide-to-lipid ratio (P:L) of 1:50, 3TAT was unable to induce leakage of PM/EE LUVs. In contrast, 3TAT caused dramatic leakage of soluble lumenal dye from LE LUVs (Figure 2-4a; ~40%, 100% leakage being obtained after treatment of LUVs with the detergent Triton X-100). 3TAT did not induce leakage when BMP was substituted with its structural isomer PG. Because PG is negatively charged like BMP, this suggests that electrostatic interactions between the cationic peptide and an anionic lipid are not sufficient to induce leakage. This in turn implies that a relative specificity is involved in the interaction between 3TAT and BMP. Furthermore, addition of 250 μg/mL of anti-BMP was sufficient to inhibit 3TAT-mediated leakage. In this assay, the amount of peptide added exceeds that anti-BMP by a factor of 3×10^6 (5 μM vs 1.7×10^{-6} μM). As previously reported, anti-BMP does not block peptide binding to the lipid membrane. Instead, it inhibits contact

between BMP-containing liposomes (202,238). Notably, preincubation with anti-IgG had no effect on the leakage. Together, these results mirror those obtained *in cellulo* and further validate the involvement of the late endosome and of its lipid BMP in the process of endosomal escape.

To establish how 1TAT, 2TAT and 3TAT differ in their membrane-disruption activities, LE liposomes were treated with the peptides and leakage was quantified (total lipid concentrations are kept constant). At low P:L, both 2TAT and 3TAT induced leakage, 3TAT being consistently more active than 2TAT. In contrast, 1TAT showed negligible membrane disruption. When increasing peptide concentration and P:L ratio, the leakage activity of both 2TAT and 3TAT reach a maximum but, instead of displaying a continual increase, the extent of induced leakage declines to levels comparable to 1TAT. Interestingly, we observed that the leakage activity of 2TAT and 3TAT appeared to be correlated with the turbidity of the liposomal suspensions. For instance, upon centrifugation, a pellet of liposomes coated with the red-colored 3TAT was obtained at a P:L ratio of 1:50, a condition leading to liposomal leakage (Figure 2-4a-c). Because the liposomes do not form a pellet in the absence of peptide at the centrifugation speed used here (data not shown), this suggests that 3TAT can cause liposomes in suspension to flocculate and sediment. Remarkably, at a P:L ratio of 1:10, the liposomes did not form a noticeable pellet upon centrifugation. This behavior correlated with an inversion of charge on the surface of liposomes, as indicated by zeta potential measurements (Figure 2-4c). In particular, addition of increasing amounts of peptide changes the zeta potential of the particles from highly negative (zeta potential of

−58.9 V for BMP- containing liposomes in the absence of peptide) to highly positive (e.g., +39.7 V at 1:10 3TAT:L; zeta potential measurements were not possible when excessive flocculation takes place at intermediate P:L). Together, these results are consistent with the notion that as 3TAT coats the surface of liposomes, the negative charges of the lipids are neutralized. Liposomes may then flocculate either because of the absence of repulsive electrostatic forces, or because of the bridging action of the peptide itself. In contrast, as the amount of peptide partitioning on the surface of liposomes increases, particles become positively charged and repulsion is restored (our data also suggest that coating of the liposome surface with peptide happens faster than leakage does). Notably, similar behaviors were observed with 1TAT and 2TAT with the exceptions that higher P:L were necessary to abolish flocculation. In addition, it is worth noting that 3TAT induced flocculation even at low P:L and that overall, 2TAT can do what 3TAT does (i.e., leakage, flocculation and liposomes charge inversion), albeit at higher concentrations. It is, however, clear that while 1TAT can also bind to liposomes and induce their flocculation, it fails to induce significant leakage. Overall, while contact between liposomes appears to be necessary for leakage, it may not be sufficient.

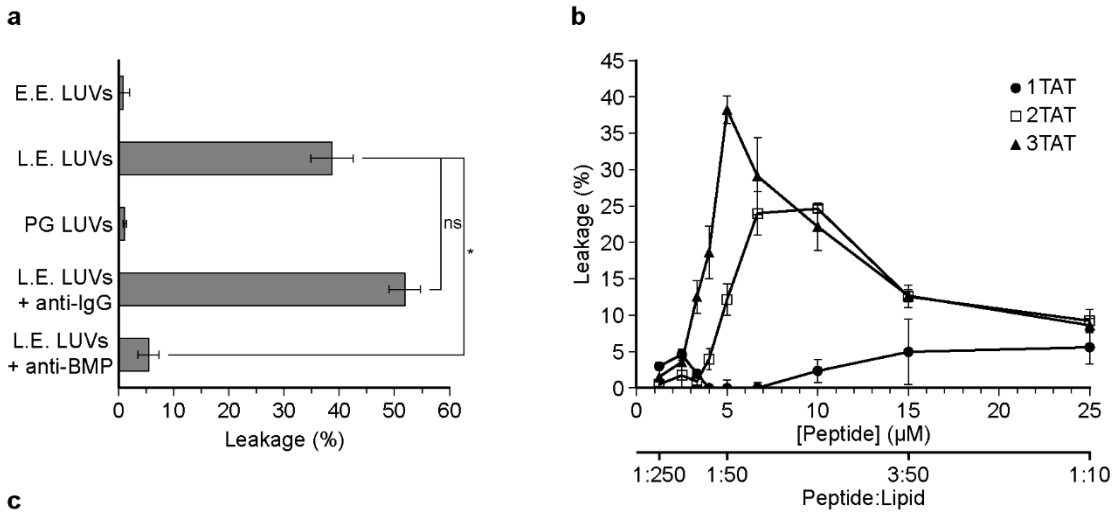

c

P:L	1:250			1:50			1:10			3:10	1.5:10
Peptide	1TAT	2TAT	3TAT	1TAT	2TAT	3TAT	1TAT	2TAT	3TAT	1TAT	2TAT
Zeta potential (mV)	-53.0	-50.4	-51.3	N/A	N/A	N/A	N/A	N/A	+39.7	+21.7	+35.2
Flocculation	No	No	Yes	Yes	Yes	Yes	Yes	Yes	No	No	No

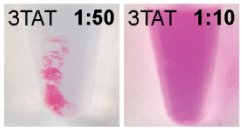

Figure 2-4 Supercharged peptides induce lysis over BMP-containing membranes. (a) 3TAT causes the leakage of LUVs with a lipid composition consistent with that of the late endosome (LE LUVs, 77:19:4 BMP:PC:PE) but does not disrupt LUVs with a lipid composition consistent with that the early endosome (EE LUVs, 65:15:20 PC:PE:Chol). LUVs (250 μM total lipid), preloaded with the green fluorophore calcein, were treated with 3TAT (5 μM) for 1 hr. Membrane leakage was assessed by measuring the release of calcein. The peptide activity is normalized against the leakage obtained after treatment of LUVs with 1% of the detergent Triton X-100. PG LUVs correspond to LE LUVs in which the lipid BMP is substituted to its isomer phosphatidyl glycerol (PG). The effects of the monoclonal antibodies anti-IgG and anti-BMP (250 μg/mL). The data represented correspond to the mean of triplicates. NS, $p>0.05$; * $p<0.05$. (b) The leakage of LE LUVs induced by 2TAT or 3TAT displays a non-linear dose response. LE LUVs (250 μM total lipid) were treated with peptides at the indicated concentrations (peptide:lipid ratios are also provided) for 1 hr. The release of calcein from LUVs was then quantified. The data reported is the mean of technical triplicates and the corresponding standard deviation. (c) Table representing the zeta potential measurements and flocculation propensity of liposomal suspensions at different peptide:lipid ratios. Flocculation was determined by visual examination of the sample after centrifugation (photographic examples of two conditions, P:L of 1:50 and 1:10 for 3TAT, are provided). Under conditions where substantial flocculation occurred, it was not possible to take zeta potential measurements as the number of particles in colloidal suspension was too low. Values in each experiment are represented as the mean percentage with resultant standard deviation of triplicate experiments. The figure is used with permission (235).

Considering both the *in cellulo* and *in vitro* results gathered thus far, it is surprising that such low activity is reported for 2TAT despite the very high activity we reported for the TAT-dimer, dfTAT. One notable difference between the 2 peptides is that 2TAT is labeled with only one fluorophore, while dfTAT is labeled with 2. To investigate whether the fluorophore plays a role in the membrane activity of 2TAT and 3TAT, non-fluorescent variants, nf2TAT and nf3TAT, were synthesized (Figure A-2g-i in Appendix A). The non-fluorescent peptides were then assayed for cell penetration, cytotoxicity, delivery of macromolecules and membrane lytic activity of late endosomes (Figure A-7 in Appendix A). Because these peptides do not contain a covalent fluorescent label, cell penetration was assayed by the ability of the non-fluorescent peptides to deliver the small molecular cargo DEAC-k5 or the enzyme TAT-Cre. In all assays, the trend observed for nf2TAT and nf3TAT across all the conditions assayed is similar to that of 2TAT and 3TAT. Namely, the peptide with 3 TAT branches is more active than the analog with only 2. However, the non-fluorescent analogs are overall less active than the fluorescent counterparts. In particular, nf3TAT requires higher concentrations than 3TAT to achieve similar cell delivery activities. The lytic activity of nf3TAT towards liposomes is also substantially less than that of 3TAT.

To gain additional insights into the complex behavior of the peptides with LE LUVs, liposomal suspensions treated with 1TAT, 2TAT and 3TAT were analyzed by Burst Analysis Spectroscopy (BAS), a single particle technique that permits quantitative analysis of liposome size distributions in heterogeneous samples (239,240). In these assays, liposomes were doped with a membrane staining carbocyanine fluorescent dye,

Vybrant DiD (0.03% of total lipid). Fluorescence bursts were first recorded from individual liposomes as they advectively flowed through the detection volume of a custom 2-channel confocal microscope at velocities much greater than the rate of particle diffusion. The underlying particle size distribution was reconstructed by BAS from the observed fluorescence burst amplitude distribution (240). The resulting BAS size distributions from the DiD channel are then directly proportional to liposome membrane con- tent, while the TMR amplitude distributions measure the amount of bound peptide. We examined samples representing P:L ratios in the range 1:2500 to 1:200. We envisioned that these conditions would be representative of the early steps in liposomal flocculation and possibly reveal how peptides and lipids interact as membrane leakage is initiated. As shown in Figure 2-5a, addition of peptides to liposomal suspension at these low P:L ratios induced a shift of the liposomes to much larger mean particle size for both 2TAT and 3TAT. This indicates that the particles detected contain a much greater level of lipid bilayer content as more peptide is added. By contrast, the shift in mean particle size upon the addition of 1TAT was far more modest. These results demonstrate that, while the binding of 1TAT does not dramatically alter the size distribution of the liposomes, the binding of 2TAT and 3TAT fundamentally restructures the liposome particles in suspension. To assess whether this restructuring can be linked to differences in peptide binding, the ratio of TMR signal to DiD signal was plotted for all correlated burst events (Figure 2-5b). At the lowest concentration of peptide tested (1 nM), the distribution of the TMR/DiD burst amplitude ratios are shifted to higher values for 2TAT and 3TAT vs 1TAT, indicating that the branched species may have a higher

binding affinity for the liposomes than the monomeric peptide. In contrast, at 5 nM, the TMR/DiD ratio distribution is similar for all 3 peptides. This strongly suggests that, for the same number of peptide molecules bound, 1TAT does not cause an increase in membrane content per particle detected but that 2TAT and 3TAT do. Importantly, each molecule bound leads to 1, 2 or 3 TAT copies being present on the surface of the lipid bilayer for 1TAT, 2TAT and 3TAT, respectively. Therefore, we next examined how the behavior of the peptides compares when differences in absolute TAT content are taken into account. For this test, the binding of 1TAT at 12.5 nM (the maximal peptide concentration accessible in our BAS experiments without causing detector saturation) was evaluated. Under this condition, a large population of liposomal particles can be observed that contain levels of bound 1TAT peptide that exceeds by several- fold (>3-fold) the amount of 2TAT and 3TAT bound at 5 nM. However, the liposomes coated with this higher amount of 1TAT retain a smaller mean particle size than liposomes coated with substantially less 2TAT or 3TAT. These results, therefore, suggest that the differential impact of 1TAT vs 2TAT or 3TAT on the liposome size distributions are not a consequence of how much peptide is bound per se, but to differences in how the peptides interact with the membrane.

To further reveal the basis for the 3TAT-mediated flocculation and leakage, liposomal samples were analyzed by cryo-electron microscopy (241). Liposomes were treated with peptides at a P:L ratio of 1:50, conditions that lead to maximal leakage for 3TAT. Untreated LE liposomes were on average bilamellar (Figure 2-5d). It is notable that BMP-containing liposomes have a propensity to spontaneously form multivesicular

structures at acidic pH (126). When treated with 1TAT, the lamellarity of the liposomes increased, albeit to a modest extent. In contrast, liposomes treated with 3TAT showed several clear differences. Consistent with both the observed propensity to sediment and increases in particle size observed by BAS, the liposomes were clustered (Figure 2-5c). The number of bilayers present per liposome was also significantly increased, with up to 20 layers observed in a single liposome (Figure 2-5d). Finally, multilamellar liposomes displayed thick external membranes. This apparent thickness is the result of several bilayers being in close proximity (Figure 2-5c). The vicinity between bilayers is particularly high. This is exemplified by the fact that, in the absence of peptide, a solvent layer is present between liposomes, even when liposomes are forced against one another (as illustrated by membrane distortion in Figure 2-5c). An interstitial solvent layer is, however, not visible when 3TAT is present. Together, these data demonstrate that 3TAT has the ability to bring lipid bilayers into close contact and reconfigure liposomes into complex multilamellar structures. However, 1TAT does not display these activities.

Figure 2-5 3TAT causes restructuring of BMP-containing membranes which leads to leakage of lumenal contents.
(a) 2TAT and 3TAT cause increases in the size and membrane content of LE LUVs when 1TAT does not. LE LUVs doped with DiD (2.5 μM total lipid, 0.03% DiD) and treated with peptide at indicated concentrations were analyzed by Burst Analysis Spectroscopy (BAS) (240). Fluorescence bursts from individual DiD-labeled liposomes in each sample are detected and quantified. Each fluorescent event is binned based on its fluorescence intensity and the overall population is represented as a heat map (242). The x-axis is a logarithmic scale of DiD fluorescence burst amplitude (which is directly proportional to liposome size) while the color of each bin is pseudo-colored blue to yellow and is proportional to the concentration of liposomes of a given size. The data represented is the compilation of triplicates. (b) Differences in binding affinity do not contribute to the lower membrane perturbing behavior of 1TAT when compared to 2TAT and 3TAT. Peptide binding to individual liposomes was assessed in two color BAS experiments by measuring the ratio of the fluorescence of the peptide ($F_{peptide}$, TMR signal) to the fluorescence of the membrane ($F_{membrane}$, DiD signal) obtained for each burst event detected during a BAS measurement. The data represented is the compilation of triplicates. (c) 3TAT causes the flocculation and fusion of LE LUVs and favors lipid bilayer contacts. LE LUVs (250 μM total lipid) were treated with 1TAT or 3TAT peptides (5 μM), sedimented, and imaged by cryo-electron microscopy (241). Untreated LE LUVs were imaged as a control. Insets represent zoomed in portions of images to highlight lipid bilayer contact or the lack there of. (d) Images of liposomes were quantified for lamellarity (number of lipid bilayers present in individual spherical liposomal structures). Each data point represents a liposomal structure observed from cryo-EM images (each experiment was duplicated, and 5 images were acquired per sample). The figure is used with permission (235).

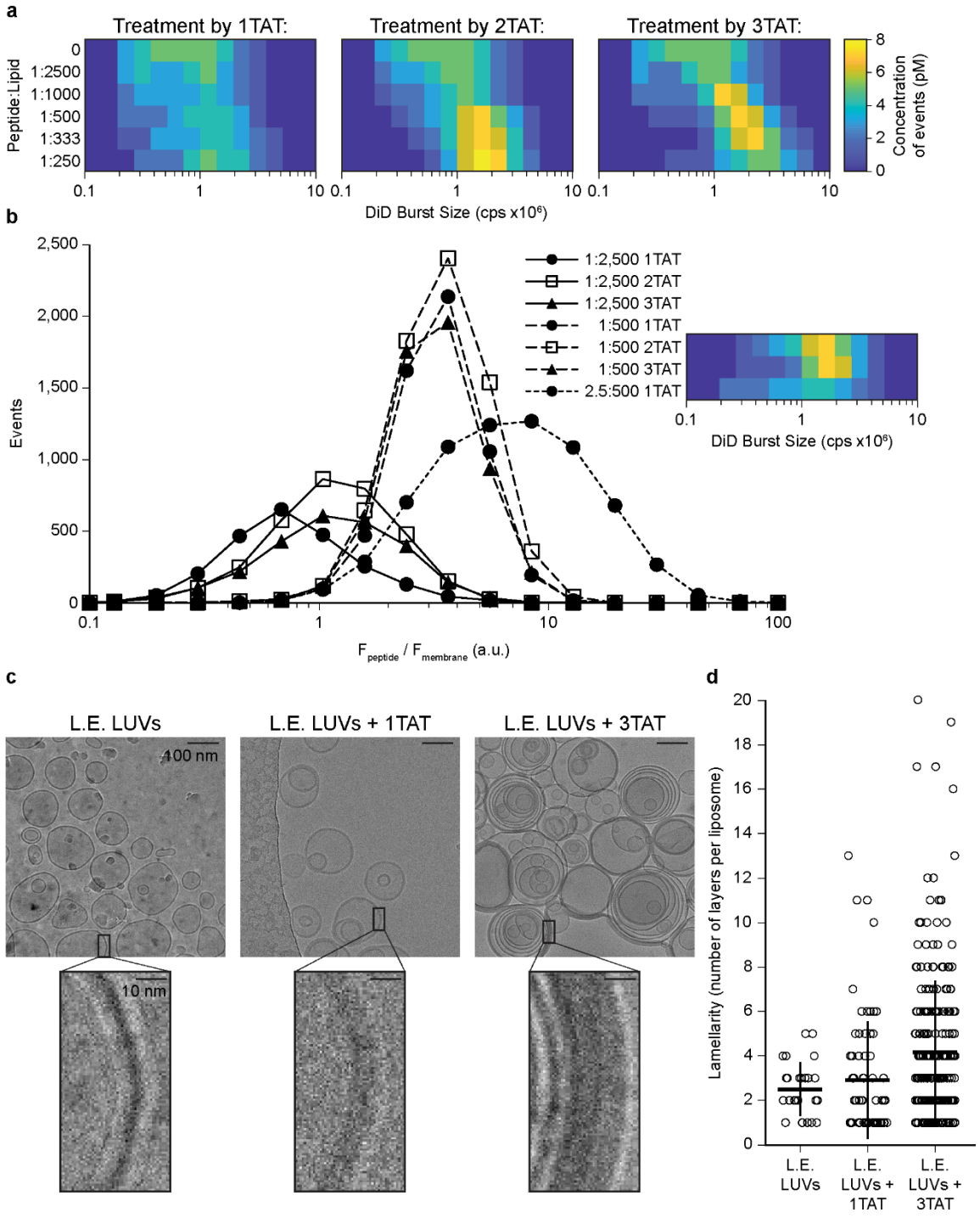
a
Treatment by 1TAT:
Treatment by 2TAT:
Treatment by 3TAT:
Peptide:Lipid
0
1:2500
1:1000
1:500
1:333
1:250
0.1
1
10
DiD Burst Size (cps x10⁶)
Concentration of events (pM)
8
6
4
2
0
b
Events
2,500
2,000
1,500
1,000
500
0
0.1
1
10
100
F peptide / F membrane (a.u.)
1:2,500 1TAT
1:2,500 2TAT
1:2,500 3TAT
1:500 1TAT
1:500 2TAT
1:500 3TAT
2.5:500 1TAT
DiD Burst Size (cps x10⁶)
c
L.E. LUVs
L.E. LUVs + 1TAT
L.E. LUVs + 3TAT
100 nm
10 nm
d
Lamellarity (number of layers per liposome)
20
18
16
14
12
10
8
6
4
2
0
L.E. LUVs
L.E. LUVs + 1TAT
L.E. LUVs + 3TAT

2.3 Discussion

The cellular assays performed in this study demonstrate that the number of branches present in the peptide constructs dramatically impact cell penetration. For instance, the efficiency of endocytosis, endosomal escape, and cargo delivery is consistently greater for 3TAT than for 2TAT. The monomeric 1TAT, an analog of the proto- typical and widely used HIV TAT peptide, is relatively poor in all activities and clearly outperformed by 3TAT. In particular, the relatively sensitive Cre recombinase assay illustrates how 1TAT can only deliver the enzyme in few cells. In turn, the SNAP-Surface assay and the monitoring of the cellular distribution of the peptide itself indicate that the delivery activity of 1TAT is too poor for microscopy detection. Notably, 1TAT and 2TAT are typically unable to produce the results obtained with 3TAT even when the concentration of the monomeric and dimeric constructs is increased to match the total amount of TAT species present in each condition. These results, therefore, highlight that covalently linking of several TAT copies produces effects that are not obtained when the same number of individual TAT peptides are present. In other words, raising the concentration of 1TAT can never reproduce what is achieved with 3TAT. One of the positive effects observed with peptide branching is a high propensity for endocytosis. In particular, the overall peptide internalization quantified in Figure 2-1e is a measure of endocytic uptake efficiency. This is because, although 3TAT distributes in the cytosol and nucleoli of cells, it needs to be first endocytosed to reach these localizations (the total amount of peptide present in the cell was, therefore, originally taken up by endocytosis first). As such, the endocytosis of 3TAT, 2TAT and 1TAT is proportional

the peptide copy numbers, indicating that a multibranch display is favoring endocytosis-inducing interactions on the cell surface. This effect is potentially mediated by the clustering of heparan sulfate proteoglycans, known interaction partners of polycationic CPPs on the cell surface (243-245). Moreover, the enhanced endocytic uptake of 3TAT may contribute to making this compound more prone than 2TAT or 1TAT at escaping endosomes. As a matter of fact, by being able to accumulate inside endosomes at higher levels than monomeric or dimeric counterparts, 3TAT may be able to reach a membrane-disruption concentration threshold more readily. However, the connection between endocytic uptake and endosomal escape may be more complicated. This is because 2TAT does not escape from endosomes as well as 3TAT, even when 2TAT is endocytosed at higher levels than 3TAT (e.g., 4.5 μM 2TAT vs 1 μM 3TAT, Figure 2-1e). Instead, our results indicate that 3TAT is also more prone to induce membrane disruption and endosomal leakage than 2TAT and 1TAT.

The enhanced membrane-disruption efficacy of 3TAT is corroborated *in vitro*, with liposomes mimicking the lipid bilayers of late endosomes. It should be noted that late endosomes are organelles with a limiting membrane and multiple intralumenal vesicles with a size and composition consistent with the liposomes tested. These membranes are also known to undergo fusion and fission endogenously, indicating that contact between these membranes is possible in the context of a living cell (126). Notably, several results point to 3TAT-mediated bilayer-to-bilayer contact, a previously unknown activity of polycationic delivery agents, as an important process involved in membrane translocation. BAS measurements indicate that 3TAT increases the total

amount of lipid per particle detected. Cryo- EM confirms that 3TAT brings lipid bilayers into close proximity, thereby causing liposome-to-liposome clustering as well as juxtaposition of lipid bilayers within an individual liposome. Interestingly, the increase in lamellarity observed by cryo-EM and the contact between bilayers has several implications. First, while multilamellar liposomes have a size comparable to that of untreated liposomes, the large increase in absolute bilayer content per liposome is indicative of fusion between many unilamellar liposomes. For instance, given that the intralumenal bilayers have a radius approximately equal to the radius of the external bilayer, formation of a liposome with 7 bilayers would require the fusion of approximately 7 unilamellar liposomes of equivalent size. However, the 3TAT-mediated fusion activity, instead of leading to larger liposomes (7 unilamellar liposomes of a radius r may fuse to a unilamellar liposome of radius $\sqrt{7}r$, or 2.6r), leads to the collapse of liposomes into smaller but multilamellar structures. This collapse could be contributed by BMP, as this lipid has a propensity to spontaneously promote multilamellarity. The fact that there is contact between bilayers of virtually identical radii (as in the "thick" membrane highlighted in Figure 2-5c) also highlight that 3TAT must act as a bridging agent that keeps the bilayers glued to one another.

Induced membrane fusion is in itself not sufficient to explain the cell penetration activity of 3TAT. This is because fusion does not imply translocation across membranes. In other words, fusion of late endosomal vesicles does not equate to endosomal escape. It is, therefore, more probably that the leakage activity of 3TAT detected *in vitro* is more pertinent to the mechanism of endosomal escape and cytosolic entry. However, we

envision that leakage and fusion are intimately related. In particular, leakage appears to decrease when liposomes cease to flocculate. Furthermore, leakage does not take place with 1TAT, a compound that also has a limited ability to induce multilamellarity and bilayer contact. The decline in leakage observed at high peptide to lipid ratios may also indicate that leakage requires liposomal contact. Indeed, liposomes do not sediment when leakage is low. Finally, anti-BMP, an antibody that can block the fusion of BMP-containing liposomes, can inhibit membrane leakage, *in vitro* and *in cellulo* (202,238). Overall, it would, therefore, seem that 3TAT, by coating the surface of liposomes, directly creates linkages between various lipid bilayers. This, in turn, causes membrane contact that overcomes liposomal repulsion and allows leakage to occur. When treated with a higher concentration of peptide, these 3TAT-bound liposomes possess a net positive charge restoring repulsion between individual liposomes resulting in no leakage. While the compounds tested clearly highlight the influence of the number of branches present in the constructs, several questions remain open. For instance, 2TAT performed poorly in our assays in comparison to the previously reported reagent dfTAT, although both reagents contain 2 TAT copies. Structural features, such as the number of fluorophores bound or the linker length between TAT branches may, therefore, play a role in membrane permeabilization. The contribution of the fluorophore in our constructs is highlighted herein by the decrease membrane-disruption activities observed for the non-fluorescent analogs. It is, therefore, possible that the fluorophore, when attached to 2TAT and 3TAT, interacts with lipid bilayers and enhances membrane destabilization. Notably, this contribution is not sufficient to cause substantial membrane leakage when

the fluorophore is linked to a single copy of the peptide, as in 1TAT. Overall, these results, therefore, indicate that, while a threshold charge density is required to induce membrane leakage by the molecules reported, other parameters, such as perhaps the relative hydrophobicity of a fluorophore, can further enhance this activity. A detailed characterization of what these parameters may be will be the object of future studies.

Another question left open is the topic of toxicity, specifically when comparing 3TAT to dfTAT. While 3TAT displays a delivery efficiency and mode of cellular entry similar to dfTAT, 3TAT is relatively toxic while dfTAT is relatively innocuous (dfTAT-mediated delivery does not noticeably impact viability, proliferation rates or transcription). On one hand, disrupting cellular membranes to gain cytosolic access can obviously be damaging to cells. It may not, therefore, be surprising that 3TAT is toxic, though it remains remarkable that dfTAT is not. Notably, because of its disulfide linkage, dfTAT is reduced into TAT monomers upon entry into the cytosolic space (137,187). The membrane-disrupting activity of the reagent is, therefore, greatly reduced after delivery is achieved. In contrast, 3TAT, while presumably susceptible to partial proteolytic cleavage, should remain trimeric and membrane active after cytosolic entry. 3TAT could, therefore, kill cells by disrupting the membrane of various intracellular organelles, a scenario that will be examined in future studies. Finally, it should be noted that our study does not directly address whether the branching design of the multivalent CPPs tested is necessary for efficient cellular penetration. For instance, it is possible that a linear peptide containing 3TAT sequence back-to-back could reproduce some of the activities observed with 3TAT. Unfortunately, we could not test this possibility because,

in our hands, the solid-phase peptide synthesis of linear constructs failed due to extremely poor coupling yields during the incorporation of residues of the second and third TAT segments. Such issue is well-known limitation of SPPS and, perhaps, this high- lights a benefit of synthesizing branched structures containing shorter sequences. Overall, because of their synthetic accessibility and of their advantageous cell penetration properties, branched CPP structures may provide new opportunities in the delivery field.

2.4 Materials and Methods

2.4.1 Peptide design, synthesis, purification, and characterization

Peptides were synthesized on Rink amide MBHA resin (Novabiochem). The amino acids used in synthesis were Fmoc-Lys (Mtt)-OH, Fmoc-Gly-OH, Fmoc-Arg(Pbf)-OH, Fmoc-Gln(Trt)-OH and Fmoc-Lys(Boc)-OH (Novabiochem) (0.78 mmol). Reactions were performed in a glass vessel at room temperature while streaming dry N_2 for effective mixing. Deprotection of Fmoc was accomplished by incubation of the peptide-bound resin with a mixture of piperidine in dimethylformamide (DMF) (Fisher Scientific) (20%, 15 mL). Two deprotections were performed for 5 and 15 min, respectively, washing with DMF in between deprotections. Coupling reactions of the amino acids to synthesize the peptide scaffold were performed for 4 hr with streaming dry N_2 at room temperature using a solution containing the Fmoc-protected amino acid (4 mmol), HCTU (Novabiochem) (3.9 mmol) and diisopropylethylamine (DIEA) (Sigma-Aldrich) (10 mmol) dissolved in DMF. In between coupling reactions, the resin was washed extensively with DMF (Fisher Scientific). Once synthesized, peptide

scaffolds were labeled using a mixture of 5(6)-TAMRA (Novabiochem), HCTU and DIEA (3, 2.9 and 7.5 eq., respectively) in DMF that was allowed to react overnight at room temperature under dry N_2. For the non-fluorescent variants, nf2TAT and nf3TAT, the scaffold's N-terminus was rendered relatively inert via standard acetic anhydride-mediated acetylation. After the peptide scaffolds were labeled with TMR or acetylated, Mtt deprotection was carried out using a solution of 1% trifluoroacetic acid (TFA) (Fisher Scientific) and 2% triisopropylsilane (TIS) (Sigma-Aldrich) in dichloromethane (DCM), and, in between deprotections, the resin was washed with DCM, DMF and methanol. For the synthesis of 1TAT, 2TAT and 3TAT, equivalents of coupling solutions were adjusted to Fmoc-protected amino acid (3, 6 and 9 mmol, respectively), HCTU (2.9, 5.8 and 8.7 mmol, respectively) and DIEA (7.5, 15 and 22.5 mmol, respectively) in DMF and allowed to react while streaming dry N_2 overnight for each coupling. Upon completion of each peptide, the N-terminal Fmoc was deprotected and the resin was washed with DCM and dried in vacuo. For cleavage of peptide from the resin, a solution containing 2.5% H_2O, 2.5% TIS and 95% TFA was added to the resin and allowed to react for 3 hr at room temperature to achieve cleavage as well as deprotection of the side chain of each amino acid. Upon completion of the cleavage, crude peptide products were allowed to precipitate in cold, anhydrous diethyl ether (Fisher Scientific). Precipitants were then resuspended in H_2O and lyophilized. Dried peptide products were then resuspended in 0.1% TFA in H_2O and then analyzed and purified by reverse-phase HPLC. rpHPLC analysis was performed on an Agilent 1200 series instrument with an analytical Biobasic-18 C18 column (Thermo Scientific) (5 μm

particle size, 4.6 × 250 mm). The flow rate was 2 mL/min, and absorbance at λ = 214, 556 nm was measured using a diode array detector (Agilent). Preparative HPLC was performed on an Ultimate 3000 preparative HPLC (Thermo Scientific) with a preparative Biobasic-18 C18 column (Thermo Scientific) (10 μm particle size, 21.2 × 250 mm). The flow rate was 20 mL/min, and absorbance at 214 and 556 nm was measured using a diode array detector (Thermo Scientific). For all analytical and preparative runs, linear gradients using 0.1% aqueous TFA (solvent A) and 90% acetonitrile, 9.9% H_2O and 0.1% TFA (solvent B). Correct peptide products were confirmed via MALDI-TOF using a Shimadzu/Kratos instrument (AXIMA-CFR). The expected mass for 1TAT was 2447.90 Da; 1TAT observed mass was [M-H+/H+] = 2448.55 Da. The expected mass for 2TAT was 3784.53 Da; 2TAT observed mass was [M-H+/H+] = 3784.53 Da. The expected mass for 3TAT was 5121.16 Da; 3TAT observed mass was [M-H+/H+] = 5121.83 Da. For the fluorescent peptides, concentration was determined using Beer's law over the absorbance of TMR. For the non-fluorescent peptides, back-calculation of the concentration was made possible by utilizing amino acid analysis (Protein Chemistry Lab, TAMU).

2.4.2 Cell penetration and delivery experiments

Cells were seeded and grown to 100% confluency after 24 hr. Prior to treatment, cells were washed twice with Leibovitz's L-15 medium (L-15) (Fisher Scientific). Cells were then either incubated with peptide or coincubated with peptide and cargo, 4 μM TAT-Cre or 50 μM SNAP-Surface 488 (NEB), at specified concentrations at 37°C for 30 min. Immediately following incubation, cells were washed twice with L-15

containing heparan (1 mg/mL) and once with L-15. To assess cytotoxicity, cells were treated with 2.5 μM SYTOX Blue or SYTOX Green 1-hr post-treatment. SYTOX dyes are cell-impermeable and are only capable of staining nucleic acids if a cell has a compromised plasma membrane. Fluorescence microscopy was performed using an inverted microscope (Olympus IX-81) with both 20× and 100× objectives as well as a heated stage (37°C) and images were taken using a Rolera-MGI Plus back-illuminated electron- multiplying CCD camera (Qimaging). Filters used in fluorescence imaging included DAPI (λex/λem = 300-388, 425-488 nm), CFP (λex/ λem = 420-450, 450-600 nm), FITC (λex/λem = 450-490, 500-550 nm) and RFP (λex/λem = 535-580, 570-670 nm) filter cubes (Chroma Technology).

Cytosolic penetration and delivery of cargo was determined, qualitatively, by 100× imaging and quantitatively by 20× imaging. Cells scored for penetration or delivery of cargo (nuclear or cytosolic fluorescence distribution) were counted using Slidebook and ImageJ software. Cells were not counted for penetration if they displayed SYTOX staining. The percentage of cells with successful penetration or delivery of cargo was determined by dividing scored cells by total cells. The total number of cells was determined by Hoechst 33342 stain (5 μM) for penetration, cells that transiently expressed EGFP using the control plasmid gWiz for TAT-Cre or cells stained with SNAP-Cell Fluorescein (5 μM) for SNAP-Surface 488. In each experiment, more than 1000 cells were counted to assess penetration and delivery efficiency, as well as cytotoxicity. Fluorescent images acquired using the 100× objective were subjected to deconvolution using the Slidebook software. Each experiment was performed in

triplicate. It is important to note that in each cell assay, individual wells were used for each condition as prolonged or repeated exposure of light to the TMR-labeled peptides can lead to the artifact of photolysis, extensively covered in the following publications.

To measure the whole cell lysate for peptide uptake, cells were grown and treated as before with each peptide at varying concentrations. Post-treatment, cells were harvested by treatment with 0.5% trypsin in PBS for 3 min followed by suspension and dilution in L-15 medium. Cells were pelleted by centrifugation at 1500×g for 10 min, resuspended in L-15 and then treated with 2× lysis buffer (50 mM Tris, pH 7.4, 2 mM EDTA, 1× HALT protease inhibitors (Thermo Scientific) and 20% Triton X-100) and vortexed to complete lysis. The cell lysates were then transferred to a 96-well plate where 3TAT fluorescence was measured using the green channel (Em = 525; Ex = 580-640 nm) of a GloMax-Multi+ detection system plate reader (Promega). Triplicate experiments were performed and measured on the same day to avoid fluctuation in fluorescence read out.

To measure colocalization of 1TAT or DEAC-k5 with LysoTracker Green (Thermo), cells were grown to 100% confluency and then treated with 9 μM 1TAT for 30 min or 25 μM DEAC-k5 for 1 hr. Cells were washed as before then treated with 500 nM LysoTracker Green at 0, 1 or 3 hr after DEAC-k5 treatment. Cells were imaged at 100× magnification using fluorescence microscopy to produce representative images of colocalization. Finally, colocalization was determined using the colocalization function of the software ImageJ. Pearson's colocalization coefficient, R, and Manders'

colocalization coefficient, M1, were reported to effectively determine the degree of colocalization.

2.4.3 Expression and purification of TAT-Cre

The gene for TAT-Cre from pTriEx-HTNC (Addgene) was cloned into the vector pTXB1 and transformed into *Escherichia coli* BL21 (DE3) cells (Agilent Technologies) using a standard heat shock method. LB media containing 100 μg/mL of ampicillin was inoculated with colonies containing the plasmid and allowed to grow shaking at 37°C overnight. Cultures were then used to inoculate 1 L of LB containing ampicillin and allowed to grow until OD_{600} = 0.6. Cultures were then induced with 1 mM Isopropyl-β-D-1-thiogalactopyranoside (IPTG) (Fisher Scientific) and grown, shaking, at 37°C for 3 hr. *Escherichia coli* cells were then pelleted by centrifugation using a J2-21 (Beckman) centrifuge and a JA-10 rotor at 4000 RPM x 30 min at 4°C. Cell pellets were then resuspended in buffer containing 20 mM NaH_2PO_4, 500 mM NaCl and 20 mM imidazole and then cells were lysed by sonication for a total sonication time of 8 min. Cell debris was removed from the whole-cell lysate by centrifugation using a JA-20 rotor at 17000 RPM x 45 min at 4°C. TAT-Cre was then purified using metal-affinity chromatography (HisTrap HP) (GE Healthcare).

2.4.4 Transfection

For experiments requiring transfections, cells were first grown to 80% confluency and then treated with transfection solutions. For TAT-Cre delivery, HeLa cells were transfected with the plasmid pCALNL (Addgene) using Lipofectamine 2000 (Thermo). For SNAP- Surface 488 (NEB) delivery, FuGene HD (Promega) was used to

transfect HeLa cells with the plasmid pSNAP-H2B (NEB). In both conditions, cells were incubated with transfection solutions for 12 (Lipofectamine 2000) or 18 hr (FuGene HD) followed by a 12- or 6-hr recovery, respectively, in DMEM supplemented with 10% FBS prior to treatment.

2.4.5 Delivery of preloaded endosomal cargo

For this experiment, cells were grown to 100% confluency and then treated with 50 μM DEAC-k5 in L-15 for 1 hr. Cells were then washed twice in L-15 and then incubated with L-15 ± 200 nM bafilomycin (Sigma-Aldrich). Following this incubation, cells were washed and finally treated with 3TAT as before (± 200 nM bafilomycin). Ten min prior to imaging, cells were treated with 2.5 μM SYTOX Green to visualize and exclude dead cells.

2.4.6 Liposome Preparation

Liposomes were prepared using the following lipids: 1,2-di-(9Z-octa-decenoyl)-*sn*-glycero-3-phosphocholine (DOPC), 1,2-di-(9Z-octadece-noyl)-*sn*-glycero-3-phosphoethanolamine (DOPE), *sn*-(3-oleoyl-2-hydroxy)-glycerol-1-phospho-sn-1'-(3'-oleoyl-2'-hydroxy)-glycerol (S,S) (BMP) and cholesterol (ovine wool) (Chol) (Avanti Polar Lipids). For BAS experiments, liposomes were doped with 0.03% DiD (Vybrant).

Lipids dissolved in chloroform, at aforementioned ratios, were transferred to a clean glass vial and dried overnight in vacuo. Lipid cakes were hydrated in LUV buffer (10 mM NaH_2PO_4, 100 mM NaCl, pH 7.4) which contained 60 mM calcein if used in leakage assays. The hydrated lipid cake underwent multiple freeze thaw cycles and the generated MLVs were extruded to 100 nm LUVs using a 0.1 μm membrane (Whatman).

For BAS experiments, liposomes were further extruded using a manifold extruder (Northern Lipids) and a 0.05 μm membrane (Whatman). Liposomes loaded with calcein were purified from free calcein using Sephadex G50 resin (Fisher Scientific).

2.4.7 Cytosolic delivery of DEAC-k5 into live cells

LUVs (250 μM total lipid) loaded with calcein were mixed with varying concentrations of peptide (1-25 μM) in LUV Buffer (10 mM NaH_2PO_4, 100 mM NaCl, pH 5.5 [LE] or 7.4 [EE/PM]). Peptides were allowed to react with LUVs for 1 hr at room temperature, rocking in the dark. A supernatant was obtained by centrifugation at 15000×g for 2 min and then the supernatant was applied to an illustra NAP-10 column (GE Healthcare Life Science) to isolate free calcein. Free calcein was pooled and the fluorescence intensity was measured using the blue channel (Ex = 490 nm, Em = 520-560 nm) of a GloMax-Multi+ detection plate reader. To normalize leakage results, a positive control was conducted by treating LUVs with 0.2% Triton X-100. Where indicated, lipid composition of LUVs varied. For leakage experiments involving antibodies, LUVs were first treated with 250 μg/mL of anti-BMP or anti-IgG for 30 min, room temperature, followed by direct addition of peptide to the reaction mixture. Extent of liposomal leakage was determined as before (138).

2.4.8 BAS experiments

BAS measurements are taken with a custom-built, multichannel con- focal microscope, as previously described (239,240). Built on a research quality, vibrationally isolated 40 × 80 optical table, the system is con- structed around a Nikon Eclipse Ti-U inverted microscope base with a 60×/1.4NA CFI Plan Fluor oil-immersion objective.

The microscope base is outfitted with a precision, 2-axis stepper motor sample stage (Optiscan II; Prior) and a custom-designed confocal optical bench with 3 independent detection channels. Each detection channel is configured with an optimized bandpass filter set for wavelength selection and a low-noise, single photon counting APD unit (SPCM- AQRH-15; Excelitas). Photon pulses were collected, and time stamped with either a multichannel hardware correlator (correlator.com) or high-speed TTL counting board (NI9402; National Instruments). Sample excitation is provided by a diode laser (642 nm; Omicron) and a diode-pumped solid-state laser (561 nm; Lasos). The free-space beams of each laser are each coupled to a 3-channel fiber combiner (PSK-000843; Gould Technologies) and the combined output is directed into the sample objective with a custom, triple-window dichroic filter (Chroma). Each laser is addressable from the integrated control and data acquisition software, custom developed using LabView (National Instruments).

Liposomes, diluted to 2.5 μM in LUV Buffer pH 5.5, were mixed with 1TAT, 2TAT or 3TAT (1-12.5 nM). Each sample was spotted onto a BSA-blocked glass coverslip held in a custom cassette. The coverslip cassette was clamped to a high-precision, computer controlled, 2-axis translation stage connected to a customized microscope system. For all experiments, dual excitation was employed with 50 μW input power (measured at the back of the objective) for both 488 and 561 nm lasers. For each experimental run, 5 min of fluorescence burst data was recorded and each experiment was repeated a minimum of 3 times. The TMR/DiD was calculated from the raw burst that were coincident in both channels.

2.4.9 Cryo-EM and image processing

LE LUVs treated with 1TAT, LE LUVs treated with 3TAT and PG LUVs treated with 3TAT were frozen in vitreous ice on a Quantfoil R2/1 holey carbon grid with an FEI Vitrobot, respectively. Cryo-EM images were acquired on a K2 Summit Direct-detection camera (Gatan) in the electron-counting mode using a TECNAI F20 cryo-electron microscope (FEI) operated at 200 kV. A nominal magnification of 19000× or 7800× was used, giving a pixel size of 1.87 Å/pixel or 4.8 Å/pixel, respectively.

CHAPTER III

MEMBRANE FLUIDITY DIRECTLY IMPACTS THE EXTENT OF SUPERCHARGED CPP-INDUCED MEMBRANE LYSIS ON BMP-CONTAINING MEMBRANES

3.1 Introduction

In previous work, it was found that the guanidinium-rich compounds dfTAT and 3TAT exhibit highly efficient cell penetration activities (137,138,235). The source of this enhanced cell penetration stems from overcoming endosomal entrapment: the bottleneck of endocytosis-mediated cell penetration. dfTAT and 3TAT achieve endosomal escape via selective lysis of organelles with BMP-containing membranes. Structural studies revealed that 3TAT-mediated membrane lysis results from 3TAT-induced membrane restructuring (235). Restructuring events included an increase in lamellarity, induced fusion and, most importantly, lipid bilayer contact of BMP-containing liposomes. While these findings advanced the understanding of the mechanism of endosomal escape, many details remain unclear.

In this study, we sought to identify additional factors that contribute to the mechanism of endosomal escape. 1TAT, 2TAT, 3TAT and their non-fluorescent variants were used as model guanidinium-rich CPPs that vary in endosomolytic activities. In this pursuit, we found that introduction of cholesterol resulted in differential 3TAT-induced membrane leakage. Based on this finding, we hypothesized that manipulation of membrane fluidity will allow us to modulate the extent of membrane leakage. Herein, we demonstrate the reliance of the membrane lytic activity of 3TAT on the fluidity of

BMP-containing membranes. In turn, these findings will bestow greater understanding of the mechanism of endosomal escape for guanidinium-rich delivery tools and can potentially be extended to the endosomal escape mechanisms of supercharged proteins and viral capsids as well.

3.2 Results

3.2.1 3TAT-induced membrane leakage and restructuring is selective towards BMP-containing membranes

In previous studies, it was found that the guanidinium-rich compound 3TAT was capable of the selective lysis of BMP-containing membranes that mimic late endosomes (235). These results have been reproduced in order to highlight this specificity (Figure 3-1a). Large unilamellar vesicles (LUVs) were prepared with membrane compositions mimicking early endosomes (65:15:20 PC:PE:Chol), late endosomes (77:19:4 *sn*-3,3'-BMP:PC:PE), or late endosomes, in which BMP has been substituted for PG (77:19:4 PG:PC:PE). Additionally, LE LUVs utilizing *sn*-2,2'-BMP were generated for comparison, as this form of the lipid as it is thought to be the most biologically relevant form (REFs). The LUVs were loaded with calcein as a reporter for extent of membrane leakage. Upon treatment of calcein-loaded LUVs with 3TAT at a 1:50 peptide-to-lipid ratio (P:L), EE LUVs and PG LE LUVs remained intact, whereas LE LUVs (consisting of either form of BMP) demonstrated marked membrane leakage. These results suggest that 3TAT-induced leakage is selective towards BMP-containing membranes. The *sn*-2,2'-BMP form demonstrated a marginally greater degree of 3TAT-induced leakage than the *sn*-3,3'-BMP form. However, attempts to synthesize *sn*-2,2'-BMP failed in our

hands. For this reason, and since there was not a substantial difference in leakage, the commercially available *sn*-3,3'-BMP form was used for the rest of this study. While 3TAT has proven highly endosomolytic, an activity that is corroborated by the aforementioned *in vitro* studies, a range of membrane lytic activities can be tested by implementation of the non-endosomolytic agent 1TAT and the lowly endosomolytic agent 2TAT. To demonstrate this capability, calcein-loaded LE LUVs were treated with 1TAT, 2TAT, or 3TAT at 1:250 – 1:10 P:L in order to determine the amount of liberated calcein resulting from membrane leakage (Figure 3-1b). While 1TAT proved relatively innocuous, 2TAT and 3TAT exhibited substantial membrane lytic activity. To complement these results, we determined if the lack of membrane leakage of PG LE LUVs was corroborated by partitioning of 3TAT into an organic phase via induced inverted micelle formation (representative of the fusogenic activity of each lipid) (Figure 3-1c). For this experiment, partitioning of 3TAT into the hexane phase was determined by measuring the fluorescence of the TMR moiety of the peptide in the aqueous phase. Calculations were performed to determine the percentage of 3TAT that had portioned into the hexane phase. While both lipids were capable of partitioning 3TAT into the hexane phase, the rate of induction of BMP inverted micelle partitioning of 3TAT was substantially higher than that of the structural isomer.

To further the mechanistic understanding of this membrane lytic behavior, our focus diverted towards identifying parameters that influence membrane lysis of BMP-containing membranes. In the leakage experiments carried out, phosphate was used as a buffering salt. At the pH (5.5), the pH at which these experiments were conducted,

phosphate (10 mM) exists predominantly in the HPO_4^{2-} form (98% as calculated by Henderson-Hasselbalch). Therefore, this divalent anionic phosphate, existing in > 10^3 excess to that of 3TAT at 1:50 P:L, can act as a "bridging unit" to oligomerize 3TAT via electrostatic interactions, which may confer extensive membrane leakage. To test this possibility, calcein LE LUVs were generated and assayed with 3TAT in LUV buffer substituting phosphate for Tris, a monovalent, cationic buffering salt incapable of this electrostatic bridging effect (Figure B-1 in Appendix B). However, switching buffering systems led to no appreciable difference in membrane leakage for the conditions tested. The LE LUVs used in this study consist of 77 mol% BMP, as this is the value reported in the late endosomal membrane lipid analysis conducted by Gruenberg et al. (125,126). However, one key difference in regard to lipid distribution remains between the organelle and synthetic doppelgänger. The inner leaflet of late endosomes is composed almost entirely of BMP, whereas there is presumably a homogenous mixture of lipid between each leaflet of the LUV, resulting in only a 77 mol% composition of BMP (238). As such, calcein-loaded LUVs composed only of BMP were generated to more closely mimic the membrane composition of the interlumenal vesicles (ILVs) and inner leaflet of late endosomes (Figure 3-1d). Upon treatment with 3TAT, a substantial enhancement in membrane lytic activity was observed. In particular, the 1:10 P:L condition yielded a 4-fold activity enhancement. Intrigued by this finding, BMP content was then modulated to test the effectiveness of 3TAT-induced membrane lysis. For this experiment, calcein-loaded LUVs were generated as before following a 77-X:X:19:4 BMP:PG:PC:PE formula where BMP content was decreased by substitution with the

structural isomer PG. Importantly, this substitution allowed for the total amount of lipid and negative charge to remain constant while still modulating BMP content. Interestingly, at all conditions tested below 77 mol% BMP, little-to-no membrane leakage was observed. Taken together, these results suggest that not only must BMP be present but that it most compose a large majority (> 50 mol%) of the membrane in order to confer 3TAT-induced membrane leakage. Another key difference between late endosomes and the LUV mimic is the presence of cholesterol in the organelle. Late endosomes serve a role in the sorting and trafficking of cellular cholesterol to different cellular membranes (202,204,246). To probe the effect that the presence of this membrane component has membrane lysis, calcein loaded LE LUVs were generated, in which the PC component (19 mol%) was substituted for cholesterol (Figure 3-1e). Upon treatment with the indicated P:L of 3TAT, a greater extent of membrane leakage was observed in the cholesterol-containing LUVs. Notably, cholesterol is a known regulator of membrane fluidity. With this in mind, these data suggest that modulating membrane fluidity may affect 3TAT-induced lysis towards BMP-containing membranes.

Figure 3-1 Identification of membrane parameters that influence the membrane lytic activity of guanidinium-rich CPPs.
(a) 3TAT-induced membrane leakage is specific to 2,2'- or 3,3'-BMP-containing membranes that mimic the late endosomal lipid composition. LUVs (250 μM total lipid), preloaded with the green water-soluble fluorophore calcein (60 mM), were treated with 3TAT (5 μM) for 1 hr. Membrane leakage was assessed by measuring the release of calcein. The peptide membrane lytic activity is normalized against the leakage obtained after treatment of LUVs with 1% of the detergent Triton X-100. EE LUVs refer to LUVs mimicking early endosomal membranes (65:15:20 PC:PE:Chol); LE LUVs refer to LUVs mimicking late endosomal membranes (77:19:4 X:PC:PE, where X = PG, 2,2'-BMP or 3,3'-BMP where indicated). (b) The resulting 2TAT- and 3TAT-induced membrane lysis presents a non-linear dose response. Calcein-loaded LE LUVs (250 μM total lipid) were treated with 1, 5, or 25 μM of each indicated peptide, resulting in 1:250, 1:50, and 1:10 peptide:lipid ratios, respectively. The leakage that ensued was measured and normalized as described previously. (c) BMP partitions 3TAT into an organic phase via induced inverted micelle formation where the structural isomer, PG does not. A solution of 3TAT (3 μM) in LE LUV buffer was added in a 1:1 mixture with hexanes to lipid films of the indicated lipids (3-3000 μM). The samples were agitated briefly via vortex mixing and separated was assisted by centrifugation. Once phase separation was complete, an aliquot of the hexane layer was taken, and the fluorescence of the TMR-labeled peptide was measured for each condition. The results shown are the fluorescence intensity of the average of technical triplicates with the corresponding standard deviation. (d) A membrane must reach a threshold of BMP content in order for 3TAT-mediated membrane lysis to occur. LUVs consisting of different BMP levels were generated and loaded with calcein as before to assess differences in the membrane lytic activity of 3TAT. The lipid content for 10-77% BMP followed the following formula: X:(77-X):19:4 – BMP:PG:PC:PE, where X is the percentage of BMP to be tested. (e) Substitution of PC with cholesterol confers greater 3TAT-mediated membrane lytic activity of BMP-containing membranes. Calcein-loaded LE LUVs were generated as described previously with a composition of 77:19:4 – BMP:PC/Chol:PE to assess the difference in 3TAT-induced membrane lytic activity. In all experiments, the data are reported as the mean of technical triplicates with the corresponding standard deviation.

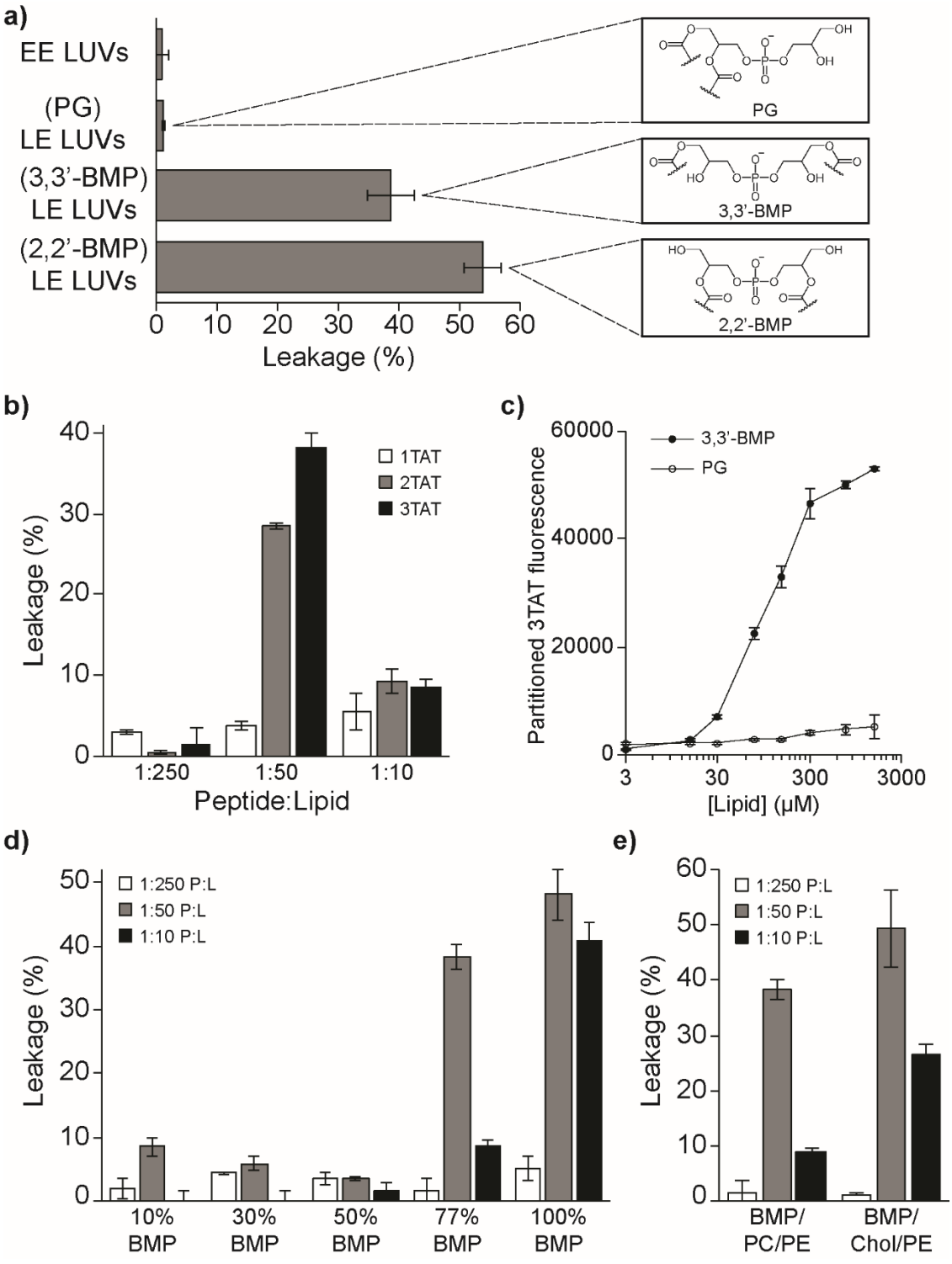
a)
EE LUVs
(PG)
LE LUVs
(3,3'-BMP)
LE LUVs
(2,2'-BMP)
LE LUVs
0 10 20 30 40 50 60
Leakage (%)
PG
3,3'-BMP
2,2'-BMP
b)
Leakage (%)
1TAT
2TAT
3TAT
1:250
1:50
1:10
Peptide:Lipid
c)
Partitioned 3TAT fluorescence
3,3'-BMP
PG
60000
40000
20000
0
3
30
300
3000
[Lipid] (μM)
d)
Leakage (%)
1:250 P:L
1:50 P:L
1:10 P:L
10% BMP
30% BMP
50% BMP
77% BMP
100% BMP
e)
Leakage (%)
1:250 P:L
1:50 P:L
1:10 P:L
BMP/ PC/PE
BMP/ Chol/PE

In the process of 3TAT-induced membrane leakage, extensive membrane restructuring results in an overall increase in membrane content manifested as an increase in lamellarity, fusion, and most notably, lipid bilayer contact (235). To gain a deeper understanding as to why PG does not behave as its structural isomer, the occurrence of these 3TAT-induced restructuring events was investigated. Utilizing burst analysis spectroscopy (BAS), overall membrane content was assessed as a metric to measure the extent of membrane restructuring between DiD-doped BMP or PG LE LUVs treated with 3TAT (Figure 3-2a). It is important to note that with this technique, resultant fluorescent burst intensity is directly proportional to the amount of lipid content. As such, BMP LE LUVs treated with 3TAT exhibited more membrane content per liposome than did PG LE LUVs. To understand this result and investigate if this difference in 3TAT-induced total lipid content is involved in the failure of PG LE LUV leakage, differences in membrane restructuring events were investigated (Figure 3-2b). For this experiment, the flocculants induced by treatment of either BMP or PG LE LUVs with 3TAT were collected, flash frozen and imaged by Cryo-EM. Both sets of liposomes seemed to undergo restructuring in the form of increased lamellarity as well as fusion (albeit, to a much greater extent in BMP LE LUVs). However, a notable absence persisted throughout imaging of PG LE LUVs; there was no observation of lipid bilayer contact. The lack of this membrane restructuring event likely explains why leakage does not take place in PG LE LUVs. Taken together, these data suggest that notable factors that influence 3TAT-induced membrane lysis include BMP structural specificity, the modulation of BMP or cholesterol content and, by proxy, membrane fluidity.

Figure 3-2 Similarities and differences of 3TAT-induced membrane restructuring between LE LUVs containing BMP or PG.
(a) BAS analysis reveals that, upon treatment with 3TAT, BMP LE LUVs possess greater lipid content than that of PG LE LUVs. BMP or PG LE LUVs doped with DiD (2.5 μM total lipid, 0.03% DiD) and treated with 10 nM 3TAT where indicated were analyzed by BAS. Fluorescence bursts from individual DiD-labeled liposomes in each sample are detected and quantified. Each fluorescent event is binned based on its fluorescence intensity, and the overall population of each condition tested is represented via a three-dimensional histogram. The x-axis is a logarithmic scale of DiD fluorescence burst amplitude (which is directly proportional to liposome size), while the y-axis represents the total number of events in each bin. (b) 3TAT selectively induces bilayer contact in BMP-containing LUVs as opposed to LUVs, where BMP was substituted for the structural isomer PG. BMP or PG LE LUVs were treated with 3TAT (1:50 P:L), sedimented by centrifugation, and flash frozen; the flocculants were subsequently imaged by Cryo-EM. Red arrows indicate events where bilayer contact was induced in BMP LE LUV flocculants; blue arrows indicate events where bilayer contact failed to occur in PG LE LUV flocculants. Provided scale bars correspond to 100 nm.

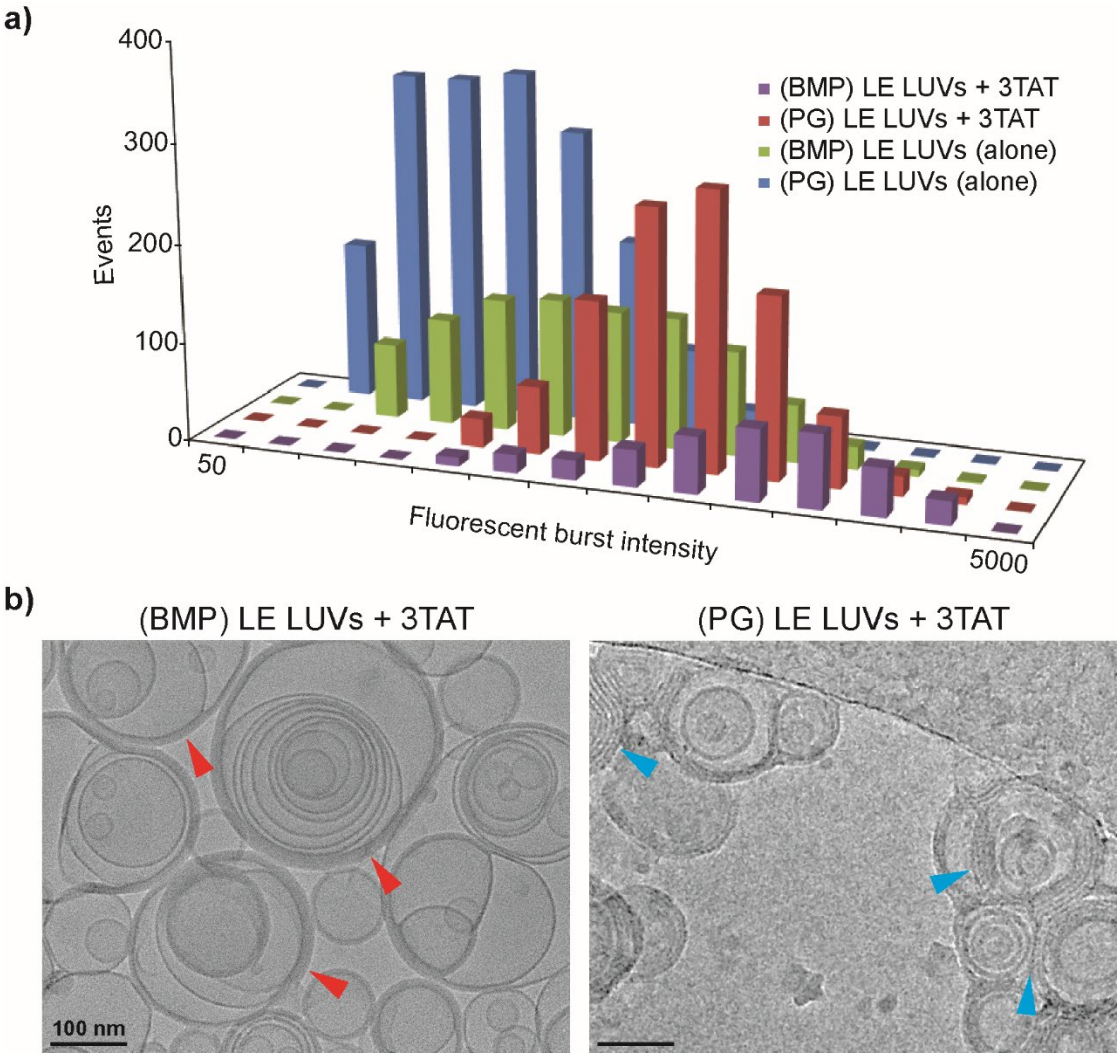
a)
400
300
200
100
0
Events
50
Fluorescent burst intensity
5000
(BMP) LE LUVs + 3TAT
(PG) LE LUVs + 3TAT
(BMP) LE LUVs (alone)
(PG) LE LUVs (alone)
b)
(BMP) LE LUVs + 3TAT
(PG) LE LUVs + 3TAT
100 nm

3.2.2 Identifying the role of membrane fluidity in 3TAT-induced membrane leakage

Assessment of membrane fluidity has been conducted *in vitro* and *in cellulo* by employing lipid-soluble fluorescent dyes as tools (247-249). Di-4-ANEPPDHQ, for example, is a potentiometric probe that, upon a change in the surrounding electric field (such as an alteration in lipid packing or change in surface charge), undergoes a shift in its electronic structure and, by proxy, fluorescent properties (248,250). This probe allows for the determination of membrane fluidity and polarity via calculation of the generalized polarization (GP) of the membrane. Generally, more positive (higher) GP values are associated with more rigid or ordered membranes, whereas more negative (lower) GP values are representative of more fluid or disordered membranes (251). With this in mind, Di-4-ANEPPDHQ was employed to investigate the effect of the membrane property of fluidity on 3TAT-induced membrane leakage. First, Di-4-ANEPPDHQ-labeled BMP or PG LE LUVs were generated in order to assess the intrinsic membrane fluidity for each set of liposomes (Figure 3-3a). While measurements for both sets of LUVs resulted in negative GP values (indicating intrinsically fluid membranes), BMP LE LUVs proved substantially more fluid than their PG LE LUV counterparts. Furthermore, upon addition of the nonendosomolytic agent nf1TAT, only a marginal change in GP was observed whereas treatment with the endosomolytic counterpart nf3TAT led to rigidification of only BMP LE LUVs (Figure 3-3a). One alternative mechanism to explain the membrane rigidification of +ΔGP membranes is the presence of a change in surface charge induced by nf3TAT. However, this mechanism seems unlikely, as the shift in GP would be realized in both sets of liposomes because the net

negative charge of each set of LUVs is equivalent. Based on these results, we hypothesized that the extent of induced leaky fusion depended on the intrinsic membrane fluidity of BMP LE LUVs. To determine if these results could be corroborated *in cellulo* to help explain the endosomolytic nature of 3TAT, Di-4-ANEPPDHQ was again employed the measure the membrane fluidity of endocytic organelles. As Di-4-ANEPPDHQ is added exogenously, it was first determined if the lipid-soluble dye could stain endocytic membranes (Figure B-2 in Appendix B). For this experiment, CHO-K1 cells were treated with a cocktail containing 5 μM Di-4-ANEPPDHQ and 500 nM LysoTracker Blue DND-22 (a fluorescent dye that selectively localizes within BMP-containing endocytic organelles). Following incubation, the cells were imaged via fluorescence microscopy, and the colocalization of LysoTracker-stained vesicles with Di-4-ANEPPDHQ-stained vesicles was calculated for regions of high puncta density within the plasma membrane of cells. The Pearson coefficient reported for this region of interest suggests that the fluorescent puncta inside cells largely represent BMP-containing endocytic vesicles. Following this experiment, CHO-K1 cells +/- treated with 10 μM of nf1TAT or nf3TAT were then stained with Di-4-ANEPPDHQ as before to determine the membrane fluidity of endocytic vesicles before and after treatment with guanidinium-rich CPPs of varying endosomolytic activities (Figure 3-3b). The inherent membrane fluidity of acidic endocytic vesicles mimicked that of BMP LE LUVs. Upon treatment with nf3TAT, acidic endocytic vesicles become more rigid while treatment with nf1TAT proved relatively innocuous in regard to acidic endocytic membrane fluidity. These results corroborate the *in vitro* findings of membrane fluidity in live cells.

Figure 3-3 BMP-containing membranes are more fluid than PG-containing or other biological membranes and undergo 3TAT-induced rigidification.
(a) BMP-containing membranes are more fluid than their PG-containing counterparts and undergo rigidification upon treatment with nf3TAT but nf1TAT induces no change in fluidity. BMP or PG LE LUVs containing 0.1% Di-4-ANEPPDHQ were generated as previously described. The fluorescence of the liposomes +/- nf1TAT or nf3TAT was then measured (λ_{ex} = 488 nm; λ_{em1} = 560 nm, λ_{em2} = 650 nm). From these measurements, generalized polarization was calculated and plotted to assess lipid fluidity. ΔGP was then calculated by subtracting the $GP_{pre\text{-}treatment}$ from $GP_{post\text{-}treatment}$ in order to represent the extent of rigidification undergone by each set of LUVs upon treatment with nf3TAT. (b) BMP-containing membranes exhibit greater fluidity than other biological membranes, and treatment with endosomolytic agents confers rigidity of endocytic vesicles, thus suggesting *in cellulo* relevance. CHO-K1 cells +/- 10 μM of each indicated peptide were costained with 5 μM Di-4-ANEPPDHQ and 500 nM LysoTracker Blue DND-22 for 30 min. Fluorescence microscopy was then performed (λ_{ex1} = 465-500 nm, λ_{em1} = 510-560 nm; λ_{ex2} = 450-490 nm, λ_{em2} = 590-670 nm). The representative fluorescence microscopy images consist of an overlay of the two fluorescent channels pseudocolored green and red. The reported GP values correspond to calculations performed over Di-4-ANEPPDHQ signals that colocalize with LysoTracker Blue DND-22 signals. The colocalized puncta represent acidic endocytic vesicles. Scale bars represent 10 μm.

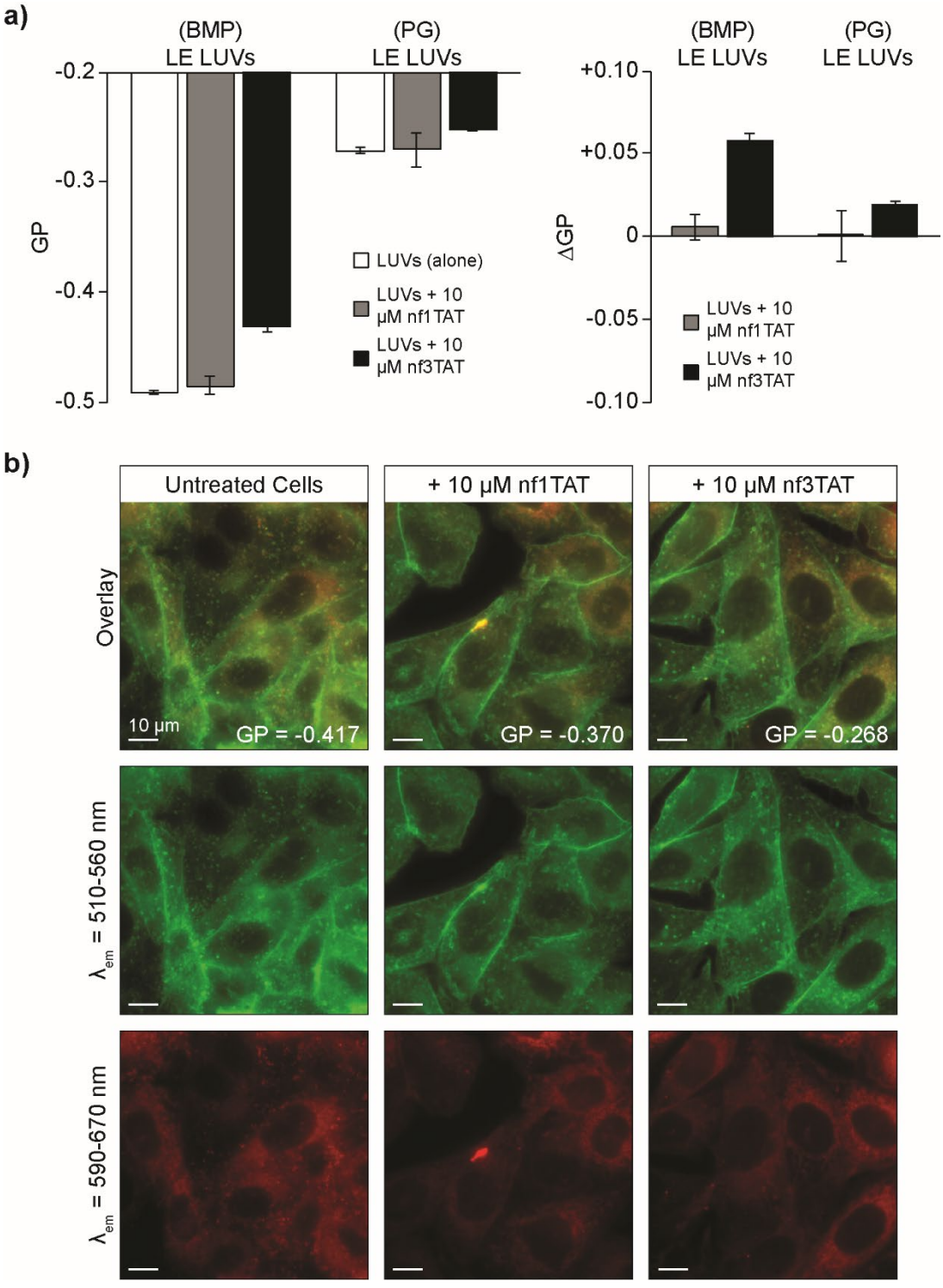
a)
(BMP) LE LUVs
(PG) LE LUVs
GP
-0.2
-0.3
-0.4
-0.5
LUVs (alone)
LUVs + 10 μM nf1TAT
LUVs + 10 μM nf3TAT
ΔGP
+0.10
+0.05
0
-0.05
-0.10
b)
Untreated Cells
+ 10 μM nf1TAT
+ 10 μM nf3TAT
Overlay
10 μm
GP = -0.417
GP = -0.370
GP = -0.268
λem = 510-560 nm
λem = 590-670 nm

Inspired by the following results, we then sought to test our hypothesis by attempting to manipulate the membrane lytic efficiencies of the guanidinium-rich CPPs by modulating the fluidity of BMP LE LUVs (Figure 3-4). The membrane fluidity of the BMP-containing LE LUV variants (18:0-3 PC LE LUVs) for the experiments that followed was modulated by introducing phosphatidylcholine (PC) with 0-3 points of unsaturation in the 18-carbon fatty acid tails (Figure 3-4a). Our logic was that introducing PC with 18:0-3 fatty acid tails would generate LUVs with a range of membrane fluidity. As PC only makes up 19 mol% of the lipid bilayer, we wanted to establish that the PC variant LE LUVs exhibited a difference in membrane fluidity (Figure 3-4b). For this experiment, 18:0-3 PC LE LUVs containing 0.1% Di-4-ANEPPDHQ were generated, and the fluorescence of the resultant LUVs was measured to determine GP. From these results, we concluded that the membrane fluidity increased as a function of the degree of fatty acid unsaturation. Next, we wanted to investigate the effects of the non-membrane lytic variant nf1TAT and its membrane lytic counterpart nf3TAT on the 18:0-3 PC LE LUVs (Figure 3-4b). Treatment with nf1TAT was relatively innocuous across each condition tested; however, 3TAT-induced rigidification of the LE LUVs was drastically increased for the more fluid 18:2 and 18:3 PC LE LUVs. We then sought to determine the effect of manipulated fluidity on the membrane lytic activities of the guanidinium-rich peptides (Figure 3-4c). Calcein-loaded 18:0-3 PC LE LUVs were treated as previously with 1TAT, 2TAT, or 3TAT at the indicated P:L ratio. These data demonstrate that the membrane lytic activities of 2TAT and 3TAT increase as a function of increased membrane fluidity. Based on these experiments, a corollary

plot was then developed to link the intrinsic membrane fluidity of BMP-containing LUVs to resultant extent of guanidinium-rich CPP-induced leakage (Figure 3-4d). Leakage percentages resulting from treatment of 18:0-3 PC LE LUVs with 5 μM of each peptide (1:50 P:L) were plotted as a function of the intrinsic membrane fluidity of each of these sets of LUVs. To establish the correlation, linear regressions were performed over each set of data points, resulting in R^2 values of 0.9984, 0.9239, and 0.9996 for 1TAT-, 2TAT-, and 3TAT-treated LUVs, respectively. These R^2 values suggest a strong correlation between the fluidity of BMP-containing membranes and resultant leakage incurred via treatment with guanidinium-rich membrane lytic agents such as 2TAT and 3TAT. Taken together, these findings highlight the influence of membrane fluidity on guanidinium-rich CPP-mediated endosomolysis.

Figure 3-4 Increasing membrane fluidity of BMP-containing membranes confers greater extent of membrane lysis mediated by guanidinium-rich CPPs.
(a) For the following experiments, LE LUVs were generated where the PC component consisted of fatty acids varying from 18:0-3 in order to induce a change in membrane fluidity. (b) As the extent of PC unsaturation increases, so too does membrane fluidity as well as the extent of nf3TAT-induced rigidification. 18:0-3 PC LE LUVs with 0.1% Di-4-ANEPPDHQ were generated as before. The fluorescence of LUVs +/- 10 μM nf1TAT or nf3TAT (where indicated) was measured as before to determine membrane fluidity. GP and ΔGP calculations were performed as previously and are represented by the reported values. (c) Increasing membrane fluidity confers greater extent of membrane lytic activity by guanidinium-rich CPPs. Calcein-loaded 18:0-3 PC LE LUVs were generated as before. LUVs were treated with 1TAT, 2TAT, or 3TAT for 1 hr at the indicated peptide:lipid ratios. Following treatment, extent of calcein leakage was measured and represented as described previously. (d) Extent of guanidinium-rich CPP-induced membrane lysis correlates strongly with membrane fluidity. A correlation was generated by plotting the extent of leakage of 18:0-3 PC LE LUVs (250 μM) treated with 5 μM of each indicated peptide (1:50 peptide:lipid ratio) against the pretreatment GP value associated with each representative liposome. In all experiments, the data are reported as the mean of technical triplicates with the corresponding standard deviation.

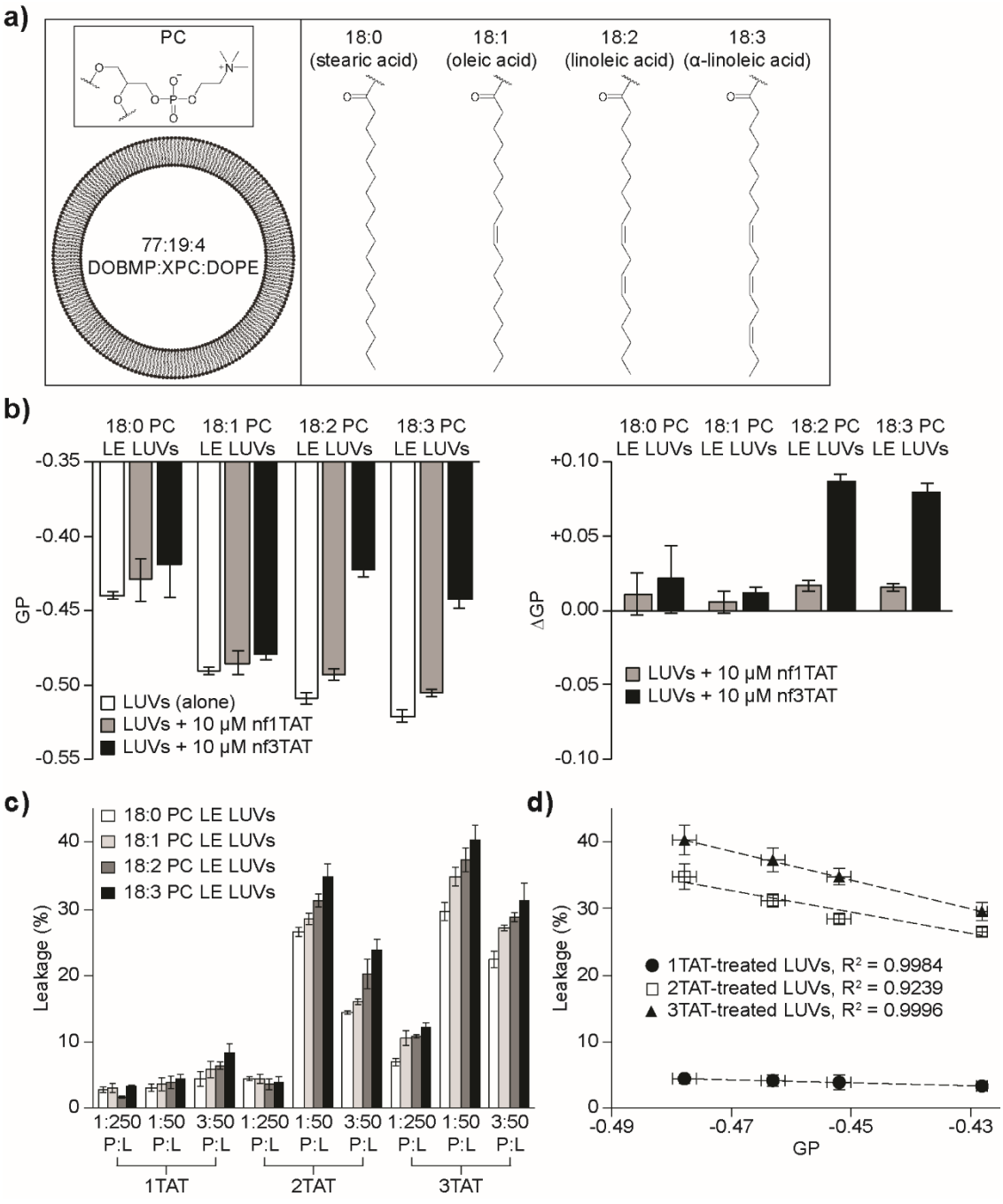
a)
PC
77:19:4
DOBMP:XPC:DOPE
18:0
(stearic acid)
18:1
(oleic acid)
18:2
(linoleic acid)
18:3
(α-linoleic acid)
b)
18:0 PC LE LUVs
18:1 PC LE LUVs
18:2 PC LE LUVs
18:3 PC LE LUVs
GP
LUVs (alone)
LUVs + 10 μM nf1TAT
LUVs + 10 μM nf3TAT
ΔGP
c)
18:0 PC LE LUVs
18:1 PC LE LUVs
18:2 PC LE LUVs
18:3 PC LE LUVs
Leakage (%)
1:250 P:L
1:50 P:L
3:50 P:L
1TAT
2TAT
3TAT
d)
1TAT-treated LUVs, R² = 0.9984
2TAT-treated LUVs, R² = 0.9239
3TAT-treated LUVs, R² = 0.9996
GP

3.3 Discussion

The assays performed throughout highlight the complexity of the mechanism of guanidinium-rich CPP endosomal escape. While the interaction between the phospholipid head of BMP and the guanidinium groups of TAT peptide variants is necessary, other factors play a role in endosomal escape as well. As identified in Figure 3-1, the introduction of greater levels of either BMP or cholesterol led to a greater extent of 3TAT-induced membrane leakage in late-endosome-mimicking liposomal systems. The introduction of greater levels of BMP seemed to be a predictable path to yield a greater extent of guanidinium-rich CPP-mediated membrane lysis. One might expect outcome, as it was previously shown that interaction of the CPP's guanidinium groups with the anionic phospholipid head of BMP triggers the fusogenic activity of the lipid, which ultimately leads to leaky fusion (138,235). However, armed with this understanding, cholesterol was perhaps a less predictable modulator of this leaky fusion event. In mammalian cells, cholesterol acts a bidirectional, temperature-dependent modulator of membrane fluidity (252-254). Cholesterol intercalates into the acyl chains of cellular membranes. This process can disrupt acyl chain packing, which makes membranes more fluid (disordered) but simultaneously rigidifies membranes (making them more ordered) by restricting more flexible unsaturated acyl chains. We then reasoned that the increase in membrane leakage was resultant of the modified membrane fluidity of the BMP-containing LE LUVs. As corroborated by both *in vitro* and *in cellulo* measurements of BMP LE LUVs and late endosomes/lysosomes, respectively, BMP causes membranes to become highly fluid (Figure 3-3). Conversely, the structural isomer

PG does not confer the same extent of membrane fluidity in PG LE LUVs. Interestingly, PG LE LUVs fail to leak upon treatment with 3TAT (Figure 3-1), an observation corroborated by the absence of 3TAT-treated LUVs with extensive membrane content or lipid bilayer contact (Figure 3-2). With these results in mind, we hypothesized that an intrinsic membrane fluidity threshold must be crossed in order for leaky fusion to occur. To test this hypothesis, we modulated the fatty acid tails of the PC component of BMP LE LUVs. PC variants with fatty acids ranging from 18:0-3 were incorporated as a means to develop a range of finely tuned LE LUVs varying in membrane fluidity (Figure 3-4). We demonstrated that guanidinium-rich CPP-induced membrane leakage increased as a function of inherent membrane fluidity.

The next logical step for this study is to attempt to modulate the membrane fluidity of late endosomes resulting in enhanced (or inhibited) cytosolic penetration of guanidinium-rich cell permeable compounds. Many molecules have been identified as tools to increase membrane fluidity, such as various fish oils and polyunsaturated fatty acids (PUFAs); fluid phospholipids, such as BMP and PE; and phospholipids with more unsaturated fatty acid chains (252,255,256). However, selectively increasing the fluidity of late endosomes has not proven to be trivial. We have tried to preincubate cells with 2,2'-BMP LE LUVs or 3,3'-BMP LUVs to increase late endosomal membrane fluidity prior to treatment with endosomolytic agents (data not shown). However, fluorescence microscopy revealed that fusion failed to occur between the artificial vesicles and either the ILVs or the limiting membrane of BMP-containing organelles. We reached this

conclusion because the intact calcein-loaded LUVs appeared as puncta that colocalized with LysoTracker after treatment with 3TAT.

To reiterate, this study highlights the fickle complexity of endosomal escape of guanidinium-rich compounds. As membrane fluidity is respective to the interacting membrane in theory, these findings can be applied not only to TAT-based delivery systems but also towards other guanidinium-rich compounds, such as supercharged viral capsid proteins. By taking the step to incorporate a moiety that enhances the membrane fluidity of BMP-containing membranes, next generation guanidinium-rich cell delivery tools may be developed for a variety of applications. Conversely, by rigidifying late endosomal membranes, the cell penetration of guanidinium-rich infectious moieties of viruses could potentially be inhibited. This could yield a novel new approach towards an "umbrella" therapeutic approach against an entire route of viral infection.

3.4 Materials and Methods

3.4.1 Materials

(S,S) Bisoleoyl-lysobisphosphatidic acid (*sn*-2,2'-BMP) was purchased from Echelon Biosciences, and all other lipids and cholesterol were purchased from Avanti Polar Lipids. All peptides were synthesized previously, and all reagents in the synthesis were purchased from Millipore Sigma. Di-4-ANEPPDHQ was purchased from Thermo Scientific. CHO-K1 cells were a gift from Dr. Patricia Pietrantonio (TAMU), and all cell culturing consumables and media were purchased from Fisher Scientific.

3.4.2 LUV preparation

LUVs for all experiments were prepared using the following protocol. Lipid films were mixed for EE (65:15:20 DOPC:DOPE:Chol), BMP LE (77:19:4 DOBMP:DOPC:DOPE; 2,2'-BMP or 3,3'-BMP were used where indicated), PG LE (77:19:4 DOPG:DOPC:DOPE), LE LUVs with cholesterol substitution (77:19:4 DOBMP:Chol:DOPE), or variable PC LE LUVs (77:19:4 DOPG:XPC:DOPE; X = stearic, oleic, linoleic, or α-linoleic acid) and allowed to dry *in vacuo* overnight. The following day, liposomes were swelled in LUV buffer (10 mM phosphate, 100 mM NaCl, pH 5.5) at 42°C for 15 min (or 70°C for 18:0 PC LE LUVs to be well above the T_c of DSPC); the liposomes were then subjected to 10 cycles of freeze/thaw performed by freezing in liquid N_2 and thawing at either 42°C or 70°C in a water bath. For leakage assays, swelling buffer contained 70 mM calcein (Sigma); for lipid packing assays, swelling buffer contained 0.1 mol% Di-4-ANEPPDHQ (relative to lipid). Following freeze/thaws, liposomes were subjected to extrusion through a 0.1 μm polycarbonate membrane 11 times to create LUVs. Calcein-loaded LUVs for leakage assays were purified from free calcein via gel filtration with Sephadex G50 resin (Sigma) purified using LUV buffer (pH 7.4).

3.4.3 Leakage assays

All LUV leakage experiments were performed, quantified, and normalized as previously reported (235). In the assays reported, LUVs (250 μM) were treated with 1:250, 1:50, 3:50, or 1:10 peptide-to-lipid ratios (1, 5, 15, or 25 μM peptide,

respectively) of 1TAT, 2TAT, 3TAT, nf1TAT, nf2TAT, or nf3TAT, where indicated. The included chemical structures were generated using ChemDraw (PerkinElmer).

3.4.4 Lipid partitioning assays

Lipid films (corresponding to a final concentration of 3-3000 μM) composed of DOBMP or DOPG were dried *in vacuo* overnight. The following day, lipid films were resuspended via vortex mixing at the phase interface between 75 μL LUV buffer (pH 5.5) and 150 μL hexanes. Lipid partitioning was initiated upon the addition and mixing (via pipetting) of 3TAT to a final aqueous concentration of 3 μM. Phase separation was assisted by centrifugation at 2,000×g for 1 min. The hexane phase was then transferred to a 96-well plate, and the fluorescence of 3TAT was measured via a Tecan Infinite M200 Pro plate reader (λ_{ex} = 556±9 nm, λ_{em} = 583±20 nm). The values were reported by normalization to a positive portioning control (fluorescence from aqueous 3 μM 3TAT) and negative portioning control (hexane alone).

3.4.5 Burst Analysis Spectroscopy

All BAS experiments were performed by Dr. Lauren Kusitigian as previously reported (235).

3.4.6 Cryo-EM

All Cryo-EM experiments were performed as previously reported (235).

3.4.7 Di-4-ANEPPDHQ-based lipid packing assays

For *in vitro* lipid packing experiments, Di-4-ANEPPDHQ-labeled BMP or PG LE LUVs (250 μM) in LE LUV buffer (pH 5.5) were mixed with 10 μM nf1TAT, nf2TAT, or nf3TAT where indicated. Immediately following, lipid packing was

determined by measuring the fluorescence of Di-4-ANEPPDHQ via a Tecan Infinite M200 PRO plate reader (λ_{ex} = 488±9 nm, λ_{em1} = 560±20 nm, λ_{em2} = 650±20 nm). GP was then calculated with the following formula: $GP = (I_{560} - I_{650}) / (I_{560} + I_{650})$ (248,257). ΔGP was calculated by subtracting the GP of untreated BMP or PG LE LUVs from the GP of BMP or PG LE LUVs treated with nf1TAT, nf2TAT, or nf3TAT, where indicated.

For *in cellulo* lipid packing experiments, CHO-K1 cells were cultured to a confluency of 70-100% on glass-bottom 8-well culture plates (Fisher). The cells were first treated with 5 μM Di-4-ANEPPDHQ in F12K medium (HyClone) containing 10% FBS for 45 min. This solution was removed, and the cells were washed twice with L15 medium (HyClone). Where indicated, cells were then treated with 10 μM nf1TAT or nf3TAT in L15 medium for 30 min. Following incubation, cells were washed twice with L15 containing heparin (1 mg/mL), once with L15, and then incubated in L15 + 10% FBS for imaging. Fluorescence microscopy was conducted using an Olympus IX-81 inverted microscope equipped with a 100× objective and heated stage (37°C). Images were captured using a Rolera-XR back-illuminated electron-multiplying CCD camera (Qimaging). Filters used in fluorescence imaging included DAPI ($\lambda_{ex}/\lambda_{em}$ = 300-388, 425-488 nm), FITC (Di-4-ANEPPDHQ channel 1) ($\lambda_{ex}/\lambda_{em}$ = 465-500, 510-560 nm) and IFRET (Di-4-ANEPPDHQ channel 2) ($\lambda_{ex}/\lambda_{em}$ = 450-490, 590-670 nm) filter cubes (Chroma Technology). GP was calculated via a macro for ImageJ (the code for this macro was derived from Gaus, et. al) (258).

CHAPTER IV

CONCLUSIONS AND FUTURE WORK

4.1 Multivalency and high guanidinium density allow for BMP-specific endosomal escape of polycationic delivery agents via a leaky fusion event

For almost 30 years, research has been conducted towards the use and improvement of CPPs as delivery tools for bioactive molecular cargo. While many approaches have been taken toward enhancement of cell penetration efficiency, constructs implementing multivalency have exhibited high levels of cell penetration. The mCPP dfTAT demonstrates an unprecedentedly high cell penetration efficiency and is able to deliver a variety of bioactive cargoes through coincubation. The cell penetration efficiency of dfTAT stems from the enhanced ability of the guanidinium-rich compound to escape the late endosome: the bottleneck in endocytosis-mediated delivery. The peptide is able to escape late endosomes through interaction with the anionic phospholipid BMP.

While many multivalent prototypes have been developed, the exact contribution of multivalency on cell penetration activity remained unclear. Through a SPPS-based approach, I was able to generate TAT constructs that vary only in their TAT valency (or copy number) and, by proxy, their charge/guanidinium density. These TAT constructs demonstrated that multivalency and guanidinium density lead to a variety of changes *in cellulo*. Multivalent constructs display drastically improved cell penetration activity compared to that of the monovalent counterpart. Although the multivalent constructs induced higher levels of endocytic uptake than monovalent TAT, this alone cannot

explain the differences in cell penetration. Notably, multivalency and higher guanidinium density impart cytotoxicity as well. Although not as guanidinium-rich as 3TAT, dfTAT exhibits high cell penetration efficiency with little-to-no cytotoxicity or observable phenotypic effects on the cell. This suggests that an upper limit to guanidinium density or multivalent exists. Finally, as demonstrated by both 3TAT and dfTAT, the efficiency of molecular cargo delivery via coincubation followed closely with their respective cell penetration efficiencies. Taken together, these findings address the effect of TAT multivalency and charge/guanidinium density on the cell penetrative and cargo delivery activities of CPPs as well as consequences associated with excessive levels of guanidinium.

More simplistic lipid bilayer models were utilized in order to understand the differences of these constructs' ability to escape late endosomes. Multivalent and endosomolytic constructs (such as 2TAT, 3TAT, or dfTAT) are highly membrane lytic towards BMP-containing LUVs mimicking late endosomes. The results presented above suggest that the lumenal contents of LE LUVs are liberated through a leaky fusion event. CPP-induced membrane restructuring was characterized by BAS and Cryo-EM. Treatment with the guanidinium-rich CPPs led to restructuring of BMP-containing membranes including flocculation, fusion, and increase in lamellarity. However, treatment with the membrane lytic variant, 3TAT, resulted in lipid bilayer contact. These data suggest that increasing the guanidinium density of cell penetrating molecules through multivalency confers glue-like activity between BMP-containing lipid bilayers. This results in leaky fusion and allows for the release of interlumenal contents.

Figure 4-1 Model depicting mCPPs such as 2TAT, 3TAT and dfTAT cause the leakage of late endosomes through interactions with the anionic lipid BMP. Guanidinium-rich mCPPs are taken up by the cell primarily through macropinocytosis. The CPPs are then trafficked along the endocytic pathway to late endosomes, a process that spans an approximately 10-45 min time window. mCPPs cause the leaky fusion of late endosomal membranes. The nature of this process remains unclear and may hypothetically involve the translocation at the limiting membrane of the late endosomes or the translocation of intraluminal vesicles. *In vitro*, mCPPs selectively permeabilize lipid bilayers that contain the late endosomal anionic lipid BMP. Permeabilization involves leaky fusion, a process where mCPPs neutralize anionic bilayers and bring them into contact. Permeabilization may also relate to the unique ability of mCPPs and BMP to partition into hydrophobic environments (hexanes, as shown in the figure, mimic the hydrophobic tails of lipids). The figure is used with permission (191).

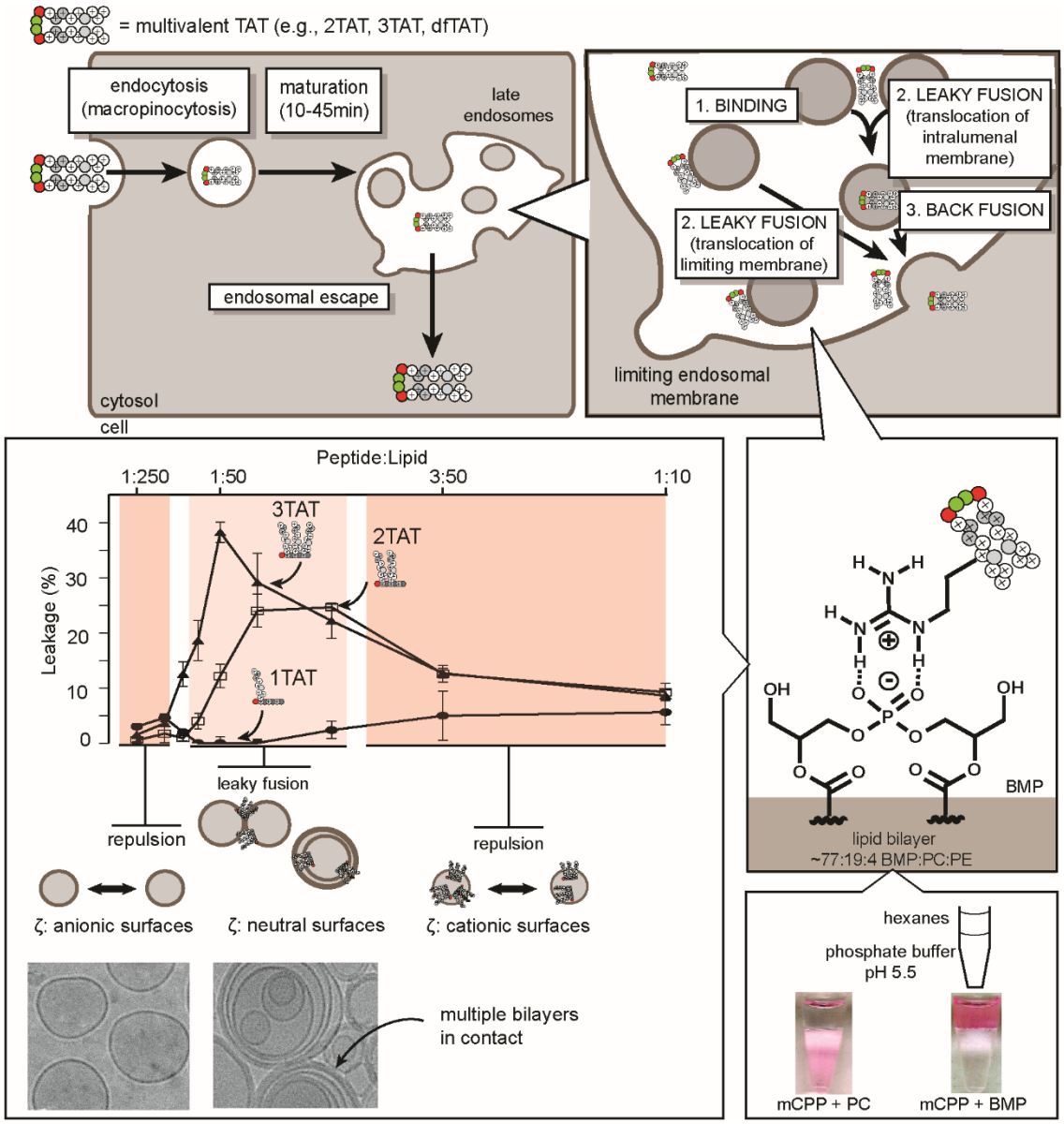
= multivalent TAT (e.g., 2TAT, 3TAT, dfTAT)
endocytosis (macropinocytosis)
maturation (10-45min)
late endosomes
endosomal escape
cytosol
cell
1. BINDING
2. LEAKY FUSION (translocation of intralumenal membrane)
3. BACK FUSION
2. LEAKY FUSION (translocation of limiting membrane)
limiting endosomal membrane
Peptide:Lipid
1:250
1:50
3:50
1:10
Leakage (%)
40
30
20
10
0
3TAT
2TAT
1TAT
leaky fusion
repulsion
repulsion
ζ: anionic surfaces
ζ: neutral surfaces
ζ: cationic surfaces
multiple bilayers in contact
OH
OH
BMP
lipid bilayer
~77:19:4 BMP:PC:PE
hexanes
phosphate buffer
pH 5.5
mCPP + PC
mCPP + BMP

4.2 The efficiency of guanidinium-rich CPP-mediated leaky fusion of BMP-containing membranes is dependent on innate membrane fluidity

While interaction between the guanidinium group of polycationic CPPs and the anionic phospholipid BMP is necessary, other factors contribute to the process of endosomal escape. Comparison of BMP LE LUVs to PG LE LUVs revealed that 3TAT and dfTAT selectively lyse BMP-containing membranes despite the net charge of the LUVs remaining constant. However, analysis by BAS and Cryo-EM suggest that many of the same 3TAT-induced membrane restructuring events are shared between BMP LE LUVs and PG LE LUVs. Notably, lipid bilayer contact was not observed for PG LE LUVs treated with 3TAT, however, this may simply be due to the poor resolution of the images. Investigation into potential modulators of membrane leakage revealed that enrichment of either BMP or cholesterol in BMP LE LUVs conferred greater extent of membrane lysis. Cholesterol regulates the fluidity of biological membranes. Upon analysis of the membrane fluidity of BMP LE LUVs and PG LE LUVs, BMP LE LUVs proved to be much more fluid or disordered than PG LE LUVs (results that were corroborated *in cellulo*). Manipulation of the fluidity of BMP-containing membranes via the substitution of fatty acids for those with a greater or lesser extent of unsaturation yielded a direct effect on the extent of membrane lysis upon treatment with mCPPs such as 3TAT. Taken together, these data suggest that the inherent disordered state of BMP-containing membranes allows for leaky fusion to occur. Pretreatment of cells with a modulator of late endosomal fluidity could potentially affect the permeation efficiency of guanidinium-rich molecules.

4.3 Implications of this work on other guanidinium-rich supercharged cell penetrating agents

In theory, this work is not restricted to guanidinium-rich CPPs but can be applied to other cationic cell permeable molecules. Cationic delivery tools, such as cationic lipids/polymers or even supercharged proteins and viral particles, are of particular interest. Cationic lipids, lipid nanoparticles (LNPs), and lipoplexes have been employed to deliver a variety of different nucleic acid cargos (259-261). In fact, lipoplexes and LNPs have been shown to enter cells through endocytosis. Upon endocytosis, it is possible that the very same electrostatic interaction between 3TAT/dfTAT and BMP could be established between the cationic lipoplex or LNP in order to escape the endosome and deliver the nucleic acid cargo. In fact, *in vitro* studies demonstrated the ability of lipoplexes to fuse with membranes containing the anionic, fusogenic phospholipid PE (262). These results suggest that the electrostatic interaction of lipoplexes with BMP is plausible, and the inherent fusogenicity of BMP could aid in the process of lipoplex endosomal escape.

Supercharged protein and viral particles share many of the same properties with the discussed mCPPs. Despite being much larger relatively, they possess many more basic residues which, in turn, bestows them with a charge density >+0.75. As previously discussed, dengue, bluetongue, and yellow fever are viruses that possess supercharged capsid proteins (214-218). It has even been demonstrated that DENV actually interacts with BMP in order to deliver its genomic cargo. It is therefore possible that other flaviviruses and viruses that possess supercharged protein components may follow in

suit by utilizing BMP for the delivery of their respective genomic cargos as well. These findings suggest that inhibiting the interaction of BMP with viral components may be a route forward towards the development of new antiviral therapeutics.

4.4 Future work

To expand upon this body of work, the paramount goal would be to reveal the final details required to fully elucidate the mechanism of endosomal escape. Being able to visualize guanidinium-rich CPP-induced endosomolysis would prove highly valuable in furthering our understanding of the mechanism of endosomal escape. However, a number of difficulties, such as the highly dynamic nature of late endosomes, makes studying this process *in cellulo* very challenging. Herein lies the value of coupling *in vitro* lipid membrane systems with emerging single particle techniques. For instance, a single liposome mimicking the late endosomal lipid profile could be optically trapped; then, using atomic force microscopy (AFM), the topography of the vesicle could be measured. Measuring the same vesicle upon treatment with a CPP would reveal even greater detail into membrane restructuring events (such as pore size, membrane ruffling, etc.) than Cryo-EM by providing a three-dimensional read out. Similarly, a real-time analysis of membrane lysis could be provided by coupling this method of optically trapping a liposome with Raman microscopy. Indeed, this approach has been recently utilized to monitor membrane leakage of DPPC or DPPC/cardiolipin liposomes loaded with a molecular cargo possessing a unique Raman signature (such as 3-nitrobenzenesulfonate, or 3-NBS) (263). This experiment would not only allow for the real-time observation of CPP-induced membrane leakage but would also yield valuable

kinetic details as well. Taken together, experiments of this nature would greatly expand our understanding or could even fully elucidate the mechanism of endosomal escape.

Additionally, work must be done to test if the mechanism of guanidinium-rich CPP endosomal escape can be applied to other supercharged moieties such as polycationic delivery tools, viral particles and viruses. If polycationic delivery tools, such as cationic lipids for DNA transfection, utilize BMP for cell penetration, then improvements can be made to make these tools more efficient and less cytotoxic. These improvements would ultimately expand the number of applications for the use of these delivery tools. If viruses possessing supercharged proteins utilize BMP for cell penetration, then therapeutics could be developed that target late endosomes and disrupt this interaction. That being said, caution should be taken in developing these therapeutics, as they may affect the biological role of BMP in regulating cholesterol trafficking and endosomal cholesterol content (202,204). This concern was realized when Gruenberg and coworkers determined that treatment of healthy cells with anti-BMP resulted in symptoms reminiscent of Niemann-Pick type C, such as cholesterol accumulation (202).

Finally, novel new approaches may be used toward enhancing the cell permeability of molecular probes and biologics. From the findings described previously, two approaches towards the enhancement of cell penetration have been revealed. The first approach includes enhancing cell penetration via chemical modification of the bioactive molecule of interest. By conjugating a small, guanidinium-rich “cell penetration tag”, many previously cell impermeable molecules of interest may become

viable effectors of intercellular targets due to this newfound cell penetrating activity. Additionally, the *in vitro* assays discussed above demonstrated that the innate membrane lytic activity of guanidinium-rich CPPs could be enhanced by increasing the inherent membrane fluidity or disorder of BMP-containing vesicles. Theoretically, if a molecule were designed to specifically target late endosomes and disrupt the lipid packing of BMP-containing membranes, then endosomal escape could be greatly enhanced. This molecule could be co-administered or even conjugated to the cell penetrating molecule of interest as an "enhancer" of endosomal escape. Perhaps then, the best way to target the late endosome is through conjugation to guanidinium-rich agents. Coupling hydrophobic moieties, such as fluorophores and endosomal escape domains (short stretches of aromatic amino acids), with guanidinium-rich CPPs has been demonstrated as a means to enhance cell penetration (75,141). Although the effect on membrane packing has not yet been investigated, it is possible that these hydrophobic moieties enhance cell penetration by disordering BMP-containing membranes.

REFERENCES

1. Fawell, S., Seery, J., Daikh, Y., Moore, C., Chen, L. L., Pepinsky, B., and Barsoum, J. (1994) Tat-mediated delivery of heterologous proteins into cells. *Proc Natl Acad Sci U S A* **91**, 664-668
2. Pan, C., Lu, B., Chen, H., and Bishop, C. E. (2010) Reprogramming human fibroblasts using HIV-1 TAT recombinant proteins OCT4, SOX2, KLF4 and c-MYC. *Mol Biol Rep* **37**, 2117-2124
3. Chakrabarti, R., Wylie, D. E., and Schuster, S. M. (1989) Transfer of monoclonal antibodies into mammalian cells by electroporation. *J Biol Chem* **264**, 15494-15500
4. Kim, T. K., and Eberwine, J. H. (2010) Mammalian cell transfection: the present and the future. *Anal Bioanal Chem* **397**, 3173-3178
5. McNeil, P. L., Murphy, R. F., Lanni, F., and Taylor, D. L. (1984) A method for incorporating macromolecules into adherent cells. *J Cell Biol* **98**, 1556-1564
6. Ortiz, D., Baldwin, M. M., and Lucas, J. J. (1987) Transient correction of genetic defects in cultured animal cells by introduction of functional proteins. *Mol Cell Biol* **7**, 3012-3017
7. Kaczmarczyk, S. J., Sitaraman, K., Young, H. A., Hughes, S. H., and Chatterjee, D. K. (2011) Protein delivery using engineered virus-like particles. *Proc Natl Acad Sci U S A* **108**, 16998-17003
8. Prior, T. I., FitzGerald, D. J., and Pastan, I. (1991) Barnase toxin: a new chimeric toxin composed of pseudomonas exotoxin A and barnase. *Cell* **64**, 1017-1023
9. Prior, T. I., FitzGerald, D. J., and Pastan, I. (1992) Translocation mediated by domain II of Pseudomonas exotoxin A: transport of barnase into the cytosol. *Biochemistry* **31**, 3555-3559
10. Renneisen, K., Leserman, L., Matthes, E., Schroder, H. C., and Muller, W. E. (1990) Inhibition of expression of human immunodeficiency virus-1 in vitro by antibody-targeted liposomes containing antisense RNA to the env region. *J Biol Chem* **265**, 16337-16342
11. van den Boorn, J. G., Schlee, M., Coch, C., and Hartmann, G. (2011) SiRNA delivery with exosome nanoparticles. *Nat Biotechnol* **29**, 325-326
12. Patel, L. N., Zaro, J. L., and Shen, W. C. (2007) Cell penetrating peptides: intracellular pathways and pharmaceutical perspectives. *Pharm Res* **24**, 1977-1992
13. Frankel, A. D., and Pabo, C. O. (1988) Cellular uptake of the tat protein from human immunodeficiency virus. *Cell* **55**, 1189-1193
14. Green, M., and Loewenstein, P. M. (1988) Autonomous functional domains of chemically synthesized human immunodeficiency virus tat trans-activator protein. *Cell* **55**, 1179-1188
15. Mann, D. A., and Frankel, A. D. (1991) Endocytosis and targeting of exogenous HIV-1 Tat protein. *EMBO J* **10**, 1733-1739
16. Milletti, F. (2012) Cell-penetrating peptides: classes, origin, and current landscape. *Drug Discov Today* **17**, 850-860

17. Deshayes, S., Morris, M. C., Divita, G., and Heitz, F. (2006) Interactions of amphipathic CPPs with model membranes. *Biochim Biophys Acta* **1758**, 328-335
18. Nishikawa, M., Otsuki, T., Ota, A., Guan, X., Takemoto, S., Takahashi, Y., and Takakura, Y. (2010) Induction of tumor-specific immune response by gene transfer of Hsp70-cell-penetrating peptide fusion protein to tumors in mice. *Mol Ther* **18**, 421-428
19. Derossi, D., Joliot, A. H., Chassaing, G., and Prochiantz, A. (1994) The third helix of the Antennapedia homeodomain translocates through biological membranes. *Journal of Biological Chemistry* **269**, 10444-10450
20. Bechara, C., and Sagan, S. (2013) Cell-penetrating peptides: 20 years later, where do we stand? *FEBS Lett* **587**, 1693-1702
21. Pooga, M., Hallbrink, M., Zorko, M., and Langel, U. (1998) Cell penetration by transportan. *FASEB J* **12**, 67-77
22. Crombez, L., Aldrian-Herrada, G., Konate, K., Nguyen, Q. N., McMaster, G. K., Brasseur, R., Heitz, F., and Divita, G. (2008) A New Potent Secondary Amphipathic Cell-penetrating Peptide for siRNA Delivery Into Mammalian Cells. *Mol Ther* **17**, 95-103
23. Lorents, A., Kodavali, P. K., Oskolkov, N., Langel, U., Hallbrink, M., and Pooga, M. (2012) Cell-penetrating peptides split into two groups based on modulation of intracellular calcium concentration. *J Biol Chem* **287**, 16880-16889
24. Montrose, K., Yang, Y., Sun, X., Wiles, S., and Krissansen, G. W. (2013) Xentry, a new class of cell-penetrating peptide uniquely equipped for delivery of drugs. *Sci Rep* **3**, 1661
25. Morris, M. C., Depollier, J., Mery, J., Heitz, F., and Divita, G. (2001) A peptide carrier for the delivery of biologically active proteins into mammalian cells. *Nat Biotech* **19**, 1173-1176
26. Munyendo, W. L., Lv, H., Benza-Ingoula, H., Baraza, L. D., and Zhou, J. (2012) Cell penetrating peptides in the delivery of biopharmaceuticals. *Biomolecules* **2**, 187-202
27. Taylor, B. N., Mehta, R. R., Yamada, T., Lekmine, F., Christov, K., Chakrabarty, A. M., Green, A., Bratescu, L., Shilkaitis, A., Beattie, C. W., and Das Gupta, T. K. (2009) Noncationic Peptides Obtained From Azurin Preferentially Enter Cancer Cells. *Cancer Research* **69**, 537
28. Oehlke, J., Scheller, A., Wiesner, B., Krause, E., Beyermann, M., Klauschenz, E., Melzig, M., and Bienert, M. (1998) Cellular uptake of an α-helical amphipathic model peptide with the potential to deliver polar compounds into the cell interior non-endocytically. *Biochimica et Biophysica Acta (BBA) - Biomembranes* **1414**, 127-139
29. Li, W., Nicol, F., and Szoka, F. C., Jr. (2004) GALA: a designed synthetic pH-responsive amphipathic peptide with applications in drug and gene delivery. *Adv Drug Deliv Rev* **56**, 967-985

30. Schafmeister, C. E., Po, J., and Verdine, G. L. (2000) An All-Hydrocarbon Cross-Linking System for Enhancing the Helicity and Metabolic Stability of Peptides. *Journal of the American Chemical Society* **122**, 5891-5892
31. Cascales, L., Henriques, S. T., Kerr, M. C., Huang, Y. H., Sweet, M. J., Daly, N. L., and Craik, D. J. (2011) Identification and characterization of a new family of cell-penetrating peptides: cyclic cell-penetrating peptides. *J Biol Chem* **286**, 36932-36943
32. Qian, Z., Martyna, A., Hard, R. L., Wang, J., Appiah-Kubi, G., Coss, C., Phelps, M. A., Rossman, J. S., and Pei, D. (2016) Discovery and Mechanism of Highly Efficient Cyclic Cell-Penetrating Peptides. *Biochemistry* **55**, 2601-2612
33. Lawrence, M. S., Phillips, K. J., and Liu, D. R. (2007) Supercharging proteins can impart unusual resilience. *J Am Chem Soc* **129**, 10110-10112
34. McNaughton, B. R., Cronican, J. J., Thompson, D. B., and Liu, D. R. (2009) Mammalian cell penetration, siRNA transfection, and DNA transfection by supercharged proteins. *Proc Natl Acad Sci U S A* **106**, 6111-6116
35. Cronican, J. J., Thompson, D. B., Beier, K. T., McNaughton, B. R., Cepko, C. L., and Liu, D. R. (2010) Potent delivery of functional proteins into Mammalian cells in vitro and in vivo using a supercharged protein. *ACS Chem Biol* **5**, 747-752
36. Thompson, D. B., Cronican, J. J., and Liu, D. R. (2012) Engineering and identifying supercharged proteins for macromolecule delivery into mammalian cells. *Methods Enzymol* **503**, 293-319
37. Mitchell, D. J., Kim, D. T., Steinman, L., Fathman, C. G., and Rothbard, J. B. (2000) Polyarginine enters cells more efficiently than other polycationic homopolymers. *J Pept Res* **56**, 318-325
38. Wender, P. A., Mitchell, D. J., Pattabiraman, K., Pelkey, E. T., Steinman, L., and Rothbard, J. B. (2000) The design, synthesis, and evaluation of molecules that enable or enhance cellular uptake: peptoid molecular transporters. *Proc Natl Acad Sci U S A* **97**, 13003-13008
39. Futaki, S., Suzuki, T., Ohashi, W., Yagami, T., Tanaka, S., Ueda, K., and Sugiura, Y. (2001) Arginine-rich peptides. An abundant source of membrane-permeable peptides having potential as carriers for intracellular protein delivery. *J Biol Chem* **276**, 5836-5840
40. Richard, J. P., Melikov, K., Vives, E., Ramos, C., Verbeure, B., Gait, M. J., Chernomordik, L. V., and Lebleu, B. (2003) Cell-penetrating peptides. A reevaluation of the mechanism of cellular uptake. *J Biol Chem* **278**, 585-590
41. Vives, E., Richard, J. P., Rispal, C., and Lebleu, B. (2003) TAT peptide internalization: seeking the mechanism of entry. *Curr Protein Pept Sci* **4**, 125-132
42. Luedtke, N. W., Carmichael, P., and Tor, Y. (2003) Cellular uptake of aminoglycosides, guanidinoglycosides, and poly-arginine. *J Am Chem Soc* **125**, 12374-12375

43. Thoren, P. E., Persson, D., Isakson, P., Goksor, M., Onfelt, A., and Norden, B. (2003) Uptake of analogs of penetratin, Tat(48-60) and oligoarginine in live cells. *Biochem Biophys Res Commun* **307**, 100-107
44. Shin, M. C., Zhang, J., Min, K. A., Lee, K., Byun, Y., David, A. E., He, H., and Yang, V. C. (2014) Cell-penetrating peptides: achievements and challenges in application for cancer treatment. *J Biomed Mater Res A* **102**, 575-587
45. Lee, Y. J., Erazo-Oliveras, A., and Pellois, J. P. (2010) Delivery of macromolecules into live cells by simple co-incubation with a peptide. *Chembiochem* **11**, 325-330
46. Kim, D. T., Mitchell, D. J., Brockstedt, D. G., Fong, L., Nolan, G. P., Fathman, C. G., Engleman, E. G., and Rothbard, J. B. (1997) Introduction of soluble proteins into the MHC class I pathway by conjugation to an HIV tat peptide. *J Immunol* **159**, 1666-1668
47. Kim, D., Kim, C. H., Moon, J. I., Chung, Y. G., Chang, M. Y., Han, B. S., Ko, S., Yang, E., Cha, K. Y., Lanza, R., and Kim, K. S. (2009) Generation of human induced pluripotent stem cells by direct delivery of reprogramming proteins. *Cell Stem Cell* **4**, 472-476
48. Takahashi, K., and Yamanaka, S. (2006) Induction of pluripotent stem cells from mouse embryonic and adult fibroblast cultures by defined factors. *Cell* **126**, 663-676
49. Whitehead, K. A., Langer, R., and Anderson, D. G. (2009) Knocking down barriers: advances in siRNA delivery. *Nat Rev Drug Discov* **8**, 129-138
50. Glover, D. J., Lipps, H. J., and Jans, D. A. (2005) Towards safe, non-viral therapeutic gene expression in humans. *Nat Rev Genet* **6**, 299-310
51. Eguchi, A., Meade, B. R., Chang, Y.-C., Fredrickson, C. T., Willert, K., Puri, N., and Dowdy, S. F. (2009) Efficient siRNA delivery into primary cells by a peptide transduction domain-dsRNA binding domain fusion protein. *Nat Biotech* **27**, 567-571
52. Kurreck, J. (2003) Antisense technologies. Improvement through novel chemical modifications. *Eur J Biochem* **270**, 1628-1644
53. Zamecnik, P. C., and Stephenson, M. L. (1978) Inhibition of Rous sarcoma virus replication and cell transformation by a specific oligodeoxynucleotide. *Proc Natl Acad Sci U S A* **75**, 280-284
54. Kole, R., Vacek, M., and Williams, T. (2004) Modification of alternative splicing by antisense therapeutics. *Oligonucleotides* **14**, 65-74
55. Krutzfeldt, J., Rajewsky, N., Braich, R., Rajeev, K. G., Tuschl, T., Manoharan, M., and Stoffel, M. (2005) Silencing of microRNAs in vivo with 'antagomirs'. *Nature* **438**, 685-689
56. Kilk, K., Elmquist, A., Saar, K., Pooga, M., Land, T., Bartfai, T., Soomets, U., and Langel, U. (2004) Targeting of antisense PNA oligomers to human galanin receptor type 1 mRNA. *Neuropeptides* **38**, 316-324
57. Wolf, Y., Pritz, S., Abes, S., Bienert, M., Lebleu, B., and Oehlke, J. (2006) Structural requirements for cellular uptake and antisense activity of peptide nucleic acids conjugated with various peptides. *Biochemistry* **45**, 14944-14954

58. Shiraishi, T., Pankratova, S., and Nielsen, P. E. (2005) Calcium ions effectively enhance the effect of antisense peptide nucleic acids conjugated to cationic tat and oligoarginine peptides. *Chem Biol* **12**, 923-929
59. Schwarze, S. R., Ho, A., Vocero-Akbani, A., and Dowdy, S. F. (1999) In vivo protein transduction: delivery of a biologically active protein into the mouse. *Science* **285**, 1569-1572
60. Brady, C. A., and Attardi, L. D. (2010) p53 at a glance. *J Cell Sci* **123**, 2527-2532
61. McCormick, F. (2001) Cancer gene therapy: fringe or cutting edge? *Nat Rev Cancer* **1**, 130-141
62. Hupp, T. R., Sparks, A., and Lane, D. P. (1995) Small peptides activate the latent sequence-specific DNA binding function of p53. *Cell* **83**, 237-245
63. Snyder, E. L., Meade, B. R., Saenz, C. C., and Dowdy, S. F. (2004) Treatment of terminal peritoneal carcinomatosis by a transducible p53-activating peptide. *PLoS Biol* **2**, E36
64. Araki, D., Takayama, K., Inoue, M., Watanabe, T., Kumon, H., Futaki, S., Matsui, H., and Tomizawa, K. (2010) Cell-penetrating D-isomer peptides of p53 C-terminus: long-term inhibitory effect on the growth of bladder cancer. *Urology* **75**, 813-819
65. Hosotani, R., Miyamoto, Y., Fujimoto, K., Doi, R., Otaka, A., Fujii, N., and Imamura, M. (2002) Trojan p16 peptide suppresses pancreatic cancer growth and prolongs survival in mice. *Clin Cancer Res* **8**, 1271-1276
66. Michl, J., Scharf, B., Schmidt, A., Huynh, C., Hannan, R., von Gizycki, H., Friedman, F. K., Brandt-Rauf, P., Fine, R. L., and Pincus, M. R. (2006) PNC-28, a p53-derived peptide that is cytotoxic to cancer cells, blocks pancreatic cancer cell growth in vivo. *Int J Cancer* **119**, 1577-1585
67. Trembley, J. H., Wang, G., Unger, G., Slaton, J., and Ahmed, K. (2009) Protein kinase CK2 in health and disease: CK2: a key player in cancer biology. *Cell Mol Life Sci* **66**, 1858-1867
68. Perea, S. E., Reyes, O., Puchades, Y., Mendoza, O., Vispo, N. S., Torrens, I., Santos, A., Silva, R., Acevedo, B., López, E., Falcón, V., and Alonso, D. F. (2004) Antitumor Effect of a Novel Proapoptotic Peptide that Impairs the Phosphorylation by the Protein Kinase 2 (Casein Kinase 2). *Cancer Research* **64**, 7127
69. Graham, S. H., Chen, J., and Clark, R. S. (2000) Bcl-2 family gene products in cerebral ischemia and traumatic brain injury. *J Neurotrauma* **17**, 831-841
70. Jo, D., Liu, D., Yao, S., Collins, R. D., and Hawiger, J. (2005) Intracellular protein therapy with SOCS3 inhibits inflammation and apoptosis. *Nat Med* **11**, 892-898
71. Rizzuti, M., Nizzardo, M., Zanetta, C., Ramirez, A., and Corti, S. (2015) Therapeutic applications of the cell-penetrating HIV-1 Tat peptide. *Drug Discov Today* **20**, 76-85

72. Tripathi, P. P., Arami, H., Banga, I., Gupta, J., and Gandhi, S. (2018) Cell penetrating peptides in preclinical and clinical cancer diagnosis and therapy. *Oncotarget* **9**, 37252-37267
73. LeCher, J. C., Nowak, S. J., and McMurry, J. L. (2017) Breaking in and busting out: cell-penetrating peptides and the endosomal escape problem. *Biomol Concepts* **8**, 131-141
74. Lundberg, M., Wikstrom, S., and Johansson, M. (2003) Cell surface adherence and endocytosis of protein transduction domains. *Mol Ther* **8**, 143-150
75. Birch, D., Christensen, M. V., Staerk, D., Franzyk, H., and Nielsen, H. M. (2017) Fluorophore labeling of a cell-penetrating peptide induces differential effects on its cellular distribution and affects cell viability. *Biochim Biophys Acta Biomembr* **1859**, 2483-2494
76. Muthukrishnan, N., Johnson, G. A., Lim, J., Simanek, E. E., and Pellois, J. P. (2012) TAT-mediated photochemical internalization results in cell killing by causing the release of calcium into the cytosol of cells. *Biochim Biophys Acta* **1820**, 1734-1743
77. Barany-Wallje, E., Gaur, J., Lundberg, P., Langel, U., and Graslund, A. (2007) Differential membrane perturbation caused by the cell penetrating peptide Tp10 depending on attached cargo. *FEBS Lett* **581**, 2389-2393
78. Fischer, R., Waizenegger, T., Kohler, K., and Brock, R. (2002) A quantitative validation of fluorophore-labelled cell-permeable peptide conjugates: fluorophore and cargo dependence of import. *Biochim Biophys Acta* **1564**, 365-374
79. Foerg, C., Ziegler, U., Fernandez-Carneado, J., Giralt, E., and Merkle, H. P. (2007) Differentiation restricted endocytosis of cell penetrating peptides in MDCK cells corresponds with activities of Rho-GTPases. *Pharm Res* **24**, 628-642
80. Hirose, H., Takeuchi, T., Osakada, H., Pujals, S., Katayama, S., Nakase, I., Kobayashi, S., Haraguchi, T., and Futaki, S. (2012) Transient focal membrane deformation induced by arginine-rich peptides leads to their direct penetration into cells. *Mol Ther* **20**, 984-993
81. Jones, A. T., and Sayers, E. J. (2012) Cell entry of cell penetrating peptides: tales of tails wagging dogs. *J Control Release* **161**, 582-591
82. Lundin, P., Johansson, H., Guterstam, P., Holm, T., Hansen, M., Langel, U., and S, E. L. A. (2008) Distinct uptake routes of cell-penetrating peptide conjugates. *Bioconjug Chem* **19**, 2535-2542
83. Trehin, R., Krauss, U., Beck-Sickinger, A. G., Merkle, H. P., and Nielsen, H. M. (2004) Cellular uptake but low permeation of human calcitonin-derived cell penetrating peptides and Tat(47-57) through well-differentiated epithelial models. *Pharm Res* **21**, 1248-1256
84. Tunnemann, G., Martin, R. M., Haupt, S., Patsch, C., Edenhofer, F., and Cardoso, M. C. (2006) Cargo-dependent mode of uptake and bioavailability of TAT-containing proteins and peptides in living cells. *FASEB J* **20**, 1775-1784

85. Duchardt, F., Fotin-Mleczek, M., Schwarz, H., Fischer, R., and Brock, R. (2007) A comprehensive model for the cellular uptake of cationic cell-penetrating peptides. *Traffic* **8**, 848-866
86. Ter-Avetisyan, G., Tünnemann, G., Nowak, D., Nitschke, M., Herrmann, A., Drab, M., and Cardoso, M. C. (2009) Cell Entry of Arginine-rich Peptides Is Independent of Endocytosis. *Journal of Biological Chemistry* **284**, 3370-3378
87. Magzoub, M., Gr, auml, and slund, A. (2004) Cell-penetrating peptides: small from inception to application. *Quarterly Reviews of Biophysics* **37**, 147-195
88. Berlose, J. P., Convert, O., Derossi, D., Brunissen, A., and Chassaing, G. (1996) Conformational and associative behaviours of the third helix of antennapedia homeodomain in membrane-mimetic environments. *Eur J Biochem* **242**, 372-386
89. Lee, M.-T., Hung, W.-C., Chen, F.-Y., and Huang, H. W. (2005) Many-Body Effect of Antimicrobial Peptides: On the Correlation Between Lipid's Spontaneous Curvature and Pore Formation. *Biophysical Journal* **89**, 4006-4016
90. Sun, D., Forsman, J., Lund, M., and Woodward, C. E. (2014) Effect of arginine-rich cell penetrating peptides on membrane pore formation and life-times: a molecular simulation study. *Phys Chem Chem Phys* **16**, 20785-20795
91. Derossi, D., Calvet, S., Trembleau, A., Brunissen, A., Chassaing, G., and Prochiantz, A. (1996) Cell internalization of the third helix of the Antennapedia homeodomain is receptor-independent. *J Biol Chem* **271**, 18188-18193
92. Conner, S. D., and Schmid, S. L. (2003) Regulated portals of entry into the cell. *Nature* **422**, 37-44
93. Fischer, R., Fotin-Mleczek, M., Hufnagel, H., and Brock, R. (2005) Break on through to the other side-biophysics and cell biology shed light on cell-penetrating peptides. *Chembiochem* **6**, 2126-2142
94. Mayor, S., and Pagano, R. E. (2007) Pathways of clathrin-independent endocytosis. *Nat Rev Mol Cell Biol* **8**, 603-612
95. Doherty, G. J., and McMahon, H. T. (2009) Mechanisms of endocytosis. *Annu Rev Biochem* **78**, 857-902
96. Plapied, L., Duhem, N., des Rieux, A., and Préat, V. (2011) Fate of polymeric nanocarriers for oral drug delivery. *Curr Opin Colloid In* **16**, 228-237
97. Nakase, I., Takeuchi, T., Tanaka, G., and Futaki, S. (2008) Methodological and cellular aspects that govern the internalization mechanisms of arginine-rich cell-penetrating peptides. *Adv Drug Deliv Rev* **60**, 598-607
98. Sakai, N., and Matile, S. (2003) Anion-mediated transfer of polyarginine across liquid and bilayer membranes. *J Am Chem Soc* **125**, 14348-14356
99. Walrant, A., Bechara, C., Alves, I. D., and Sagan, S. (2012) Molecular partners for interaction and cell internalization of cell-penetrating peptides: how identical are they? *Nanomedicine (Lond)* **7**, 133-143
100. Favretto, M. E., Wallbrecher, R., Schmidt, S., van de Putte, R., and Brock, R. (2014) Glycosaminoglycans in the cellular uptake of drug delivery vectors - bystanders or active players? *J Control Release* **180**, 81-90

101. Tumova, S., Woods, A., and Couchman, J. R. (2000) Heparan sulfate chains from glypican and syndecans bind the Hep II domain of fibronectin similarly despite minor structural differences. *J Biol Chem* **275**, 9410-9417
102. Futaki, S., Nakase, I., Tadokoro, A., Takeuchi, T., and Jones, A. T. (2007) Arginine-rich peptides and their internalization mechanisms. *Biochem Soc Trans* **35**, 784-787
103. Richard, J. P., Melikov, K., Brooks, H., Prevot, P., Lebleu, B., and Chernomordik, L. V. (2005) Cellular uptake of unconjugated TAT peptide involves clathrin-dependent endocytosis and heparan sulfate receptors. *J Biol Chem* **280**, 15300-15306
104. Suzuki, T., Futaki, S., Niwa, M., Tanaka, S., Ueda, K., and Sugiura, Y. (2002) Possible existence of common internalization mechanisms among arginine-rich peptides. *J Biol Chem* **277**, 2437-2443
105. Ziegler, A., and Seelig, J. (2008) Binding and clustering of glycosaminoglycans: a common property of mono- and multivalent cell-penetrating compounds. *Biophys J* **94**, 2142-2149
106. Ziegler, A., and Seelig, J. (2004) Interaction of the protein transduction domain of HIV-1 TAT with heparan sulfate: binding mechanism and thermodynamic parameters. *Biophys J* **86**, 254-263
107. Fuchs, S. M., and Raines, R. T. (2004) Pathway for polyarginine entry into mammalian cells. *Biochemistry* **43**, 2438-2444
108. Nakase, I., Tadokoro, A., Kawabata, N., Takeuchi, T., Katoh, H., Hiramoto, K., Negishi, M., Nomizu, M., Sugiura, Y., and Futaki, S. (2007) Interaction of arginine-rich peptides with membrane-associated proteoglycans is crucial for induction of actin organization and macropinocytosis. *Biochemistry* **46**, 492-501
109. Ridley, A. J. (1994) Membrane ruffling and signal transduction. *Bioessays* **16**, 321-327
110. Madani, F., Lindberg, S., Langel, U., Futaki, S., and Graslund, A. (2011) Mechanisms of cellular uptake of cell-penetrating peptides. *Journal of biophysics (Hindawi Publishing Corporation : Online)* **2011**, 414729
111. Kaplan, I. M., Wadia, J. S., and Dowdy, S. F. (2005) Cationic TAT peptide transduction domain enters cells by macropinocytosis. *J Control Release* **102**, 247-253
112. Fotin-Mleczek, M., Welte, S., Mader, O., Duchardt, F., Fischer, R., Hufnagel, H., Scheurich, P., and Brock, R. (2005) Cationic cell-penetrating peptides interfere with TNF signalling by induction of TNF receptor internalization. *J Cell Sci* **118**, 3339-3351
113. Nakase, I., Niwa, M., Takeuchi, T., Sonomura, K., Kawabata, N., Koike, Y., Takehashi, M., Tanaka, S., Ueda, K., Simpson, J. C., Jones, A. T., Sugiura, Y., and Futaki, S. (2004) Cellular uptake of arginine-rich peptides: roles for macropinocytosis and actin rearrangement. *Mol Ther* **10**, 1011-1022
114. Wadia, J. S., Stan, R. V., and Dowdy, S. F. (2004) Transducible TAT-HA fusogenic peptide enhances escape of TAT-fusion proteins after lipid raft macropinocytosis. *Nat Med* **10**, 310-315

115. Fittipaldi, A., Ferrari, A., Zoppe, M., Arcangeli, C., Pellegrini, V., Beltram, F., and Giacca, M. (2003) Cell membrane lipid rafts mediate caveolar endocytosis of HIV-1 Tat fusion proteins. *J Biol Chem* **278**, 34141-34149
116. Gump, J. M., June, R. K., and Dowdy, S. F. (2010) Revised role of glycosaminoglycans in TAT protein transduction domain-mediated cellular transduction. *J Biol Chem* **285**, 1500-1507
117. Swanson, J. A. (2008) Shaping cups into phagosomes and macropinosomes. *Nat Rev Mol Cell Biol* **9**, 639-649
118. Stoorvogel, W., Oorschot, V., and Geuze, H. J. (1996) A novel class of clathrin-coated vesicles budding from endosomes. *J Cell Biol* **132**, 21-33
119. Fridolfsson, H. N., Roth, D. M., Insel, P. A., and Patel, H. H. (2014) Regulation of intracellular signaling and function by caveolin. *FASEB J* **28**, 3823-3831
120. Huotari, J., and Helenius, A. (2011) Endosome maturation. *EMBO J* **30**, 3481-3500
121. Gruenberg, J., Griffiths, G., and Howell, K. E. (1989) Characterization of the early endosome and putative endocytic carrier vesicles in vivo and with an assay of vesicle fusion in vitro. *J Cell Biol* **108**, 1301-1316
122. Gruenberg, J. (2001) The endocytic pathway: a mosaic of domains. *Nat Rev Mol Cell Biol* **2**, 721-730
123. Stenmark, H. (2009) Rab GTPases as coordinators of vesicle traffic. *Nat Rev Mol Cell Biol* **10**, 513-525
124. Griffiths, G., Hoflack, B., Simons, K., Mellman, I., and Kornfeld, S. (1988) The mannose 6-phosphate receptor and the biogenesis of lysosomes. *Cell* **52**, 329-341
125. Kobayashi, T., Stang, E., Fang, K. S., de Moerloose, P., Parton, R. G., and Gruenberg, J. (1998) A lipid associated with the antiphospholipid syndrome regulates endosome structure and function. *Nature* **392**, 193-197
126. Kobayashi, T., Beuchat, M. H., Chevallier, J., Makino, A., Mayran, N., Escola, J. M., Lebrand, C., Cosson, P., Kobayashi, T., and Gruenberg, J. (2002) Separation and characterization of late endosomal membrane domains. *J Biol Chem* **277**, 32157-32164
127. Yang, S. T., Zaitseva, E., Chernomordik, L. V., and Melikov, K. (2010) Cell-penetrating peptide induces leaky fusion of liposomes containing late endosome-specific anionic lipid. *Biophys J* **99**, 2525-2533
128. Cooper, G. M. (2000) *The Cell: A Molecular Approach*, 2nd ed., Sinauer Associates, Sunderland (MA)
129. Xu, H., and Ren, D. (2015) Lysosomal physiology. *Annu Rev Physiol* **77**, 57-80
130. Aits, S., and Jäättelä, M. (2013) Lysosomal cell death at a glance. *Journal of Cell Science* **126**, 1905-1912
131. Lee, Y. J., Datta, S., and Pellois, J. P. (2008) Real-time fluorescence detection of protein transduction into live cells. *J Am Chem Soc* **130**, 2398-2399
132. Gillmeister, M. P., Betenbaugh, M. J., and Fishman, P. S. (2011) Cellular trafficking and photochemical internalization of cell penetrating peptide linked cargo proteins: a dual fluorescent labeling study. *Bioconjug Chem* **22**, 556-566

133. Appelbaum, J. S., LaRochelle, J. R., Smith, B. A., Balkin, D. M., Holub, J. M., and Schepartz, A. (2012) Arginine topology controls escape of minimally cationic proteins from early endosomes to the cytoplasm. *Chem Biol* **19**, 819-830
134. Burlina, F., Sagan, S., Bolbach, G., and Chassaing, G. (2006) A direct approach to quantification of the cellular uptake of cell-penetrating peptides using MALDI-TOF mass spectrometry. *Nat. Protocols* **1**, 200-205
135. Paramelle, D., Subra, G., Vezenkov, L. L., Maynadier, M., Andre, C., Enjalbal, C., Calmes, M., Garcia, M., Martinez, J., and Amblard, M. (2010) A straightforward approach for cellular-uptake quantification. *Angewandte Chemie* **49**, 8240-8243
136. Loison, F., Nizard, P., Sourisseau, T., Le Goff, P., Debure, L., Le Drean, Y., and Michel, D. (2005) A ubiquitin-based assay for the cytosolic uptake of protein transduction domains. *Mol Ther* **11**, 205-214
137. Erazo-Oliveras, A., Najjar, K., Dayani, L., Wang, T.-Y., Johnson, G. A., and Pellois, J.-P. (2014) Protein delivery into live cells by incubation with an endosomolytic agent. *Nat Meth* **11**, 861-867
138. Erazo-Oliveras, A., Najjar, K., Truong, D., Wang, T.-Y., Brock, D. J., Prater, A., and Pellois, J.-P. (2016) The Late Endosome and Its Lipid BMP Act as Gateways for Efficient Cytosolic Access of the Delivery Agent dfTAT and Its Macromolecular Cargos. *Cell chemical biology* **23**, 598-607
139. Erazo-Oliveras, A., Muthukrishnan, N., Baker, R., Wang, T. Y., and Pellois, J. P. (2012) Improving the endosomal escape of cell-penetrating peptides and their cargos: strategies and challenges. *Pharmaceuticals (Basel)* **5**, 1177-1209
140. El-Sayed, A., Futaki, S., and Harashima, H. (2009) Delivery of macromolecules using arginine-rich cell-penetrating peptides: ways to overcome endosomal entrapment. *AAPS J* **11**, 13-22
141. Lönn, P., Kacsinta, A. D., Cui, X.-S., Hamil, A. S., Kaulich, M., Gogoi, K., and Dowdy, S. F. (2016) Enhancing Endosomal Escape for Intracellular Delivery of Macromolecular Biologic Therapeutics. *Scientific Reports* **6**, 32301
142. Ciftci, K., and Levy, R. J. (2001) Enhanced plasmid DNA transfection with lysosomotropic agents in cultured fibroblasts. *Int J Pharm* **218**, 81-92
143. Erbacher, P., Roche, A. C., Monsigny, M., and Midoux, P. (1996) Putative role of chloroquine in gene transfer into a human hepatoma cell line by DNA/lactosylated polylysine complexes. *Exp Cell Res* **225**, 186-194
144. Caron, N. J., Quenneville, S. P., and Tremblay, J. P. (2004) Endosome disruption enhances the functional nuclear delivery of Tat-fusion proteins. *Biochem Biophys Res Commun* **319**, 12-20
145. Shiraishi, T., and Nielsen, P. E. (2006) Enhanced delivery of cell-penetrating peptide-peptide nucleic acid conjugates by endosomal disruption. *Nat Protoc* **1**, 633-636
146. Forgac, M. (2007) Vacuolar ATPases: rotary proton pumps in physiology and pathophysiology. *Nat Rev Mol Cell Biol* **8**, 917-929

147. Wharton, S. A., Martin, S. R., Ruigrok, R. W., Skehel, J. J., and Wiley, D. C. (1988) Membrane fusion by peptide analogues of influenza virus haemagglutinin. *J Gen Virol* **69 (Pt 8)**, 1847-1857
148. Michiue, H., Tomizawa, K., Wei, F. Y., Matsushita, M., Lu, Y. F., Ichikawa, T., Tamiya, T., Date, I., and Matsui, H. (2005) The NH2 terminus of influenza virus hemagglutinin-2 subunit peptides enhances the antitumor potency of polyarginine-mediated p53 protein transduction. *J Biol Chem* **280**, 8285-8289
149. Maiolo, J. R., 3rd, Ottinger, E. A., and Ferrer, M. (2004) Specific redistribution of cell-penetrating peptides from endosomes to the cytoplasm and nucleus upon laser illumination. *J Am Chem Soc* **126**, 15376-15377
150. Matsushita, M., Noguchi, H., Lu, Y. F., Tomizawa, K., Michiue, H., Li, S. T., Hirose, K., Bonner-Weir, S., and Matsui, H. (2004) Photo-acceleration of protein release from endosome in the protein transduction system. *FEBS Lett* **572**, 221-226
151. Srinivasan, D., Muthukrishnan, N., Johnson, G. A., Erazo-Oliveras, A., Lim, J., Simanek, E. E., and Pellois, J. P. (2011) Conjugation to the cell-penetrating peptide TAT potentiates the photodynamic effect of carboxytetramethylrhodamine. *PLoS One* **6**, e17732
152. Muthukrishnan, N., Johnson, G. A., Erazo-Oliveras, A., and Pellois, J. P. (2013) Synergy between cell-penetrating peptides and singlet oxygen generators leads to efficient photolysis of membranes. *Photochemistry and photobiology* **89**, 625-630
153. Choi, Y., McCarthy, J. R., Weissleder, R., and Tung, C. H. (2006) Conjugation of a photosensitizer to an oligoarginine-based cell-penetrating peptide increases the efficacy of photodynamic therapy. *ChemMedChem* **1**, 458-463
154. Lee, Y. C., Townsend, R. R., Hardy, M. R., Lonngren, J., Arnarp, J., Haraldsson, M., and Lonn, H. (1983) Binding of synthetic oligosaccharides to the hepatic Gal/GalNAc lectin. Dependence on fine structural features. *J Biol Chem* **258**, 199-202
155. Mammen, M., Choi, S.-K., and Whitesides, G. M. (1998) Polyvalent Interactions in Biological Systems: Implications for Design and Use of Multivalent Ligands and Inhibitors. *Angewandte Chemie International Edition* **37**, 2754-2794
156. Kiessling, L. L., Gestwicki, J. E., and Strong, L. E. (2000) Synthetic multivalent ligands in the exploration of cell-surface interactions. *Curr Opin Chem Biol* **4**, 696-703
157. Sung, M., Poon, G. M., and Gariepy, J. (2006) The importance of valency in enhancing the import and cell routing potential of protein transduction domain-containing molecules. *Biochim Biophys Acta* **1758**, 355-363
158. Torchilin, V. P., Rammohan, R., Weissig, V., and Levchenko, T. S. (2001) TAT peptide on the surface of liposomes affords their efficient intracellular delivery even at low temperature and in the presence of metabolic inhibitors. *Proceedings of the National Academy of Sciences* **98**, 8786-8791
159. Torchilin, V. P. (2002) TAT peptide-modified liposomes for intracellular delivery of drugs and DNA. *Cell Mol Biol Lett* **7**, 265-267

160. Torchilin, V. P., Levchenko, T. S., Rammohan, R., Volodina, N., Papahadjopoulos-Sternberg, B., and D'Souza, G. G. (2003) Cell transfection in vitro and in vivo with nontoxic TAT peptide-liposome-DNA complexes. *Proc Natl Acad Sci U S A* **100**, 1972-1977
161. Zhao, M., Kircher, M. F., Josephson, L., and Weissleder, R. (2002) Differential conjugation of tat peptide to superparamagnetic nanoparticles and its effect on cellular uptake. *Bioconjug Chem* **13**, 840-844
162. Koch, A. M., Reynolds, F., Merkle, H. P., Weissleder, R., and Josephson, L. (2005) Transport of surface-modified nanoparticles through cell monolayers. *Chembiochem* **6**, 337-345
163. Kircher, M. F., Allport, J. R., Graves, E. E., Love, V., Josephson, L., Lichtman, A. H., and Weissleder, R. (2003) In vivo high resolution three-dimensional imaging of antigen-specific cytotoxic T-lymphocyte trafficking to tumors. *Cancer Res* **63**, 6838-6846
164. Lewin, M., Carlesso, N., Tung, C. H., Tang, X. W., Cory, D., Scadden, D. T., and Weissleder, R. (2000) Tat peptide-derivatized magnetic nanoparticles allow in vivo tracking and recovery of progenitor cells. *Nat Biotechnol* **18**, 410-414
165. Johnson, C. R., Morin, P. E., Arrowsmith, C. H., and Freire, E. (1995) Thermodynamic analysis of the structural stability of the tetrameric oligomerization domain of p53 tumor suppressor. *Biochemistry* **34**, 5309-5316
166. Phelan, A., Elliott, G., and O'Hare, P. (1998) Intercellular delivery of functional p53 by the herpesvirus protein VP22. *Nat Biotechnol* **16**, 440-443
167. Kawamura, K. S., Sung, M., Bolewska-Pedyczak, E., and Gariepy, J. (2006) Probing the impact of valency on the routing of arginine-rich peptides into eukaryotic cells. *Biochemistry* **45**, 1116-1127
168. Lee, W., Harvey, T. S., Yin, Y., Yau, P., Litchfield, D., and Arrowsmith, C. H. (1994) Solution structure of the tetrameric minimum transforming domain of p53. *Nat Struct Biol* **1**, 877-890
169. Chen, M., Won, D. J., Krajewski, S., and Gottlieb, R. A. (2002) Calpain and mitochondria in ischemia/reperfusion injury. *J Biol Chem* **277**, 29181-29186
170. Wang, J., Dai, H., Yousaf, N., Moussaif, M., Deng, Y., Boufelliga, A., Swamy, O. R., Leone, M. E., and Riedel, H. (1999) Grb10, a positive, stimulatory signaling adapter in platelet-derived growth factor BB-, insulin-like growth factor I-, and insulin-mediated mitogenesis. *Mol Cell Biol* **19**, 6217-6228
171. Kang, H., DeLong, R., Fisher, M. H., and Juliano, R. L. (2005) Tat-conjugated PAMAM dendrimers as delivery agents for antisense and siRNA oligonucleotides. *Pharm Res* **22**, 2099-2106
172. Juliano, R. L. (2006) Intracellular delivery of oligonucleotide conjugates and dendrimer complexes. *Ann N Y Acad Sci* **1082**, 18-26
173. Kim, J. B., Choi, J. S., Nam, K., Lee, M., Park, J. S., and Lee, J. K. (2006) Enhanced transfection of primary cortical cultures using arginine-grafted PAMAM dendrimer, PAMAM-Arg. *J Control Release* **114**, 110-117

174. Pantos, A., Tsiourvas, D., Nounesis, G., and Paleos, C. M. (2005) Interaction of functional dendrimers with multilamellar liposomes: design of a model system for studying drug delivery. *Langmuir* **21**, 7483-7490
175. Medina, S. H., and El-Sayed, M. E. (2009) Dendrimers as carriers for delivery of chemotherapeutic agents. *Chem Rev* **109**, 3141-3157
176. Sheldon, K., Liu, D., Ferguson, J., and Gariepy, J. (1995) Loligomers: design of de novo peptide-based intracellular vehicles. *Proc Natl Acad Sci U S A* **92**, 2056-2060
177. Singh, D., Kiarash, R., Kawamura, K., LaCasse, E. C., and Gariepy, J. (1998) Penetration and intracellular routing of nucleus-directed peptide-based shuttles (loligomers) in eukaryotic cells. *Biochemistry* **37**, 5798-5809
178. Singh, D., Bisland, S. K., Kawamura, K., and Gariepy, J. (1999) Peptide-based intracellular shuttle able to facilitate gene transfer in mammalian cells. *Bioconjug Chem* **10**, 745-754
179. Kawamura, K. S., Su, R. C., Nguyen, L. T., Elford, A. R., Ohashi, P. S., and Gariepy, J. (2002) In vivo generation of cytotoxic T cells from epitopes displayed on peptide-based delivery vehicles. *J Immunol* **168**, 5709-5715
180. Angeles-Boza, A. M., Erazo-Oliveras, A., Lee, Y. J., and Pellois, J. P. (2010) Generation of endosomolytic reagents by branching of cell-penetrating peptides: tools for the delivery of bioactive compounds to live cells in cis or trans. *Bioconjug Chem* **21**, 2164-2167
181. Dawson, P. E., Muir, T. W., Clark-Lewis, I., and Kent, S. B. (1994) Synthesis of proteins by native chemical ligation. *Science* **266**, 776-779
182. Rudolph, C., Schillinger, U., Ortiz, A., Tabatt, K., Plank, C., Muller, R. H., and Rosenecker, J. (2004) Application of novel solid lipid nanoparticle (SLN)-gene vector formulations based on a dimeric HIV-1 TAT-peptide in vitro and in vivo. *Pharm Res* **21**, 1662-1669
183. Lee, S. J., Yoon, S. H., and Doh, K. O. (2011) Enhancement of gene delivery using novel homodimeric tat peptide formed by disulfide bond. *J Microbiol Biotechnol* **21**, 802-807
184. Joshi, V. G., Dighe, V. D., Thakuria, D., Malik, Y. S., and Kumar, S. (2013) Multiple antigenic peptide (MAP): a synthetic peptide dendrimer for diagnostic, antiviral and vaccine strategies for emerging and re-emerging viral diseases. *Indian journal of virology : an official organ of Indian Virological Society* **24**, 312-320
185. Vivès, E., Brodin, P., and Lebleu, B. (1997) A Truncated HIV-1 Tat Protein Basic Domain Rapidly Translocates through the Plasma Membrane and Accumulates in the Cell Nucleus. *Journal of Biological Chemistry* **272**, 16010-16017
186. Lian, X., Erazo-Oliveras, A., Pellois, J. P., and Zhou, H. C. (2017) High efficiency and long-term intracellular activity of an enzymatic nanofactory based on metal-organic frameworks. *Nat Commun* **8**, 2075
187. Najjar, K., Erazo-Oliveras, A., Brock, D. J., Wang, T. Y., and Pellois, J. P. (2017) An l- to d-Amino Acid Conversion in an Endosomolytic Analog of the

Cell-penetrating Peptide TAT Influences Proteolytic Stability, Endocytic Uptake, and Endosomal Escape. *J Biol Chem* **292**, 847-861
188. Authier, F., Posner, B. I., and Bergeron, J. J. (1996) Endosomal proteolysis of internalized proteins. *FEBS Lett* **389**, 55-60
189. Chatterjee, B., Smed-Sorensen, A., Cohn, L., Chalouni, C., Vandlen, R., Lee, B. C., Widger, J., Keler, T., Delamarre, L., and Mellman, I. (2012) Internalization and endosomal degradation of receptor-bound antigens regulate the efficiency of cross presentation by human dendritic cells. *Blood* **120**, 2011-2020
190. Diment, S., and Stahl, P. (1985) Macrophage endosomes contain proteases which degrade endocytosed protein ligands. *J Biol Chem* **260**, 15311-15317
191. Allen, J. K., Brock, D. J., Kondow-McConaghy, H. M., and Pellois, J. P. (2018) Efficient Delivery of Macromolecules into Human Cells by Improving the Endosomal Escape Activity of Cell-Penetrating Peptides: Lessons Learned from dfTAT and its Analogs. *Biomolecules* **8**, 50
192. LaRochelle, J. R., Cobb, G. B., Steinauer, A., Rhoades, E., and Schepartz, A. (2015) Fluorescence correlation spectroscopy reveals highly efficient cytosolic delivery of certain penta-arg proteins and stapled peptides. *J Am Chem Soc* **137**, 2536-2541
193. Brock, D. J., Kondow-McConaghy, H. M., Hager, E. C., and Pellois, J.-P. (2019) Endosomal Escape and Cytosolic Penetration of Macromolecules Mediated by Synthetic Delivery Agents. *Bioconjugate Chemistry* **30**, 293-304
194. Glover, D. J., Leyton, D. L., Moseley, G. W., and Jans, D. A. (2010) The efficiency of nuclear plasmid DNA delivery is a critical determinant of transgene expression at the single cell level. *J Gene Med* **12**, 77-85
195. Pollard, H., Remy, J. S., Loussouarn, G., Demolombe, S., Behr, J. P., and Escande, D. (1998) Polyethylenimine but not cationic lipids promotes transgene delivery to the nucleus in mammalian cells. *Journal of Biological Chemistry* **273**, 7507-7511
196. Xu, Y., and Szoka, F. C., Jr. (1996) Mechanism of DNA release from cationic liposome/DNA complexes used in cell transfection. *Biochemistry* **35**, 5616-5623
197. Rezgui, R., Blumer, K., Yeoh-Tan, G., Trexler, A. J., and Magzoub, M. (2016) Precise quantification of cellular uptake of cell-penetrating peptides using fluorescence-activated cell sorting and fluorescence correlation spectroscopy. *Biochim Biophys Acta* **1858**, 1499-1506
198. Takayama, K., Nakase, I., Michiue, H., Takeuchi, T., Tomizawa, K., Matsui, H., and Futaki, S. (2009) Enhanced intracellular delivery using arginine-rich peptides by the addition of penetration accelerating sequences (Pas). *J Control Release* **138**, 128-133
199. Yang, B., Ming, X., Cao, C., Laing, B., Yuan, A., Porter, M. A., Hull-Ryde, E. A., Maddry, J., Suto, M., Janzen, W. P., and Juliano, R. L. (2015) High-throughput screening identifies small molecules that enhance the pharmacological effects of oligonucleotides. *Nucleic Acids Res* **43**, 1987-1996
200. Selbo, P. K., Weyergang, A., Hogset, A., Norum, O. J., Berstad, M. B., Vikdal, M., and Berg, K. (2010) Photochemical internalization provides time- and space-

controlled endolysosomal escape of therapeutic molecules. *J Control Release* **148**, 2-12
201. Huang, C. H., Chen, P. M., Lu, T. C., Kung, W. M., Chiou, T. J., Yang, M. H., Kao, J. Y., and Wu, K. J. (2010) Purified recombinant TAT-homeobox B4 expands CD34(+) umbilical cord blood and peripheral blood progenitor cells ex vivo. *Tissue Eng Part C Methods* **16**, 487-496
202. Kobayashi, T., Beuchat, M. H., Lindsay, M., Frias, S., Palmiter, R. D., Sakuraba, H., Parton, R. G., and Gruenberg, J. (1999) Late endosomal membranes rich in lysobisphosphatidic acid regulate cholesterol transport. *Nat Cell Biol* **1**, 113-118
203. Matsuo, H., Chevallier, J., Mayran, N., Le Blanc, I., Ferguson, C., Faure, J., Blanc, N. S., Matile, S., Dubochet, J., Sadoul, R., Parton, R. G., Vilbois, F., and Gruenberg, J. (2004) Role of LBPA and Alix in multivesicular liposome formation and endosome organization. *Science* **303**, 531-534
204. Chevallier, J., Chamoun, Z., Jiang, G., Prestwich, G., Sakai, N., Matile, S., Parton, R. G., and Gruenberg, J. (2008) Lysobisphosphatidic acid controls endosomal cholesterol levels. *J Biol Chem* **283**, 27871-27880
205. Théry, C., Boussac, M., Véron, P., Ricciardi-Castagnoli, P., Raposo, G., Garin, J., and Amigorena, S. (2001) Proteomic Analysis of Dendritic Cell-Derived Exosomes: A Secreted Subcellular Compartment Distinct from Apoptotic Vesicles. *The Journal of Immunology* **166**, 7309
206. Garin, J., Diez, R., Kieffer, S., Dermine, J.-F., Duclos, S., Gagnon, E., Sadoul, R., Rondeau, C., and Desjardins, M. (2001) The Phagosome Proteome. *The Journal of Cell Biology* **152**, 165
207. Odorizzi, G., Katzmann, D. J., Babst, M., Audhya, A., and Emr, S. D. (2003) Bro1 is an endosome-associated protein that functions in the MVB pathway in Saccharomyces cerevisiae. *Journal of Cell Science* **116**, 1893
208. Falguieres, T., Luyet, P. P., Bissig, C., Scott, C. C., Velluz, M. C., and Gruenberg, J. (2008) In vitro budding of intralumenal vesicles into late endosomes is regulated by Alix and Tsg101. *Mol Biol Cell* **19**, 4942-4955
209. Goldstein, J. L., Brown, M. S., Anderson, R. G., Russell, D. W., and Schneider, W. J. (1985) Receptor-mediated endocytosis: concepts emerging from the LDL receptor system. *Annu Rev Cell Biol* **1**, 1-39
210. Liscum, L., and Klansek, J. J. (1998) Niemann–Pick disease type C. *Current Opinion in Lipidology* **9**, 131-135
211. Chavrier, P., Parton, R. G., Hauri, H. P., Simons, K., and Zerial, M. (1990) Localization of low molecular weight GTP binding proteins to exocytic and endocytic compartments. *Cell* **62**, 317-329
212. Escola, J. M., Kleijmeer, M. J., Stoorvogel, W., Griffith, J. M., Yoshie, O., and Geuze, H. J. (1998) Selective enrichment of tetraspan proteins on the internal vesicles of multivesicular endosomes and on exosomes secreted by human B-lymphocytes. *J Biol Chem* **273**, 20121-20127
213. Kornfeld, S. (1992) Structure and function of the mannose 6-phosphate/insulinlike growth factor II receptors. *Annu Rev Biochem* **61**, 307-330

214. Zaitseva, E., Yang, S. T., Melikov, K., Pourmal, S., and Chernomordik, L. V. (2010) Dengue virus ensures its fusion in late endosomes using compartment-specific lipids. *PLoS pathogens* **6**, e1001131
215. Patel, A., Mohl, B. P., and Roy, P. (2016) Entry of Bluetongue Virus Capsid Requires the Late Endosome-specific Lipid Lysobisphosphatidic Acid. *J Biol Chem* **291**, 12408-12419
216. Freire, J. M., Veiga, A. S., Conceicao, T. M., Kowalczyk, W., Mohana-Borges, R., Andreu, D., Santos, N. C., Da Poian, A. T., and Castanho, M. A. (2013) Intracellular nucleic acid delivery by the supercharged dengue virus capsid protein. *PLoS One* **8**, e81450
217. Freire, J. M., Almeida Dias, S., Flores, L., Veiga, A. S., and Castanho, M. A. (2015) Mining viral proteins for antimicrobial and cell-penetrating drug delivery peptides. *Bioinformatics* **31**, 2252-2256
218. Freire, J. M., Santos, N. C., Veiga, A. S., Da Poian, A. T., and Castanho, M. A. (2015) Rethinking the capsid proteins of enveloped viruses: multifunctionality from genome packaging to genome transfection. *FEBS J* **282**, 2267-2278
219. Mukhopadhyay, S., Kuhn, R. J., and Rossmann, M. G. (2005) A structural perspective of the flavivirus life cycle. *Nat Rev Microbiol* **3**, 13-22
220. Ma, L., Jones, C. T., Groesch, T. D., Kuhn, R. J., and Post, C. B. (2004) Solution structure of dengue virus capsid protein reveals another fold. *Proc Natl Acad Sci U S A* **101**, 3414-3419
221. Brooks, H., Lebleu, B., and Vives, E. (2005) Tat peptide-mediated cellular delivery: back to basics. *Adv Drug Deliv Rev* **57**, 559-577
222. Kay, M. A., Glorioso, J. C., and Naldini, L. (2001) Viral vectors for gene therapy: the art of turning infectious agents into vehicles of therapeutics. *Nature Medicine* **7**, 33-40
223. Samal, S. K., Dash, M., Van Vlierberghe, S., Kaplan, D. L., Chiellini, E., van Blitterswijk, C., Moroni, L., and Dubruel, P. (2012) Cationic polymers and their therapeutic potential. *Chem Soc Rev* **41**, 7147-7194
224. Zelphati, O., Wang, Y., Kitada, S., Reed, J. C., Felgner, P. L., and Corbeil, J. (2001) Intracellular delivery of proteins with a new lipid-mediated delivery system. *J Biol Chem* **276**, 35103-35110
225. Cleal, K., He, L., Watson, P. D., and Jones, A. T. (2013) Endocytosis, intracellular traffic and fate of cell penetrating peptide based conjugates and nanoparticles. *Curr Pharm Des* **19**, 2878-2894
226. Fotin-Mleczek, M., Fischer, R., and Brock, R. (2005) Endocytosis and cationic cell-penetrating peptides--a merger of concepts and methods. *Curr Pharm Des* **11**, 3613-3628
227. Chesnoy, S., and Huang, L. (2000) Structure and function of lipid-DNA complexes for gene delivery. *Annual review of biophysics and biomolecular structure* **29**, 27-47
228. Cronican, J., Beier, K., Davis, T., Tseng, J.-C., Li, W., Thompson, D., Shih, A., May, E., Cepko, C., Kung, A., Zhou, Q., and Liu, D. (2011) A class of human

proteins that deliver functional proteins into mammalian cells in vitro and in vivo. *Chemistry & biology* **18**, 833-838
229. Futaki, S., Nakase, I., Suzuki, T., Youjun, Z., and Sugiura, Y. (2002) Translocation of branched-chain arginine peptides through cell membranes: flexibility in the spatial disposition of positive charges in membrane-permeable peptides. *Biochemistry* **41**, 7925-7930
230. Jeong, C., Yoo, J., Lee, D., and Kim, Y.-C. (2016) A branched TAT cell-penetrating peptide as a novel delivery carrier for the efficient gene transfection. *Biomaterials Research* **20**, 28-28
231. Liu, Z., Li, M., Cui, D., and Fei, J. (2005) Macro-branched cell-penetrating peptide design for gene delivery. *J Control Release* **102**, 699-710
232. Backlund, C. M., Takeuchi, T., Futaki, S., and Tew, G. N. (2016) Relating structure and internalization for ROMP-based protein mimics. *Biochim Biophys Acta* **1858**, 1443-1450
233. Fretz, M. M., Penning, N. A., Al-Taei, S., Futaki, S., Takeuchi, T., Nakase, I., Storm, G., and Jones, A. T. (2007) Temperature-, concentration- and cholesterol-dependent translocation of L- and D-octa-arginine across the plasma and nuclear membrane of CD34+ leukaemia cells. *Biochem J* **403**, 335-342
234. Najjar, K., Erazo-Oliveras, A., Mosior, J. W., Whitlock, M. J., Rostane, I., Cinclair, J. M., and Pellois, J. P. (2017) Unlocking Endosomal Entrapment with Supercharged Arginine-Rich Peptides. *Bioconjug Chem* **28**, 2932-2941
235. Brock, D. J., Kustigian, L., Jiang, M., Graham, K., Wang, T. Y., Erazo-Oliveras, A., Najjar, K., Zhang, J., Rye, H., and Pellois, J. P. (2018) Efficient cell delivery mediated by lipid-specific endosomal escape of supercharged branched peptides. *Traffic* **19**, 421-435
236. Peitz, M., Pfannkuche, K., Rajewsky, K., and Edenhofer, F. (2002) Ability of the hydrophobic FGF and basic TAT peptides to promote cellular uptake of recombinant Cre recombinase: a tool for efficient genetic engineering of mammalian genomes. *Proc Natl Acad Sci U S A* **99**, 4489-4494
237. Sun, X., Zhang, A., Baker, B., Sun, L., Howard, A., Buswell, J., Maurel, D., Masharina, A., Johnsson, K., Noren, C. J., Xu, M. Q., and Correa, I. R., Jr. (2011) Development of SNAP-tag fluorogenic probes for wash-free fluorescence imaging. *Chembiochem* **12**, 2217-2226
238. Kobayashi, T., Startchev, K., Whitney, A. J., and Gruenber, J. (2001) Localization of lysobisphosphatidic acid-rich membrane domains in late endosomes. *Biol Chem* **382**, 483-485
239. Brooks, A., Shoup, D., Kustigian, L., Puchalla, J., Carr, C. M., and Rye, H. S. (2015) Single particle fluorescence burst analysis of epsin induced membrane fission. *PLoS One* **10**, e0119563
240. Puchalla, J., Krantz, K., Austin, R., and Rye, H. (2008) Burst analysis spectroscopy: a versatile single-particle approach for studying distributions of protein aggregates and fluorescent assemblies. *Proc Natl Acad Sci U S A* **105**, 14400-14405

241. Araç, D., Chen, X., Khant, H., Ubach, J., Ludtke, S., Kikkawa, M., Johnson, A., Chiu, W., Südhof, T., and Rizo, J. (2006) Close membrane-membrane proximity induced by Ca(2+)-dependent multivalent binding of synaptotagmin-1 to phospholipids. *Nature Structural & Molecular Biology* **13**, 209-217
242. Brooks, A., Shoup, D., Kustigian, L., Puchalla, J., Carr, C., and Rye, H. (2015) Single particle fluorescence burst analysis of epsin induced membrane fission. *PloS one* **10**, e0119563-e0119563
243. Argyris, E., Kulkosky, J., E Meyer, M., Xu, Y., Mukhtar, M., J Pomerantz, R., and Williams, K. J. (2005) *The perlecan heparan sulfate proteoglycan mediates cellular uptake of HIV-1 Tat through a pathway responsible for biological activity*,
244. Rusnati, M., Coltrini, D., Oreste, P., Zoppetti, G., Albini, A., Noonan, D., d'Adda di Fagagna, F., and Giacca, M., and Presta, M. (1997) *Interaction of HIV-1 Tat Protein with Heparin. Role of the backbone structure, sulfation, and size*,
245. Tyagi, M., Rusnati, M., Presta, M., and Giacca, M. (2001) *Internalization of HIV-1 Tat Requires Cell Surface Heparan Sulfate Proteoglycans*,
246. Puri, V., Watanabe, R., Dominguez, M., Sun, X., Wheatley, C. L., Marks, D. L., and Pagano, R. E. (1999) Cholesterol modulates membrane traffic along the endocytic pathway in sphingolipid-storage diseases. *Nat Cell Biol* **1**, 386-388
247. Harris, F. M., Best, K. B., and Bell, J. D. (2002) Use of laurdan fluorescence intensity and polarization to distinguish between changes in membrane fluidity and phospholipid order. *Biochimica et Biophysica Acta (BBA) - Biomembranes* **1565**, 123-128
248. Jin, L., Millard, A. C., Wuskell, J. P., Dong, X., Wu, D., Clark, H. A., and Loew, L. M. (2006) Characterization and application of a new optical probe for membrane lipid domains. *Biophys J* **90**, 2563-2575
249. Dinic, J., Biverstahl, H., Maler, L., and Parmryd, I. (2011) Laurdan and di-4-ANEPPDHQ do not respond to membrane-inserted peptides and are good probes for lipid packing. *Biochim Biophys Acta* **1808**, 298-306
250. Jin, L., Millard, A. C., Wuskell, J. P., Clark, H. A., and Loew, L. M. (2005) Cholesterol-Enriched Lipid Domains Can Be Visualized by di-4-ANEPPDHQ with Linear and Nonlinear Optics. *Biophysical Journal* **89**, L04-L06
251. Yu, W., So, P. T., French, T., and Gratton, E. (1996) Fluorescence generalized polarization of cell membranes: a two-photon scanning microscopy approach. *Biophys J* **70**, 626-636
252. Dawaliby, R., Trubbia, C., Delporte, C., Noyon, C., Ruysschaert, J. M., Van Antwerpen, P., and Govaerts, C. (2016) Phosphatidylethanolamine Is a Key Regulator of Membrane Fluidity in Eukaryotic Cells. *J Biol Chem* **291**, 3658-3667
253. Holthuis, J. C., and Menon, A. K. (2014) Lipid landscapes and pipelines in membrane homeostasis. *Nature* **510**, 48-57
254. Yeagle, P. L. (1985) Cholesterol and the cell membrane. *Biochim Biophys Acta* **822**, 267-287

255. Chapman, D., and Quinn, P. J. (1976) A method for the modulation of membrane fluidity: homogeneous catalytic hydrogenation of phospholipids and phospholipids and phospholipid-water model biomembranes. *Proc Natl Acad Sci U S A* **73**, 3971-3975
256. Kamada, T., Yamashita, T., Baba, Y., Kai, M., Setoyama, S., Chuman, Y., and Otsuji, S. (1986) Dietary sardine oil increases erythrocyte membrane fluidity in diabetic patients. *Diabetes* **35**, 604-611
257. Obaid, A. L., Loew, L. M., Wuskell, J. P., and Salzberg, B. M. (2004) Novel naphthylstyryl-pyridium potentiometric dyes offer advantages for neural network analysis. *J Neurosci Methods* **134**, 179-190
258. Owen, D. M., Rentero, C., Magenau, A., Abu-Siniyeh, A., and Gaus, K. (2011) Quantitative imaging of membrane lipid order in cells and organisms. *Nat Protoc* **7**, 24-35
259. Gilleron, J., Querbes, W., Zeigerer, A., Borodovsky, A., Marsico, G., Schubert, U., Manygoats, K., Seifert, S., Andree, C., Stöter, M., Epstein-Barash, H., Zhang, L., Koteliansky, V., Fitzgerald, K., Fava, E., Bickle, M., Kalaidzidis, Y., Akinc, A., Maier, M., and Zerial, M. (2013) Image-based analysis of lipid nanoparticle–mediated siRNA delivery, intracellular trafficking and endosomal escape. *Nature Biotechnology* **31**, 638
260. Juliano, R. L., and Carver, K. (2015) Cellular uptake and intracellular trafficking of oligonucleotides. *Adv Drug Deliv Rev* **87**, 35-45
261. Zuhorn, I. S., Kalicharan, R., and Hoekstra, D. (2002) Lipoplex-mediated transfection of mammalian cells occurs through the cholesterol-dependent clathrin-mediated pathway of endocytosis. *J Biol Chem* **277**, 18021-18028
262. Koltover, I., Salditt, T., Radler, J. O., and Safinya, C. R. (1998) An inverted hexagonal phase of cationic liposome-DNA complexes related to DNA release and delivery. *Science* **281**, 78-81
263. Kitt, J. P., Bryce, D. A., Minteer, S. D., and Harris, J. M. (2017) Raman Spectroscopy Reveals Selective Interactions of Cytochrome c with Cardiolipin That Correlate with Membrane Permeability. *J Am Chem Soc* **139**, 3851-3860

APPENDIX A

SUPPORTING INFORMATION FOR EFFICIENT CELL DELIVERY

MEDIATED BY LIPID-SPECIFIC ENDOSOMAL ESCAPE OF

SUPERCHARGED BRANCHED PEPTIDES

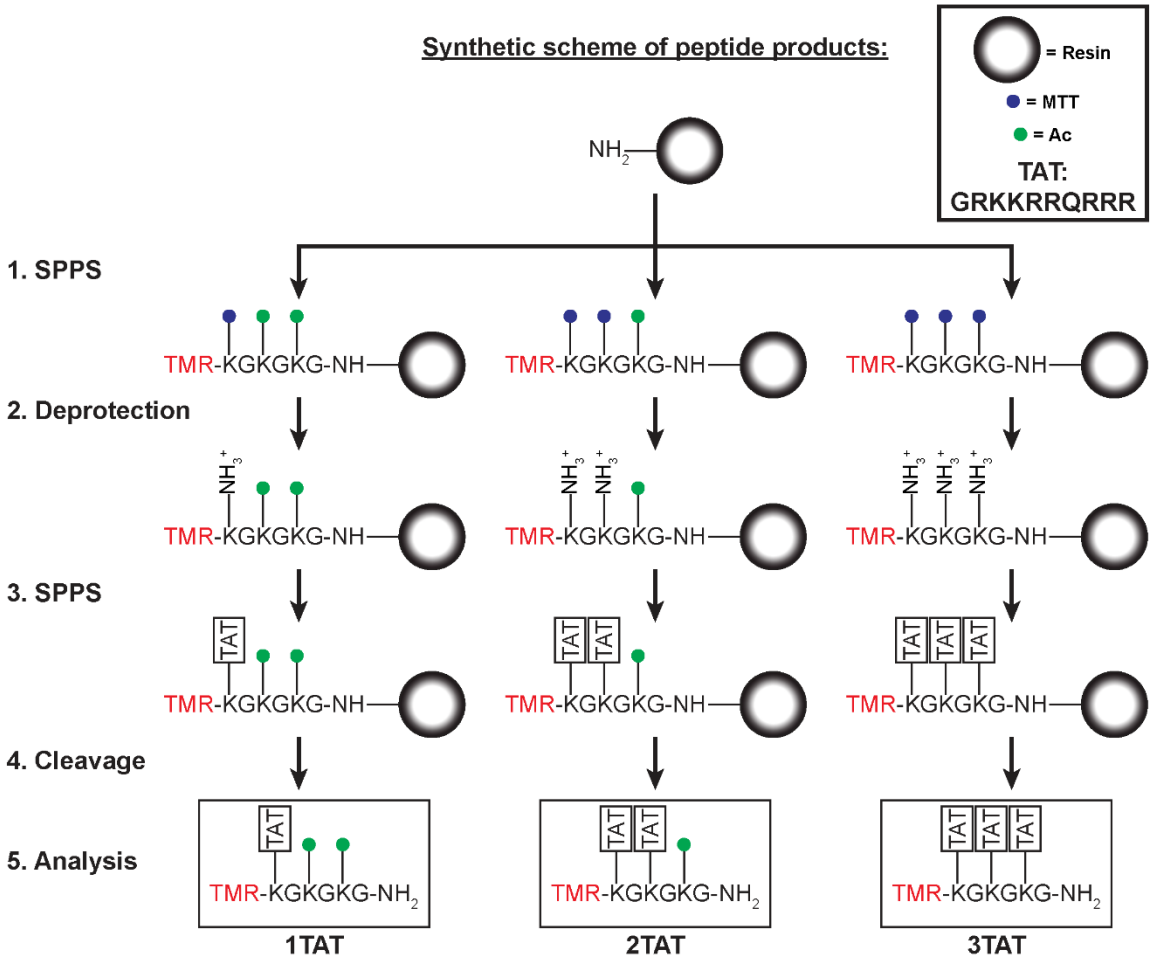

Figure A-1 Synthetic route used for the generation of the peptides 1TAT, 2TAT, 3TAT. Scaffold peptides were first synthesized via solid phase peptide synthesis (SPPS) using standard Fmoc-chemistry. Lysine residues containing cleavable (MTT) or non-cleavable (Ac) protecting groups on the ε-N are introduced at different positions in the scaffold sequence. Following Fmoc removal, the N-terminus of the scaffold peptide is capped with the fluorophore TMR. Next, MTT groups are selectively cleaved under 1% TFA. The TAT peptide branches are then assembled off the ε-N of each deprotected lysine residues. Completed products are cleaved from the solid support by treatment with 95% TFA.

Figure A-2 Characterization of 1TAT, 2TAT and 3TAT.
(a) Structure of 1TAT. (b) rpHPLC analysis and MALDI-TOF MS spectrum of purified 1TAT (retention time (rt): 15.04 min, 0-73% solvent B in 0-30 min) (1TAT, expected mass = 2447.42, observed mass: $(M-H^+)/H^+$ = 2449.55). (c) Structure of 2TAT. (d) rpHPLC analysis and MALDI-TOF MS spectrum of purified 2TAT (retention time (rt): 13.94 min, 0-73% solvent B in 0-30 min) (2TAT, expected mass = 3783.29, observed mass: $(M-H^+)/H^+$ = 3784.53). (e) Structure of 3TAT. (f) rpHPLC analysis and MALDI-TOF MS spectrum of purified 3TAT (retention time (rt): 13.54 min, 0-73% solvent B in 0-30 min) (3TAT, expected mass = 5119.16, observed mass: $(M-H^+)/H^+$ = 5121.03). (g) Structure of nf2TAT. (h) rpHPLC analysis and MALDI-TOF MS spectrum of purified nf2TAT (retention time (rt): 9.25 min, 0-30% solvent B in 0-30 min) (nf2TAT, expected mass = 3413.15, observed mass: $(M-H^+)/H^+$ = 3414.22). (i) Structure of nf3TAT. (j) rpHPLC analysis and MALDI-TOF MS spectrum of purified nf3TAT (retention time (rt): 9.52 min, 0- 30% solvent B in 0-30 min) (nf3TAT, expected mass = 4750.02, observed mass: $(M-H^+)/H^+$ = 4750.53).

a)

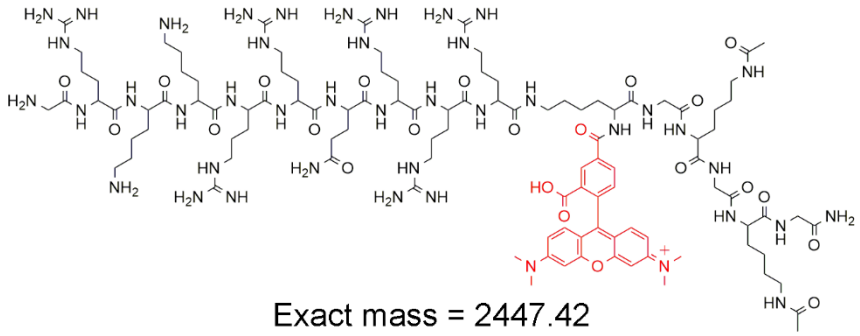

Exact mass = 2447.42

b)

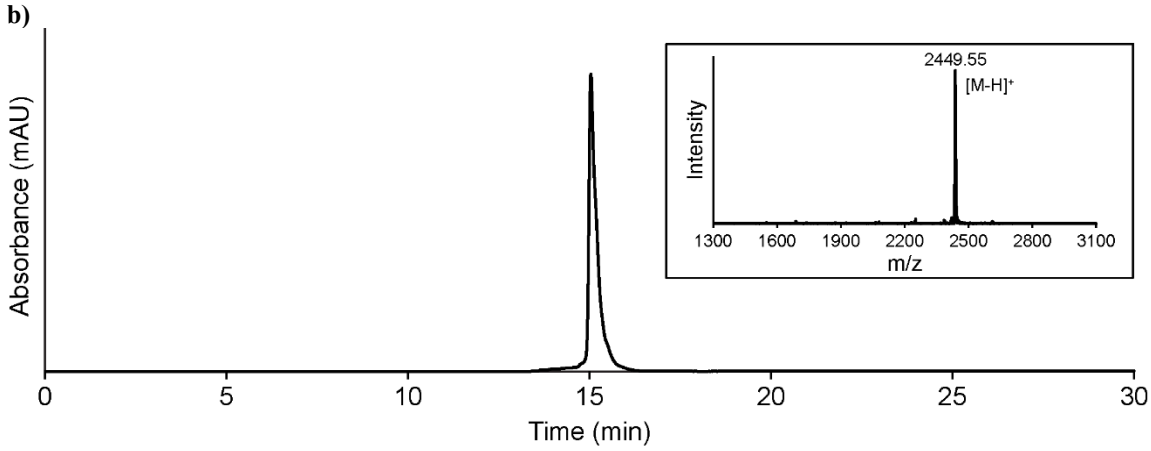

c)

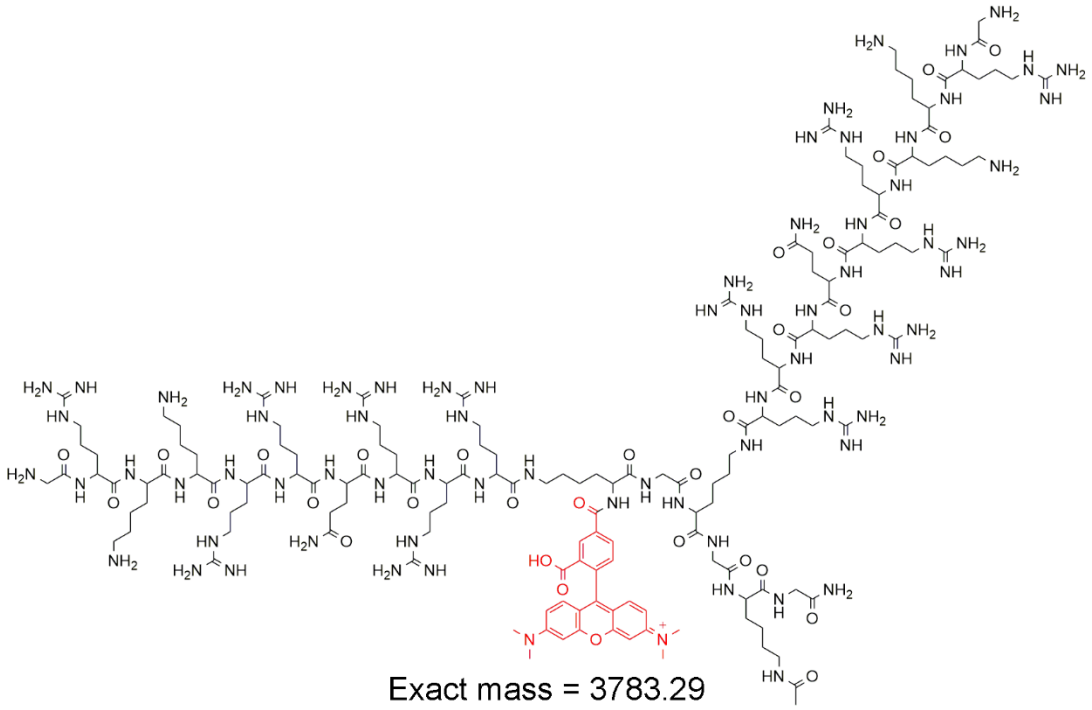

d)

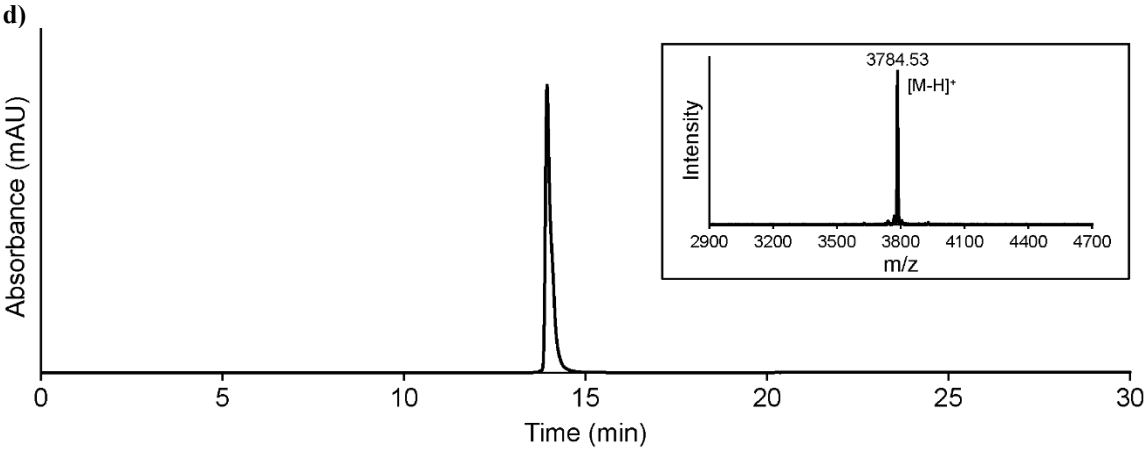

Figure A-2 continued.

e)

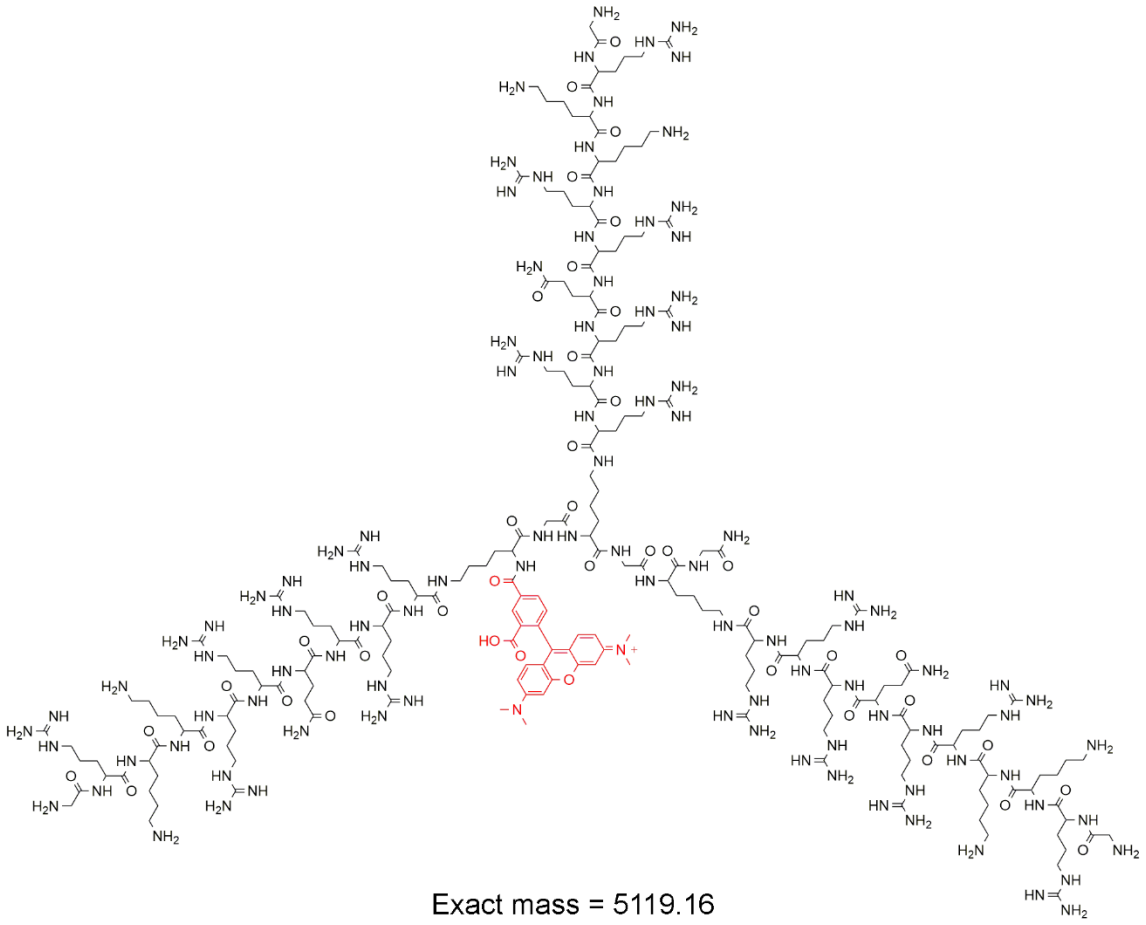

f)

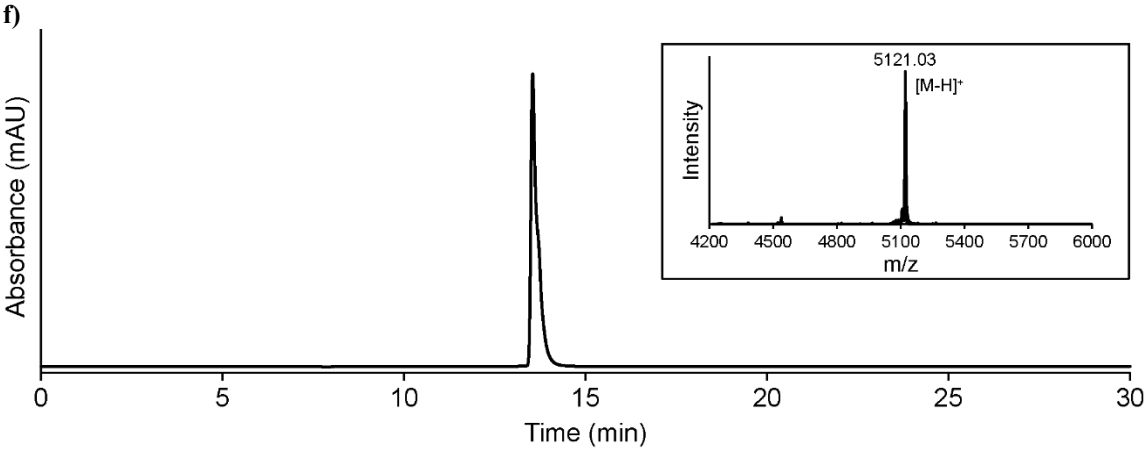

Figure A-2 continued.

g)

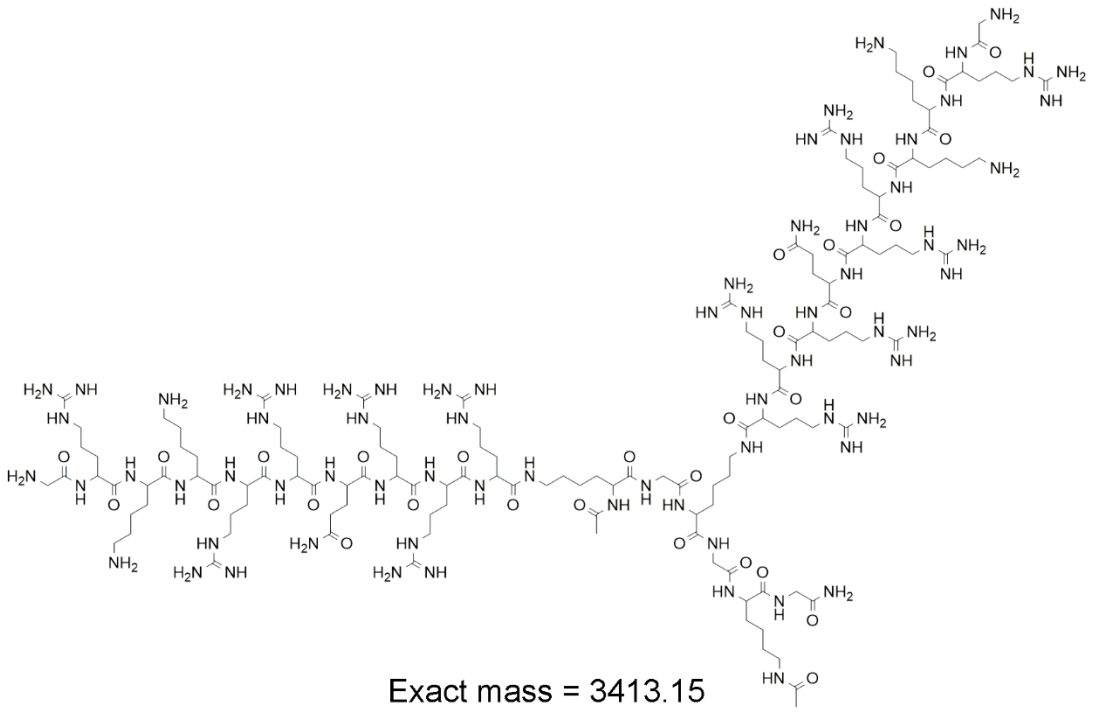

h)

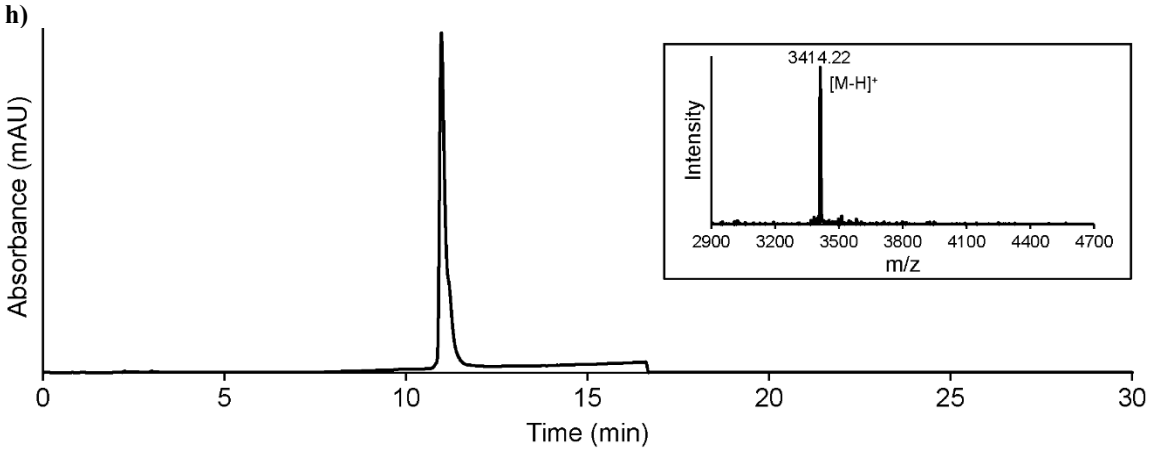

Figure A-2 continued.

i)

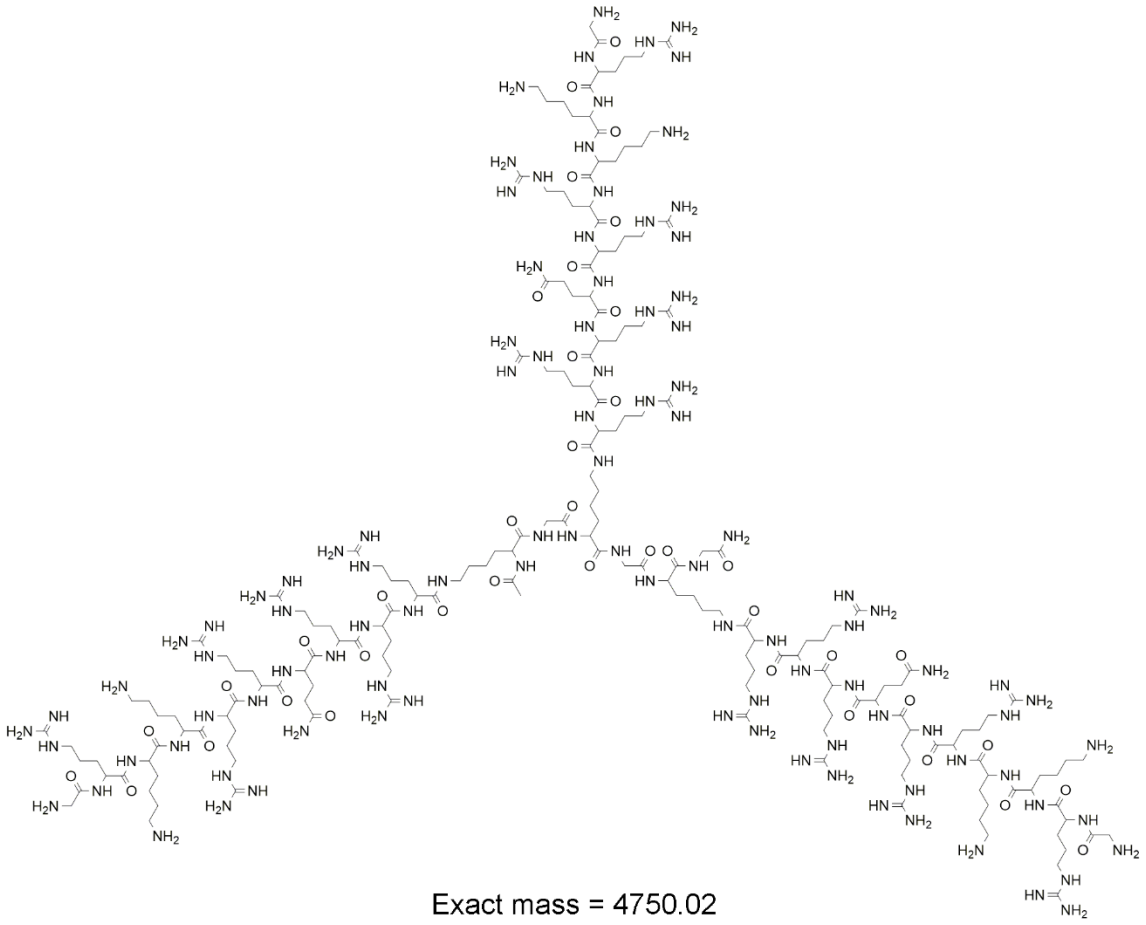

j)

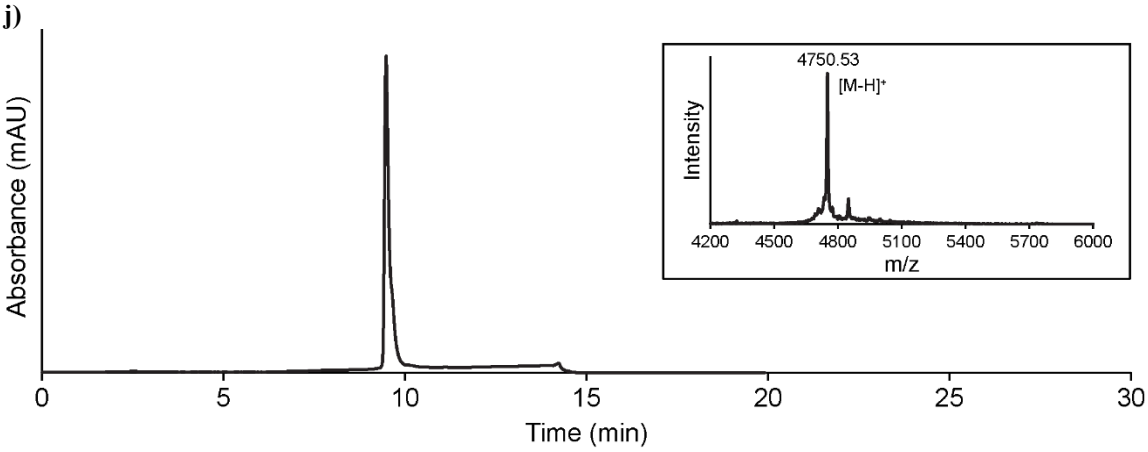

Figure A-2 continued.

Figure A-3 1TAT colocalizes inside cells with LysoTracker Green.
Cells were incubated with 1TAT (3 µM) for 30 min at 37°C and washed thereafter. Next, cells were incubated in L-15 medium for indicated times (exp 1 = 0 hr, exp 2 = 0.75 hr, exp 3 = 2.75 hr) and then stained with LysoTracker Green (500 nM), a marker of acidified endocytic organelles, as well as Hoechst 33342 (5 µM) for nuclear visualization. Representative fluorescence microscopy images taken under 100× magnification were obtained for 1TAT (pseudocolored red), LysoTracker Green (pseudocolored green) and an overlay of 1TAT, LysoTracker green and Hoechst 33342 (pseudocolored blue). Colocalization analysis was performed over zoomed-in sections of 1TAT and LysoTracker images of each condition. Pearson's R and Manders' M1 coefficients are reported to represent the extent of colocalization. Student's t-test was performed to compare the R_{avg} of each condition. Scale bars: 100× images: 10 µm, zoomed images: 2 µm. NS, $p>0.05$; *, $p<0.05$.

These data suggest that the accumulation of 1TAT in lysotracker-stained organelles, late endosomes and lysosomes increases overtime.

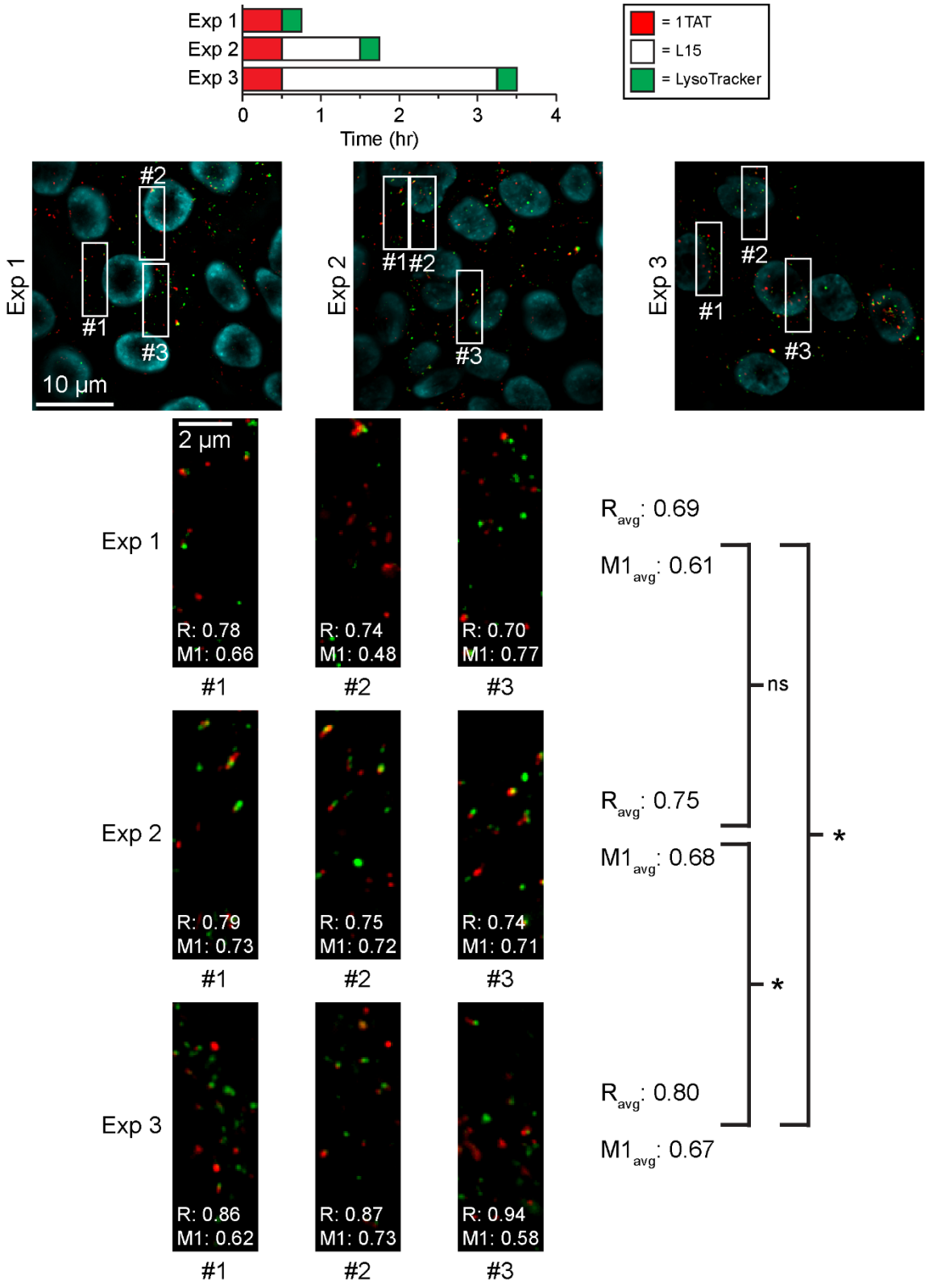
Exp 1
Exp 2
Exp 3
0
1
2
3
4
Time (hr)
= 1TAT
= L15
= LysoTracker
Exp 1
Exp 2
Exp 3
#1
#2
#3
10 µm
2 µm
R: 0.78
M1: 0.66
R: 0.74
M1: 0.48
R: 0.70
M1: 0.77
R: 0.79
M1: 0.73
R: 0.75
M1: 0.72
R: 0.74
M1: 0.71
R: 0.86
M1: 0.62
R: 0.87
M1: 0.73
R: 0.94
M1: 0.58
R_avg: 0.69
M1_avg: 0.61
R_avg: 0.75
M1_avg: 0.68
R_avg: 0.80
M1_avg: 0.67
ns
*
*

Figure A-4 Cytotoxicity upon 24 hr exposure of HeLa cells to 1TAT, 2TAT, and 3TAT.
(a) Representative fluorescence microscopy images of a SYTOX exclusion assay over HeLa cells treated with each peptide for 24 hr. HeLa cells were incubated with the peptides at the listed concentrations for 24 hr. Post-treatment, cells were washed and stained with SYTOX Green and Hoechst 33342 as before. Fluorescence microscopy was performed over the cells under each condition, and representative images were taken at 20× magnification (scale bars: 20×: 50 µm). (b) Evaluation of the toxicity of the peptides via a SYTOX Green exclusion assay. Cells were treated as in a. The number of cells displaying a nucleus stained by SYTOX Green were counted. The data represented correspond to the mean of technical triplicates (>500 cells counted per experiment). (c) Evaluation of the viability of cells treated with the peptides via an MTT viability assay. Cells were treated as in a and b. Post-treatment; cell viability was assessed using a standard MTT viability assay. Each condition was replicated (n=7) and represented as the normalized mean ± standard deviation.

These data suggest that the majority of the cytotoxic effect conferred by the addition of the peptides occurs initially, that is, within the first 30 min of addition. Little to no additional deleterious effects were observed upon prolonged exposure of the cells to the peptides.

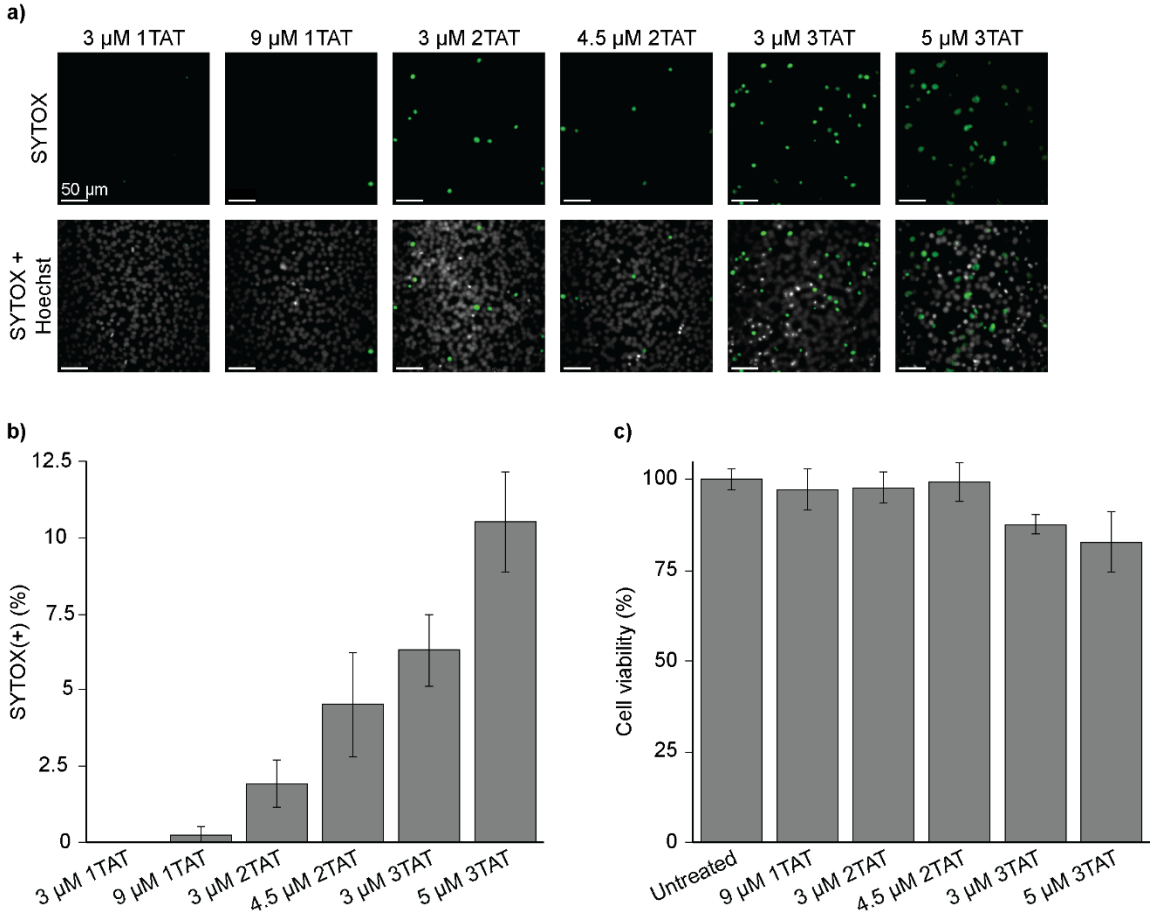
a)
3 μM 1TAT
9 μM 1TAT
3 μM 2TAT
4.5 μM 2TAT
3 μM 3TAT
5 μM 3TAT
SYTOX
50 μm
SYTOX + Hoechst
b)
SYTOX(+) (%)
12.5
10
7.5
5
2.5
0
3 μM 1TAT
9 μM 1TAT
3 μM 2TAT
4.5 μM 2TAT
3 μM 3TAT
5 μM 3TAT
c)
Cell viability (%)
100
75
50
25
0
Untreated
9 μM 1TAT
3 μM 2TAT
4.5 μM 2TAT
3 μM 3TAT
5 μM 3TAT

Figure A-5 DEAC-k5 colocalizes with LysoTracker Green.
Cells were incubated with DEAC-k5 (25 µM) for 1 hr at 37°C and washed thereafter. Next, cells were incubated in L-15 medium for indicated times (exp 1 = 0 hr, exp 2 = 0.75 hr, exp 3 = 2.75 hr) and then stained with LysoTracker Green (500 nM) as well as Hoechst 33342 (5 µM) for nuclear visualization. Representative fluorescence microscopy images at under 100× magnification were taken for DEAC-k5 (pseudocolored red), LysoTracker Green (pseudocolored green) and an overlay of DEAC-k5, LysoTracker green and Hoechst 33342 (pseudocolored blue). Colocalization analysis was performed over zoomed-in sections of DEAC-k5 and LysoTracker images of each condition. Pearson's R and Manders' M1 coefficients are reported to represent the extent of colocalization. Student's t-test was performed to compare the R_{avg} of each condition. DEAC-k5 was pseudocolored red in the images provided to enhance the contrast between the peptide and LysoTracker Green (as opposed to comparing blue and green). Scale bars: 100× images: 10 µm, zoomed images: 2 µm. NS, $p>0.05$; *, $p<0.05$; **, $p<0.01$.

These data suggest that the accumulation of DEAC-k5 in lysotracker-stained organelles, late endosomes and lysosomes, increases overtime.

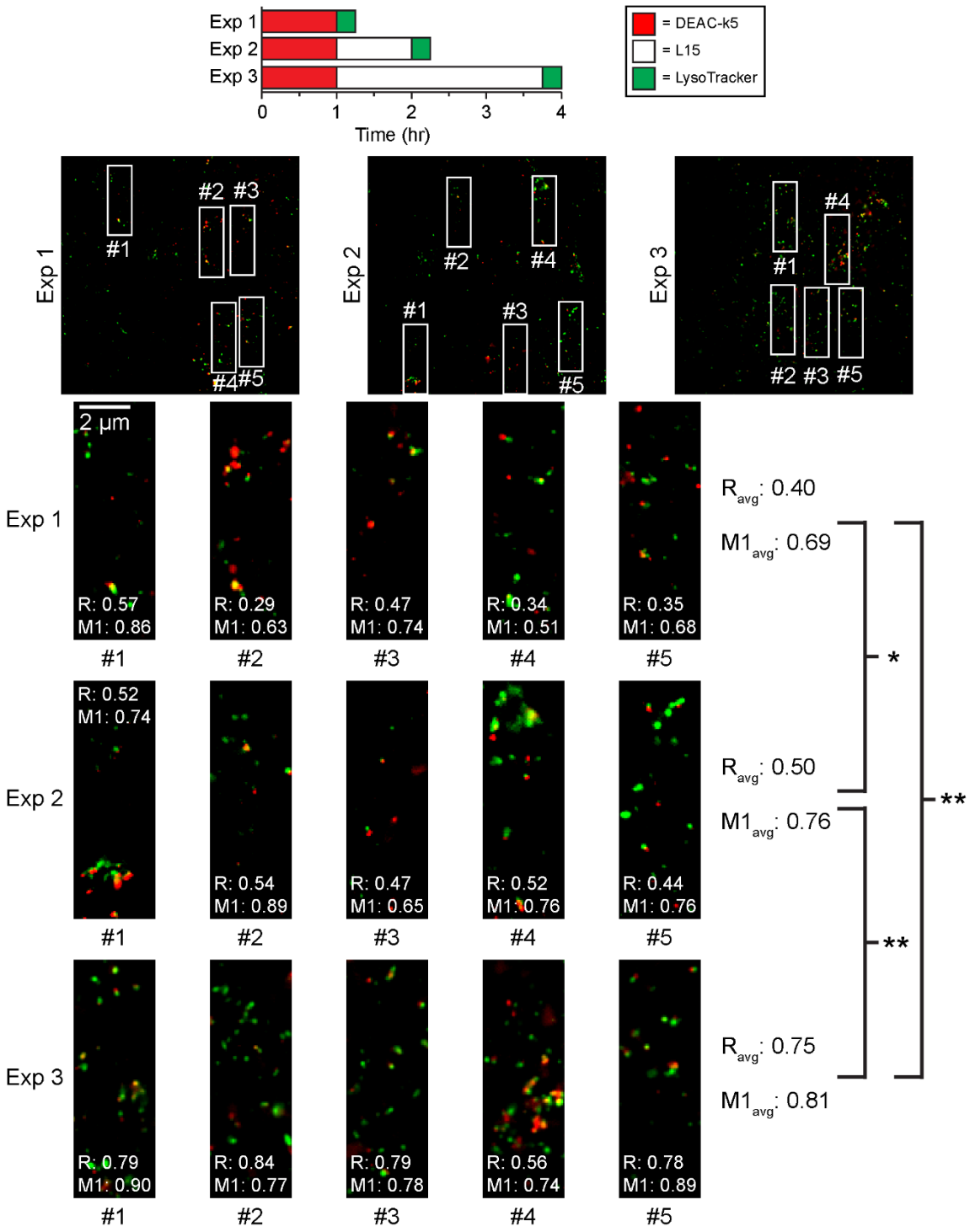
Exp 1
Exp 2
Exp 3
0
1
2
3
4
Time (hr)
= DEAC-k5
= L15
= LysoTracker
Exp 1
#1
#2 #3
#4 #5
Exp 2
#1
#2
#3
#4
#5
Exp 3
#1
#4
#2 #3 #5
2 µm
Exp 1
R: 0.57
M1: 0.86
R: 0.29
M1: 0.63
R: 0.47
M1: 0.74
R: 0.34
M1: 0.51
R: 0.35
M1: 0.68
#1
#2
#3
#4
#5
R_avg: 0.40
M1_avg: 0.69
*
Exp 2
R: 0.52
M1: 0.74
R: 0.54
M1: 0.89
R: 0.47
M1: 0.65
R: 0.52
M1: 0.76
R: 0.44
M1: 0.76
#1
#2
#3
#4
#5
R_avg: 0.50
M1_avg: 0.76
**
**
Exp 3
R: 0.79
M1: 0.90
R: 0.84
M1: 0.77
R: 0.79
M1: 0.78
R: 0.56
M1: 0.74
R: 0.78
M1: 0.89
#1
#2
#3
#4
#5
R_avg: 0.75
M1_avg: 0.81

Figure A-6 DEAC-k5 does not affect cell penetration or endosomolytic activities of 3TAT.
(a) DEAC-k5 does not affect cellular uptake of 3TAT. Cells were treated with 3 μM 3TAT ± DEAC-k5 (25 μM) for 30 min, 37°C. Following treatment, cells were washed, trypsinized, and lysed as described previously. Cellular uptake of 3TAT was determined by measuring the red fluorescence of the cell lysates. The data represented correspond to the mean of technical triplicates (>500 cells counted per experiment) with corresponding standard deviation. NS, p>0.05. (b) DEAC-k5 does not affect endosomal escape of 3TAT. Cells were treated with 3 μM 3TAT and/or DEAC-k5 (25 μM) for 30 min, 37°C. Following treatment, cells were washed and then stained with Hoechst 33342 (2.5 μM) 30 min later. Representative fluorescence microscopy images at 20× magnification were taken of DEAC-k5 (pseudocolored blue), 3TAT (pseudocolored red) and Hoechst 33342 (pseudocolored white). (Scale bars: 20×: 50 μm). (c) DEAC-k5 does not affect membrane lysis of liposomes treated with 3TAT. LE LUVs (250 μM total lipid) were treated with 3TAT (5 μM), DEAC-k5 (25 μM), or both peptides for 1 hr. The release of calcein from LUVs was then quantified. The data reported is the mean of technical triplicates and the corresponding standard deviation. Means were normalized to the leakage induced by 3TAT alone.

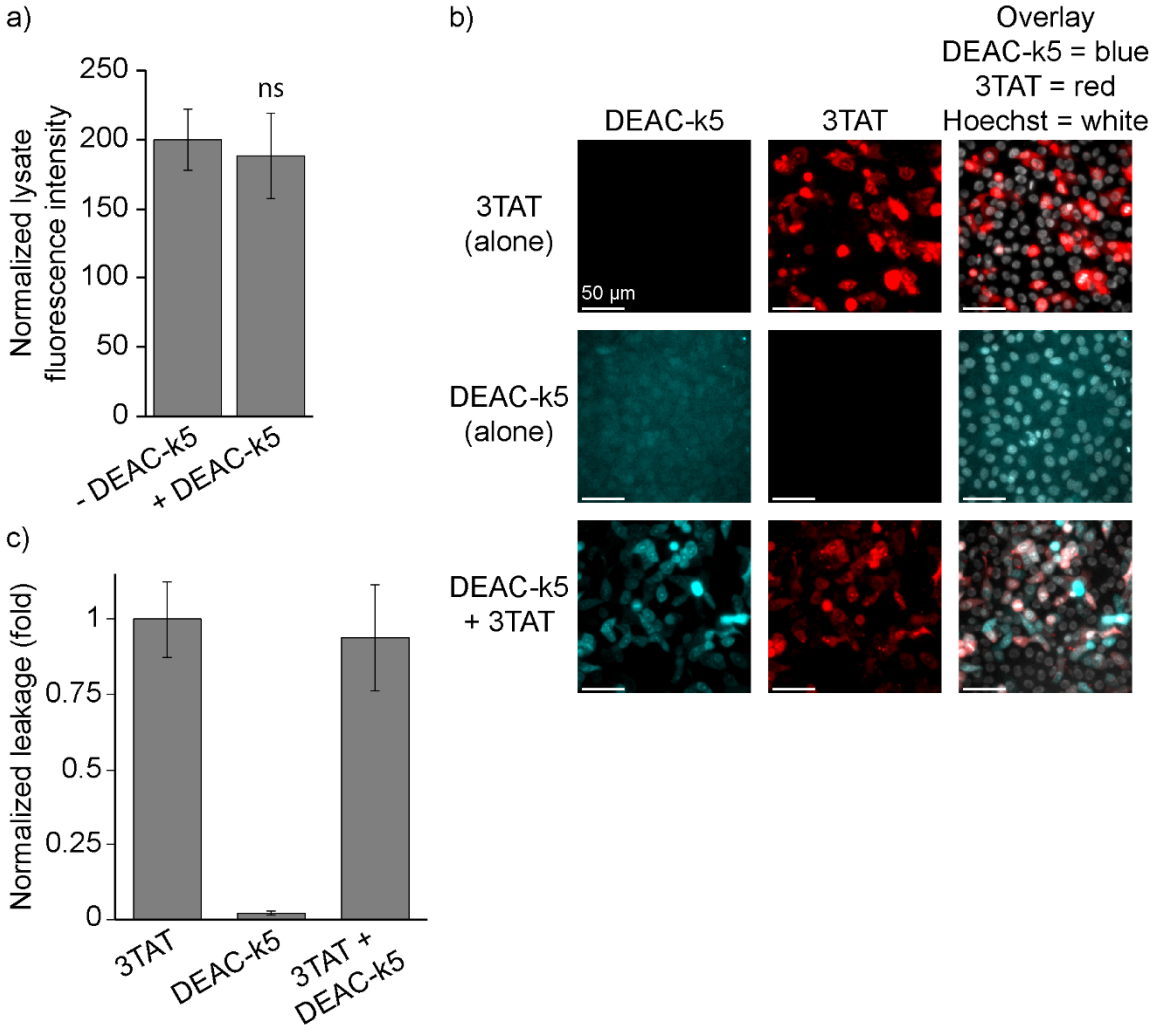
a)
Normalized lysate fluorescence intensity
250
200
150
100
50
0
ns
- DEAC-k5
+ DEAC-k5
b)
Overlay
DEAC-k5 = blue
3TAT = red
Hoechst = white
DEAC-k5
3TAT
3TAT (alone)
50 µm
DEAC-k5 (alone)
DEAC-k5 + 3TAT
c)
Normalized leakage (fold)
1
0.75
0.5
0.25
0
3TAT
DEAC-k5
3TAT + DEAC-k5

Figure A-7 Non-fluorescent variants of nf2TAT and nf3TAT confer similar *in cellulo* and *in vitro* activities to their fluorescent counterparts, albeit with poorer efficiency.
(a) Non-fluorescent peptide-mediated delivery of DEAC-k5 into HeLa cells. DEAC-k5 delivered by nf2TAT and nf3TAT allows for the quantification of cell penetration efficiency. Representative fluorescence microscopy images of cells coincubated with DEAC-k5 (25 μM) and each peptide at indicated concentrations for 30 min, washed, and stained with DRAQ7 (cell impermeable nucleic acid stain) and the nuclear stain Hoechst 33342. Cells were imaged 1 hr after incubation with peptides. Images are an overlay of DEAC-k5 (pseudocolored blue) and Hoechst 33342 (pseudocolored white). Scale bars: 20×: 50 μm. (b) The cell penetration activity of nf3TAT is superior to that of nf2TAT with a marked decrease from the activity of the fluorescent variant, 3TAT. Cells were treated as in a. Quantitative evaluation of the percentage of cells positive for penetration/delivery of DEAC-k5 (i.e., showing nucleolar staining by DEAC-k5 while excluding DRAQ7(+) cells. The data reported represent the mean of biological triplicates with corresponding standard deviation (>500 cells counted per experiment). (c) At high concentrations, nf3TAT is toxic to cells but significantly less toxic than 3TAT. Evaluation of the toxicity of the peptides by a DRAQ7 exclusion assay. Cells were treated as in b and c. The number of cells displaying a nucleus stained by DRAQ7 were counted. The data reported represent the mean of biological triplicates (>500 cells counted per experiment). (d) nf2TAT and nf3TAT deliver the biologically active enzyme TAT-Cre into HeLa cells. Cells transfected with a plasmid containing EGFP downstream of an LSL cassette were coincubated with TAT-Cre (4 μM) and each peptide at indicated concentrations for 30 min. Because successful cellular entry of TAT-Cre results in EGFP expression, the number of cells positive for EGFP fluorescence were counted 24 hr after each peptide/TAT-Cre incubations. Fluorescence microscopy images, pseudocolored green for EGFP, are representative examples of the cells 24 hr after enzyme delivery (scale bars: 20×: 50 μm, 100×: 10 μm). Quantification of cells positive for TAT-Cre delivery were scored and reported as the mean of biological triplicates (>500 cells per experiment) with corresponding standard deviation. (e) The leakage of LE LUVs induced by nf2TAT or nf3TAT displays a non-linear dose-dependent response. LE LUVs (250 μM total lipid) were treated with peptides at the indicated concentrations (peptide:lipid ratios are also provided) for 1 hr. The release of calcein from LUVs was then quantified. The data reported is the mean of technical triplicates and the corresponding standard deviation.

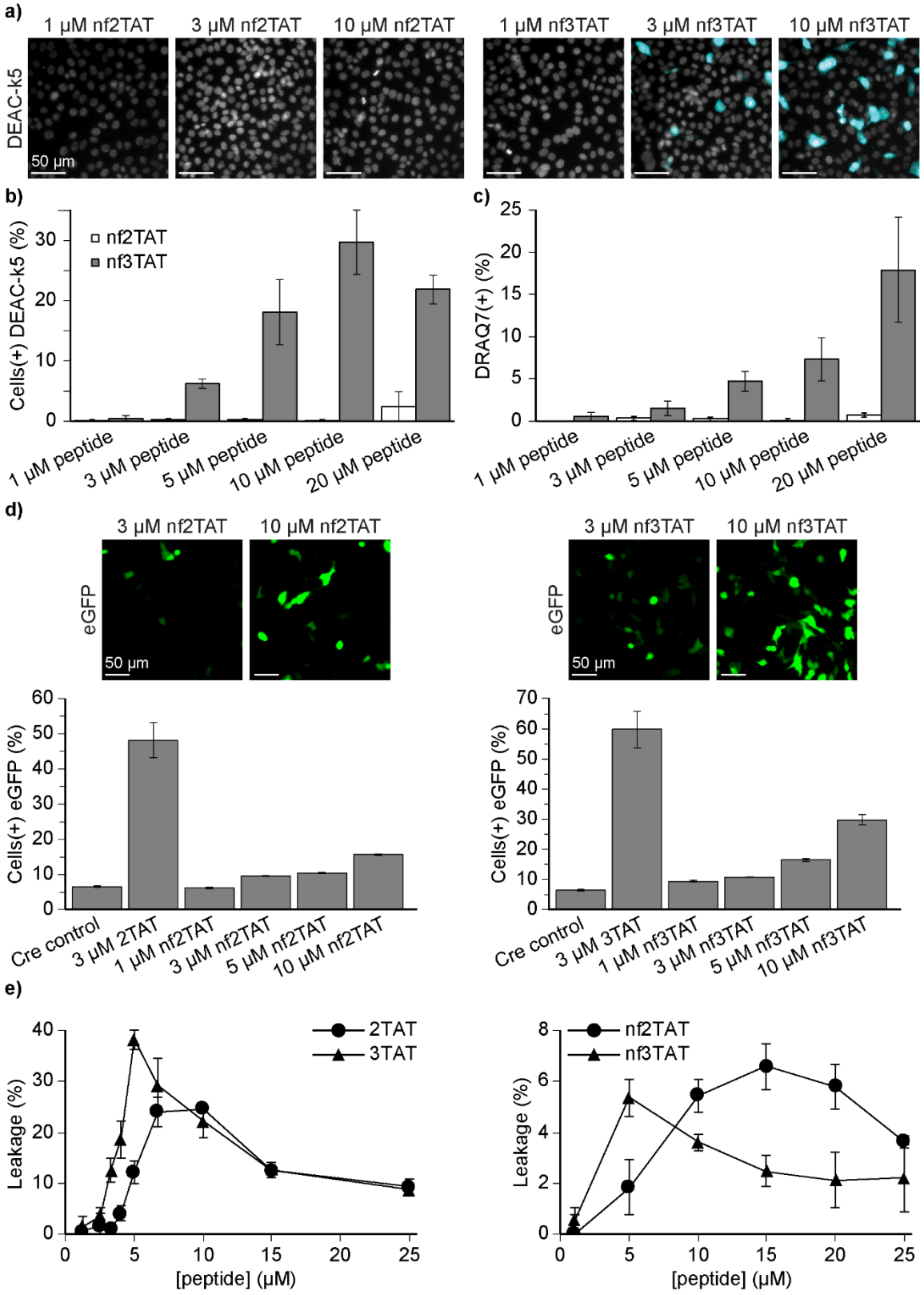
a)
1 μM nf2TAT
3 μM nf2TAT
10 μM nf2TAT
1 μM nf3TAT
3 μM nf3TAT
10 μM nf3TAT
DEAC-k5
50 μm
b)
Cells(+) DEAC-k5 (%)
nf2TAT
nf3TAT
1 μM peptide
3 μM peptide
5 μM peptide
10 μM peptide
20 μM peptide
c)
DRAQ7(+) (%)
d)
3 μM nf2TAT
10 μM nf2TAT
3 μM nf3TAT
10 μM nf3TAT
eGFP
50 μm
Cells(+) eGFP (%)
Cre control
3 μM 2TAT
1 μM nf2TAT
3 μM nf2TAT
5 μM nf2TAT
10 μM nf2TAT
3 μM 3TAT
1 μM nf3TAT
3 μM nf3TAT
5 μM nf3TAT
10 μM nf3TAT
e)
Leakage (%)
2TAT
3TAT
[peptide] (μM)
nf2TAT
nf3TAT

Figure A-8 Representative fluorescence microscopy images of 3TAT-mediated DEAC-k5 cellular delivery under different conditions.
Cells were treated as described in the main text Figure 3b. Fluorescence microscopy images, at 20× and 100× magnification, were taken over treated cells. Images are reported over the cells (bright field), DEAC-k5 (pseudocolored blue), and 3TAT (pseudocolored red). In experiments 4 and 7, the DEAC-k5 channel contrast of 20× magnification images was adjusted in an attempt to show the minimal level of staining of cells with the peptide. In the 100× magnification images of experiment 5, white arrows are superimposed to highlight the nucleoli-staining characteristic shared by both DEAC-k5 and 3TAT. Scale bars: 20×: 50 μm, 100×: 10 μm.

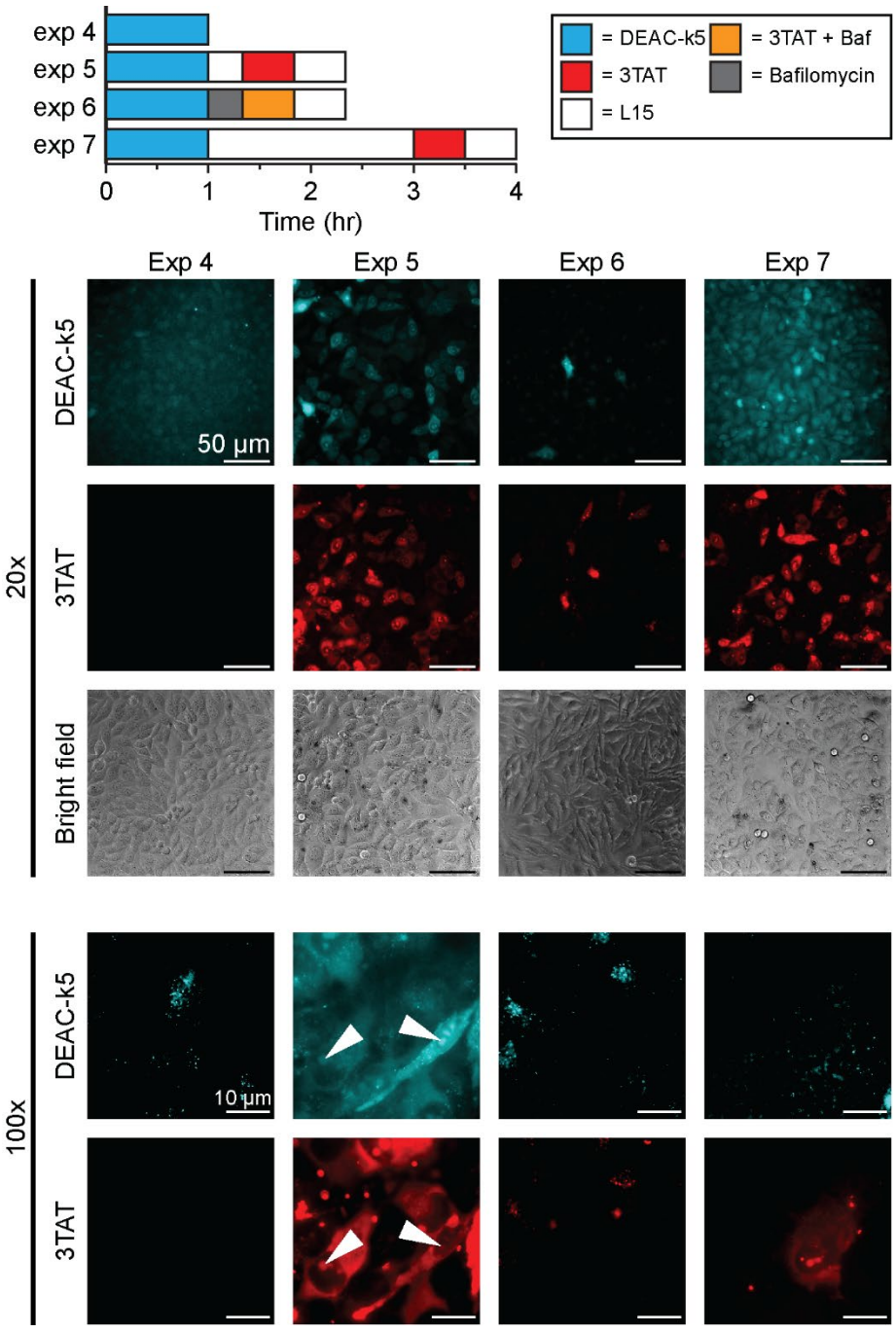
exp 4
exp 5
exp 6
exp 7
0
1
2
3
4
Time (hr)
= DEAC-k5
= 3TAT + Baf
= 3TAT
= Bafilomycin
= L15
Exp 4
Exp 5
Exp 6
Exp 7
20x
DEAC-k5
3TAT
Bright field
50 µm
100x
DEAC-k5
3TAT
10 µm

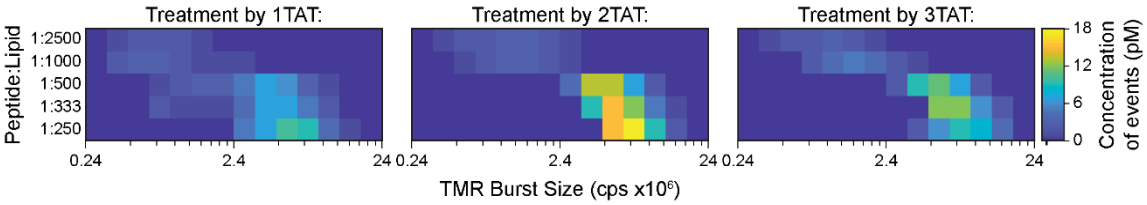

Figure A-9 Quantification of peptides bound to LE LUVs by BAS. LE LUVs doped with DiD (2.5 µM total lipid, 0.03% DiD) and treated with peptide at indicated concentrations were analyzed by Burst Analysis Spectroscopy (BAS). Fluorescence bursts from individual TMR-labeled peptides coincident with fluorescence bursts of DiD-labeled liposomes in each sample were detected and quantified. Each fluorescent event is binned based on its fluorescence intensity, and the overall population is represented as a heat map. The x-axis is a logarithmic scale of TMR fluorescence burst amplitude, while the color of each bin is pseudo-colored blue to yellow and is proportional to the concentration of peptide bound to liposomes. The data represented is the compilation of triplicates.

APPENDIX B

SUPPORTING INFORMATION FOR MEMBRANE FLUIDITY DIRECTLY IMPACTS THE EXTENT OF SUPERCHARGED CPP-INDUCED MEMBRANE LYSIS ON BMP-CONTAINING MEMBRANES

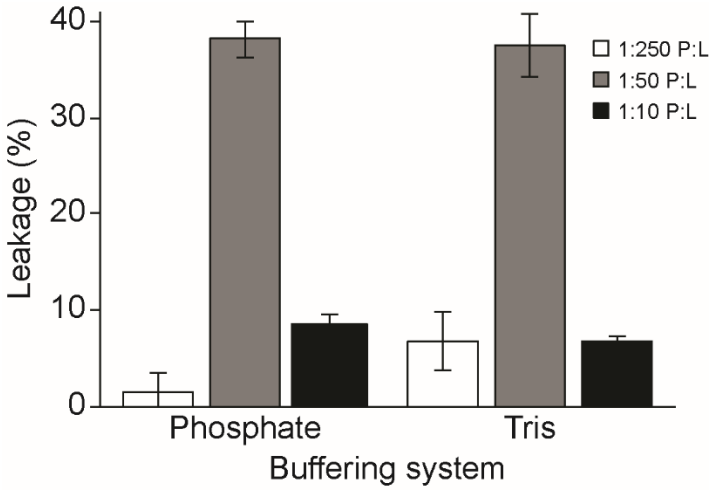

Figure B-1 The buffering system used does not play a role in 3TAT-mediated lysis of BMP-containing membranes.
Calcein-loaded LE LUVs were generated and treated with indicated peptide:lipid ratios of 3TAT in either a phosphate or Tris buffering system to monitor differences in membrane lytic activity. Values reported are the mean of technical triplicates and corresponding standard deviations.

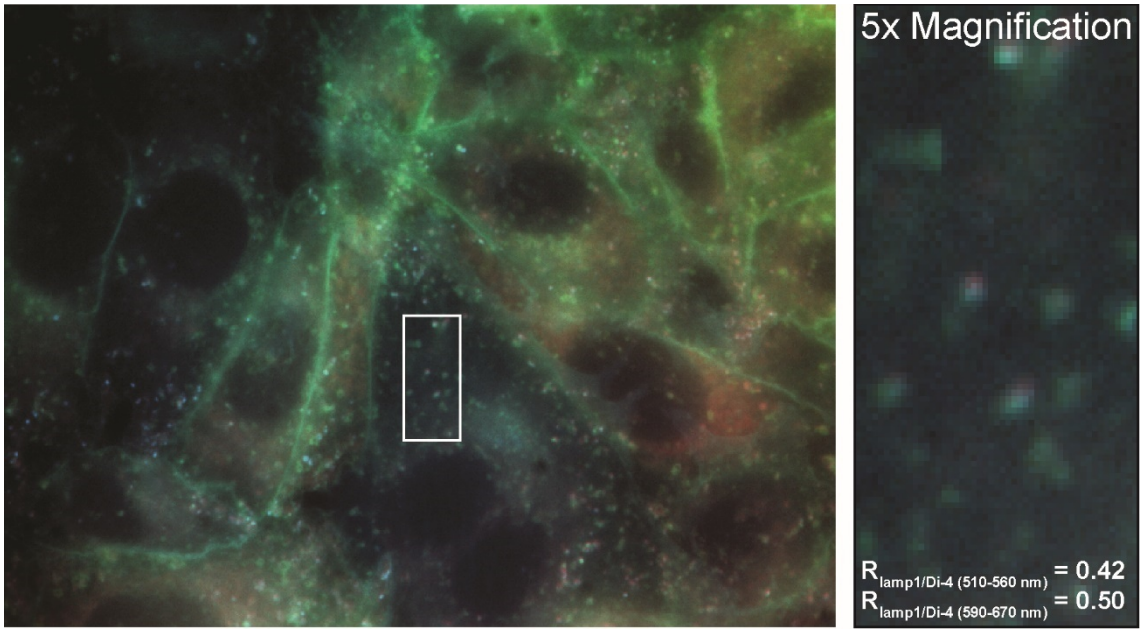

Figure B-2 Di-4-ANEPPDHQ is capable of staining BMP-containing endocytic membranes. CHO-K1 cells were stained with 5 µM Di-4-ANEPPDHQ and allowed to incubate for 30 min prior to addition of 500 nM LysoTracker Blue DND-22. Following LysoTracker incubation, cells were imaged by fluorescence microscopy in order to determine the extent of colocalization between LysoTracker-stained membranes and Di-4-ANEPPDHQ-stained membranes. Colocalization calculations were performed for the indicated regions of interest with high puncta density. The Pearson colocalization coefficient, R, was reported for colocalization of the LysoTracker channel with either the λ_{ex} = 510-560 nm or λ_{ex} = 590-670 nm Di-4-ANEPPDHQ channels.